

# DESIGN AND IMPLEMENTATION OF MODULATION AND DETECTION STRATEGIES FOR SPATIAL MODULATION MIMO SYSTEMS

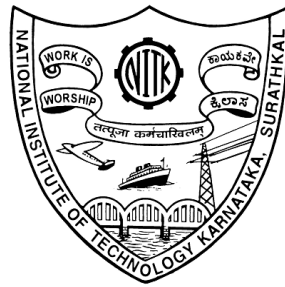
Thesis

Submitted in partial fulfillment of the requirements for the degree of

DOCTOR OF PHILOSOPHY

by

GOUTHAM SIMHA G.D.



DEPARTMENT OF ELECTRONICS AND COMMUNICATION ENGINEERING

NATIONAL INSTITUTE OF TECHNOLOGY KARNATAKA

SURATHKAL, MANGALORE - 575025

JUNE, 2018



## DECLARATION

I hereby *declare* that the Research Thesis entitled "**DESIGN AND IMPLEMENTATION OF MODULATION AND DETECTION STRATEGIES FOR SPATIAL MODULATION MIMO SYSTEMS**" which is being submitted to the **National Institute of Technology Karnataka, Surathkal** in partial fulfillment of the requirements for the award of the Degree of **Doctor of Philosophy in Electronics and Communication Engineering** is a *bonafide report of the research work carried out by me*. The material contained in this Research Thesis has not been submitted to any University or Institution for the award of any degree.

Goutham Simha G.D.

Reg. No.: 123040 EC12F04

Department of Electronics and Communication Engineering

Place: NITK, Surathkal.

Date: JUNE-2018



## **CERTIFICATE**

This is to *certify* that the Research Thesis entitled "**DESIGN AND IMPLEMENTATION OF MODULATION AND DETECTION STRATEGIES FOR SPATIAL MODULATION MIMO SYSTEMS**" submitted by **GOUTHAM SIMHA G.D.**, (Reg. No.: 123040 EC12F04) as the record of the research work carried out by him, is *accepted as the Research Thesis submission* in partial fulfillment of the requirements for the award of degree of **Doctor of Philosophy**.

(Prof. U Shripathi Acharya)  
Research Supervisor

Chairman - DRPC



# ACKNOWLEDGMENT

I would like to take this opportunity to thank those people who have made this thesis possible.

Firstly, I would like to express my sincere gratitude to my advisor Prof. U Shripathi Acharya for the continuous support for my Ph.D study and related research. I always adore his patience, motivation, and immense knowledge about the subject which has inspired me to do research at NITK, Surathkal. His guidance helped me in all the time of research and writing of this thesis. I could not have imagined a better advisor and mentor for my Ph.D study. My sincere Namaskarams at his feet. I would also like to thank Gayatri Amma w/o Shripathi sir for providing her indebted love and support.

Besides my advisor, I would like to thank the rest of my thesis committee: Prof. Muralidhar Kulkarni, Prof. B.R Shankar, Prof M.S Bhat and Prof. T Laxminidhi, for their insightful comments and encouragement throughout my Ph.D study.

I would like to thank Prof Prashantha Kumar H for his wonderful insight and motivation at every stage.

From bottom part of my heart I thank my fellow lab mate Shriharsha K, who stood by me with his ever lasting support drenched with magnificent insight and thought process towards the research and equipping me with all the minute technical details. I would like to sincerely thank Raghavendra M A N S for his awe-inspiring discussions on complex analytical upper bounds, that had helped me in understanding and realizing the closed form solutions. My wholehearted thanks to Neha for the wonderful discussions about channel estimation experiment. My heartfelt thanks to Shrutkirthi G for her exceptional skills, that revamped my journal papers. I thank R Prasad Naik for his valuable comments, support and suggestions. Thank you very much every lab mate for the sleepless nights we were working together before deadlines, and for all the fun we have had in the last five years.

Finally, I am thankful to the two most precious jewels of my life, father Dattathreya and mother Sathyavathi for their unceasingly intense love towards me.

Place: NITK, Surathkal

Goutham Simha G.D.

Date: JUNE-2018



*Dedicated to the Lotus feet of these Great Masters who have  
Reformed my life.*

**Babaji Maharaj.**  
my dad **Dattathreya.**  
and my mom **Sathyavathi.**



# Abstract

It is well known that MIMO communication systems possess higher spectral efficiency when compared with SISO systems. A novel MIMO technique that tried to combine the advantages of multiple antenna communication while simultaneously conserving energy was proposed by Mesleh [Mesleh et al. (2008)]. This technique uses only one active antenna out of the available multiple antennas to communicate information. The advantage of this scheme is that the active antenna index is also used to communicate information and only a single RF chain is required at the transmitter. Since certain symbols are conveyed by means of the antenna index, they need not be physically radiated. This has the effect of increasing spectral efficiency while reducing the power consumed by the transmitting circuits.

A study of relevant literature shows that the performance of all SM schemes deteriorate under Spatially Correlated (SC) fading channel conditions. To combat the impact of SC, Trellis Coded Spatial Modulation (TCSM) was introduced by [Mesleh et al. (2010)]. In TCSM, the impact of correlation on the performance of SM is reduced by segregating antennas into subsets. This offers maximum spatial separation between the antennas within the same set, though a minimum of four transmit antennas are needed to make the subsets. In this thesis, we have developed and synthesized modulation schemes which are capable of delivering good BER performance under uncorrelated as well as correlated channel conditions. Our primary concern is on practical hand held devices which exhibit spatial correlation quite often. We have designed a scheme called Redesigned Spatial Modulation (ReSM) which can be employed under spatially correlated channel conditions (Chapter-3). This scheme exhibits significant advantage over TCSM and other SM schemes in terms of ABER performance improvement. An experimental setup was established in order to realize the working of the proposed ReSM scheme for indoor environment and a comparative study over SM scheme was performed. The observed results clearly indicate the superiority of ReSM over SM

schemes.

In the next chapter (Chapter-4), we have attempted to design SM schemes with an underlying Space Time Block Code (STBC). This is motivated by the desire to further improve the integrity of information transfer. A study of relevant literature lead us to explore the class of codes bearing good rank distance properties. We converged on the class of  $n$ -length cyclic codes over  $GF(q^m)$  which have good rank distance properties. We have synthesized several Non Orthogonal Space Time Block Codes for MIMO systems. These schemes achieve high rate, are spectrally efficient and can serve as alternatives to traditional STBC schemes. The improvement achieved in terms of ABER by the use of these Non Orthogonal STBCs is explored in Chapter-4.

In the following chapters, different aspects of varied Spatial Modulation schemes have been explored. The BER performance of various SM schemes in the presence and absence of channel state information in MIMO environments for various fading channels has been determined. We have employed a high rate spectrally efficient modulation scheme, designated as Double Spatial Modulation (DSM) which yields a performance that is superior to all known variants of SM under these conditions. The performance of DSM under conditions of non-uniform phase distribution which is associated with several real world channel scenarios (Nakagami- $m$ ) have been simulated and synthesized in Chapter-5.

In Chapter-6, we have synthesized SM schemes which preserve spectral efficiency while being compatible with the requirements of LTE-Advanced and 5G systems employing MIMO architecture with single and Multistream configurations. This is achieved through the use of non-uniform constellations derived from multiplicative groups of Gaussian and Eisenstein integers.

In the last part of our work, the advantages of a Multistream Spatial Modulation (MSM) scheme has been explored. The simulation results show that, MSM scheme can yield impressive SNR gains in all possible uncorrelated fading environments. This encouraged us to formulate, a new design employing MSM under conditions of high spatial correlation. The observed results reveal that the proposed Multistream Spatial Modulation scheme yields performance improvement of the order  $\sim 2.5$  dB over all

conventional Multistream SM schemes in SC channels.

In summary, the focus of the thesis has been on the design of uncoded and codes SM schemes which have high spectral efficiency, moderate decoding complexity and BER performance that is superior to known SM constructions, over various channel fading models in the presence and absence of Channel State Information. Further, the SM systems designed and described in the thesis have employed the notions of non-uniform constellation design and the effect of Multistream configurations. Every design was formulated keeping in mind the adaptation to the latest communication setup and standards. We have also proposed certain extensions to this body of work which can bring about further improvements to the integrity of information transfer while conserving resources such as spectrum and energy.



# Contents

Abstract . . . . .	i
Acronyms and Abbreviations . . . . .	ix
List of Symbols . . . . .	xi
List of Figures . . . . .	xiv
List of Tables . . . . .	xx
<b>1 Introduction</b>	<b>1</b>
1.1 Motivation for this Research work . . . . .	1
<b>2 Background</b>	<b>5</b>
2.1 MIMO wireless communication systems . . . . .	5
2.1.1 System Models . . . . .	6
2.1.2 Channel Models . . . . .	7
2.1.3 Summary . . . . .	9
<b>3 Redesigned Spatial Modulation for Spatially Correlated channels</b>	<b>11</b>
3.1 Introduction . . . . .	12
3.2 ReSM construction and Design . . . . .	14
3.2.1 Methodology of antenna selection algorithm in ReSM . . . . .	17
3.2.2 Optimal Maximum Likelihood detection criterion: . . . . .	18
3.3 Analytical Treatment for ReSM . . . . .	19
3.4 Receiver Computational Complexity Comparison . . . . .	21
3.4.1 Computational Complexity of the Proposed ReSM . . . . .	23
3.5 Simulation Results . . . . .	24
3.6 Real time Measurements . . . . .	29
3.6.1 A detailed procedure for channel estimation using USRP B210 . . . . .	29
3.7 Summary . . . . .	35

<b>4</b>	<b>Full Rank Non Orthogonal STBC design for SM-MIMO Systems from Cyclic codes: A Complete Framework.</b>	<b>37</b>
4.1	Introduction . . . . .	37
4.2	Design of Non Orthogonal Full Rank Space Time Block Coded Spatial Modulation (NSTBC-SM) . . . . .	39
4.2.1	Transform Domain description of cyclic codes . . . . .	39
4.2.2	Cyclotomic coset . . . . .	39
4.2.3	Galois Field Fourier Transforms (GFFT) . . . . .	40
4.2.4	Characterization of cyclic codes for Rank metric . . . . .	41
4.2.5	Cyclic Codes as STBC . . . . .	43
4.3	Non Orthogonal Full Rank Space Time Block Coded Spatial Modulation (NSTBC-SM) . . . . .	45
4.3.1	Spectral Efficiency Calculation for NSTBC-SM . . . . .	50
4.3.2	ML decoder for the proposed NSTBC-SM . . . . .	50
4.4	NSTBC-SM Analytical Performance . . . . .	52
4.5	Computational Complexity Analysis . . . . .	56
4.6	Simulation Results and Performance Analysis . . . . .	56
4.6.1	Performance Analysis under Rayleigh Channel conditions . . . . .	57
4.6.2	STBC construction for 4 bpcu . . . . .	57
4.6.3	STBC construction for 4.5 bpcu using Eisenstein map . . . . .	59
4.6.4	STBC construction for 5.5 bpcu using Gaussian map . . . . .	60
4.6.5	STBC construction for 6 bpcu using Gaussian map . . . . .	62
4.6.6	Performance Analysis Under Rician Channel Conditions: . . . . .	65
4.6.7	Performance Analysis Under Spatially Correlated Channel Conditions . . . . .	67
4.7	Summary . . . . .	67
<b>5</b>	<b>A Comprehensive Framework for Double Spatial Modulation Under Imperfect Channel State Information</b>	<b>69</b>
5.1	Introduction . . . . .	70
5.2	System and Channel Model . . . . .	71
5.2.1	Rayleigh and Rician Fading Channels . . . . .	73



5.2.2	Nakagami-m Fading Channels . . . . .	73
5.2.3	Optimal ML and Suboptimal OB-MMSE decoding strategies for DSM . . . . .	75
5.2.4	Optimal ML detection . . . . .	75
5.2.5	Suboptimal OB-MMSE detection . . . . .	75
5.3	Analytical treatment for DSM under fading scenarios: . . . . .	77
5.3.1	<b>Case 1: Perfect-CSI</b> . . . . .	77
5.3.2	<b>Case 2: Imperfect-CSI</b> . . . . .	80
5.4	Simulation Results and observations: . . . . .	81
5.5	Summary . . . . .	88
<b>6</b>	<b>Signal Constellations Employing Multiplicative Groups of Gaussian and Eisenstein Integers for Enhanced Spatial Modulation</b>	<b>91</b>
6.1	Introduction . . . . .	92
6.2	System and Channel Model . . . . .	93
6.2.1	Gaussian and Eisenstein-Jacobi integers . . . . .	93
6.2.2	Enhanced SM (ESM) . . . . .	94
6.2.3	Quadrature SM (QSM) . . . . .	96
6.2.4	Enhanced SM (ESM) type-1 and type-2 . . . . .	96
6.2.5	ESM design from Gaussian and Eisenstein integers (GESM) . . . . .	96
6.2.6	Generalization to Multistream SM systems . . . . .	103
6.2.7	Quasi Static Rayleigh Fading Channels . . . . .	105
6.3	Analytical treatment for proposed GESM . . . . .	105
6.4	Computational Complexity Analysis . . . . .	106
6.5	Simulation Results and Observations . . . . .	107
6.6	Summary . . . . .	110
<b>7</b>	<b>Modified Signal Design for Multistream Spatial Modulation over Spatially Correlated Channels</b>	<b>113</b>
7.1	Introduction . . . . .	114
7.2	System Models . . . . .	115
7.2.1	Enhanced SM (ESM) . . . . .	115
7.2.2	Quadrature SM (QSM) . . . . .	115

7.2.3	Double SM (DSM)	116
7.2.4	Modified Multistream SM (MSM)	116
7.2.5	Antenna Selection in modified MSM	116
7.3	Analytical Treatment for Modified MSM	119
7.4	Simulation Results and Observations	120
7.5	Summary	124
<b>8</b>	<b>Conclusions and Future works:</b>	<b>125</b>
8.1	Future work	127
	Bibliography	128

## Acronyms and Abbreviations

ABEP	Average Bit Error Probability
ABER	Average Bit Error Ratio
ADC	Analog to Digital Conversion
AoA	Angle of Arrival
AoD	Angle of Departure
APEP	Average Pairwise Error Probability
AS	Angular Spread
AWGN	Additive White Gaussian Noise
BLAST	Bell Lab Layered Space Time
CDF	Cumulative Distribution Function
CPEP	Conditional Pairwise Error Probability
DAC	Digital to Analog Conversion
DSM	Double Spatial Modulation
EJ	Eisenstein-Jacobi
ESM	Enhanced Spatial Modulation
GESM	Gaussian ESM
GF	Galois Field
GFFT	Galois Field Fourier Transform
GNSM	Generalized Spatial Modulation
IGFFT	Inverse Galois Field Fourier Transform
i.i.d	Independent and Identically Distributed
IM	Index Modulation
Imp-CSI	Imperfect Channel State Information
ISI	Inter Symbol Interference
ISM	Improved Spatial Modulation
LoS	Line of Sight
LS	Least Square
LTE	Long Term Evolution

MIMO	Multiple Input Multiple Output
ML	Maximum Likelihood
MMSE	Minimum Mean Square Error
MRRC	Maximal Receive Ratio Combining
MSM	Multistream Spatial Modulation
NLoS	Non Line of Sight
NSTBC	Non-Orthogonal Space Time Block Code
OB-MMSE	Ordered Block Minimum Mean Square Error
OSTBC	Orthogonal Space Time Block Code
P-CSI	Perfect Channel State Information
PDF	Probability Density Function
PEP	Pairwise Error Probability
QOSTBC	Quasi Orthogonal Space Time Block Code
QSM	Quadrature Spatial Modulation
ReSM	Redesigned Spatial Modulation
RS	Reed-Solomon
RX Separation	Receive antenna Separation
SC	Spatially Correlated
SISO	Single Input Single Output
SM	Spatial Modulation
SMX	Spatial Multiplexing
SNR	Signal to Noise Ratio
ST	Space Time
STBC	Space Time Block Codes
STC	Space Time Codes
TAC	Transmit Antenna Combination
TCSM	Trellis Coded Spatial Modulation
TX separation	Transmit antenna Separation
USRP	Universal Software Radio Peripheral
VGSM	Variable Generalized Spatial Modulation
Wi-Max	Worldwide Interoperability for Microwave Access
3GPP	3 <sup>rd</sup> Generation Partnership Project
4G	4 <sup>th</sup> Generation
5G	5 <sup>th</sup> Generation

## List of Symbols

Symbol	Explanation
<b>S</b>	Information Symbol
<b>X</b>	Transmitted symbol vector
<b>H</b>	Channel Matrix
<b>Y</b>	Received symbol vector
$\hat{\mathbf{S}}$	Estimation of <b>S</b>
$N_t$	Number of transmit antennas
$N_r$	Number of receive antennas
$N_a$	Number of active antennas
$\rho$	Average SNR
$M$	Modulation order
<b>n</b>	Noise vector
<b>H<sub>c</sub></b>	Correlated channel matrix
$K$	Rician factor
$\bar{\mathbf{H}}$	All one matrix
$R_{(m,n)}$	Correlation between signals from any two antenna elements $m, n$
$d_a$	Distance of separation between the antenna elements
$\theta_0, \sigma_\theta$	AoA and AS.
<b>R<sub>TRAN</sub></b>	Transmit correlation matrix
<b>R<sub>TRAN</sub></b>	Receiver correlation matrix
$\lambda$	Wavelength
$h_{ij}$	Channel gain from $j^{th}$ transmit antenna to $i^{th}$ receive antenna
$h_{rp}$	Channel gain from $p^{th}$ transmit antenna to $r^{th}$ receive antenna
$\eta$	Spectral efficiency
$\hat{j}_{ML}$	Information about active transmit antenna index
$\hat{q}_{ML}$	Information about signal constellation symbol
$(\cdot)^H$	Hermitian operator

<b>Symbol</b>	<b>Explanation</b>
$N(x_{n_t, s_t}, x_{n, s})$	Total number of bits in error between $x_{n_t, s_t}, x_{n, s}$
$\ \bullet\ _F^2$	Frobenius norm
$E_H\{\cdot\}$	Expectation across the channel matrix $\mathbf{H}$
$Q(\cdot)$	Q function
$\Gamma$	The gamma function
$\mathcal{L}_H$	Covariance matrix
$\check{\mathbf{H}}$	The mean matrix
$\otimes$	Kronecker product
$vec(\mathbf{H})$	Column of matrix $\mathbf{H}$
$I_n$	$n \times n$ identity matrix
$\sigma_n^2$	Noise variance
$n$	Length of a cyclic code
$[f]^d$	Cardinality of $f$
$\mathbf{a}$	$n$ -tuple value over finite field
$\mathbf{A}_j$	GIFFT
$\mathbf{a}_i$	IGFFT
$P$	Characteristic of a finite field element
$C$	Cyclic code
$e_j$	Size of the Cyclotomic coset
$Rank_q(\cdot)$	Rank of a Cyclic code over $GF(q)$
$\alpha$	Primitive polynomial
$\Pi$	Eisenstein prime number
$G_\pi$	Gaussian Integer modulo $\pi$
$Z_i$	Gaussian prime number
$[\cdot]$	Rounding to the next nearest integer
$J_\Pi$	Residue class of $J \bmod \Pi$
$\mathfrak{Z}$	$\zeta$ or $\xi$ depends on map
$\log_2(\Psi)$	Bits from antenna selection
$M_{ant}$	Antenna selection bits
$\mathbb{M}$	Input bits (Algorithm-1 Chapter-4)
$T$	Output bits
$\mathbb{M}_{info}$	Information bits
$\phi$	variable to store mapped bits
$\lfloor \cdot \rfloor$	Floor operation
$\hat{\mathbb{M}}$	Total estimated bits

---

<b>Symbol</b>	<b>Explanation</b>
$\Gamma$	The Gamma function (Chapter-4)
$\mathbf{C}$	Codeword vector
$[\cdot]^T$	Transpose operator
$\Theta$	Optimum rotation angle
$\mathbb{Z}_i^R, \mathbb{Z}_i^I$	Circularly symmetric i.i.d Gaussian RV (Real and Imaginary)
$\varphi$	Random variable
$P(\varpi)$	Nakagami variance parameter
$P(\phi)$	Phase of Nakagami-m
$m$	Nakagami parameter
$\mathbf{E}$	Estimation error
$V_{th}$	Threshold value
$Q(\cdot)$	Digital modulator/demodulator function
$\sigma_e^2$	Signal variance
$\sigma_n^2$	Noise variance
$\bar{\gamma}$	Average SNR per bit
$P_c$	Primary constellation
$S_c$	Secondary constellation
$\mathbb{L}$	Group of constellations
$\rho$	Eisenstein integer value
$\hat{\mathbf{X}}$	Estimation of vector $\mathbf{X}$
$l_{min}^2$	Euclidean distance between two codewords

---





# List of Figures

2.1	MIMO system model with $N_t$ transmit antennas and $N_r$ receive antennas [Mesleh (2007)] . . . . .	6
3.1	Block diagram of the proposed Redesigned Spatial Modulation system	14
3.2	Block diagram of the proposed Redesigned Spatial Modulation system	24
3.3	BER performance of $4 \times 4$ systems with TX separation $=0.1\lambda$ and RX separation $=0.5\lambda$ yielding $\eta =6$ bpcu spectral efficiency, in a SC channel.	25
3.4	BER performance of $4 \times 4$ systems with TX separation $=0.1\lambda$ and RX separation $=0.3\lambda$ yielding $\eta =6$ bpcu spectral efficiency, in a SC channel.	26
3.5	BER performance of $4 \times 4$ systems with TX separation $=0.1\lambda$ and RX separation $=0.1\lambda$ yielding $\eta =6$ bpcu spectral efficiency, in a SC channel.	27
3.6	BER performance of $2 \times 4$ systems with TX separation $=0.1\lambda$ and RX separation $=0.1\lambda$ yielding $\eta =4$ bpcu spectral efficiency, in a SC channel.	28
3.7	BER performance of $4 \times 4$ systems with TX separation $=0.1\lambda$ and RX separation $=0.5\lambda$ yielding $\eta =6$ bpcu spectral efficiency, in a Rician fading channel with $K=3$ . . . . .	28
3.8	BER performance of $4 \times 4$ systems with TX separation $=0.1\lambda$ and RX separation $=0.5\lambda$ yielding $\eta =6$ bpcu spectral efficiency, in a Rician fading channel with $K=3$ . . . . .	29
3.9	Histograms of $h_{(mag_{ratio})}$ values computed for transmit/receive antenna separation of $1\lambda$ , $0.5\lambda$ and $0.1\lambda$ . . . . .	32
3.10	Histograms of $h_{(angle_{diff})}$ values computed for transmit/receive antenna separation of $1\lambda$ , $0.5\lambda$ and $0.1\lambda$ . . . . .	33
3.11	Comparison of PDF-CDF between Rician and measured indoor channel with TX separation $=0.1\lambda$ ,RX separation $=0.5\lambda$ . . . . .	33

3.12	Real measurements of $2 \times 2$ MIMO systems with a total distance TX-RX separation of 3 meters TX separation $=0.1\lambda$ and RX separation $=0.5\lambda$ yielding $\eta=4$ bpcu spectral efficiency operating in an indoor environment. . . . .	34
3.13	Performance results of SM $2 \times 2$ and ReSM $2 \times 2$ under SC channel with channel coefficients obtained by USRP B210 at TX-RX separation of 3 meters. TX separation $=0.1\lambda$ , RX separation $=0.5\lambda$ yielding $\eta=4$ bpcu. . . . .	35
4.1	Block diagram for NSTBC-SM system . . . . .	45
4.2	Illustration of Antenna selection (corresponding to first time slot as shown in (4.14). Symbol 0 is mapped to $G_{2+i}$ , $G_{3+2\rho}$ , $G_{3+2i}$ , $G_{4+i}$ for different maps which yield different spectral efficiencies.) . . . . .	49
4.3	Gaussian Map Signal Constellation for $G_{2+i}$ . . . . .	58
4.4	BER performance at 4 bpcu, for NSTBC-SM,with theoretical upper bounds . . . . .	59
4.5	Eisenstein Map Signal Constellation for $G_{3+2\rho}$ . . . . .	60
4.6	BER performance at 4 and 4.5 bpcu, for NSTBC-SM, STBC-SM, and SM in a Rayleigh Channel . . . . .	61
4.7	Gaussian Map Signal Constellation for $G_{3+2i}$ . . . . .	62
4.8	BER performance at 5 and 5.5 bpcu, exception for NSTBC-SM $\eta=5.5$ bpcu, STBC-SM ( $\eta=5$ ), and SM ( $\eta=5$ ) over Rayleigh fading Channel. . . . .	63
4.9	Gaussian Map Signal Constellation for $G_{4+i}$ . . . . .	64
4.10	Analytical and simulated ABER performance of NSTBC-SM. . . . .	65
4.11	ABER performance comparison of various schemes with NSTBC-SM achieving $\eta = 6$ bpcu with $N_t = 4$ , $N_r = 4$ and $N_a=2$ . . . . .	66
4.12	BER performance at 6 bpcu for NSTBC-SM, STBC-SM, VGSM, GNSM, ESM, QSM and SM in a Rician fading Channel with $K=3$ . . . . .	66
4.13	BER performance at 6 bits/s/Hz for NSTBC-SM, STBC-SM, and SM in a quasi-static flat channel Spatially Correlated channel with a inter antenna separation $0.1\lambda$ at the TX and $0.5\lambda$ at the RX. . . . .	68
5.1	Block diagram for DSM system [Yigit and Basar (2016)] . . . . .	72

5.2	BER performance analysis of DSM in Imp-CSI ( $\sigma_e^2 = \frac{1}{SNR} = 0.01$ ) and variants of SM schemes (DSM,ESM,QSM) over a Rayleigh fading environment with $N_t = 4, N_r = 4$ , yielding $\eta = 8$ bpcu. . . . .	82
5.3	BER performance analysis of DSM in Imp-CSI ( $\sigma_e^2 = \frac{1}{SNR} = 0.01$ ) and variants of SM schemes (DSM,ESM,QSM) in P-CSI over a Rician fading environment ( $K=3$ ) with $N_t = 4, N_r = 4$ , yielding $\eta = 8$ bpcu. . . . .	83
5.4	BER performance analysis of DSM in Imp-CSI ( $\sigma_e^2 = \frac{1}{SNR} = 0.01$ ) and variants of SM schemes (DSM,ESM,QSM,SM) in P-CSI over Nakagami-m fading environment ( $m=1$ ) with $N_t = 4, N_r = 4$ , yielding $\eta = 8$ bpcu. . . . .	84
5.5	BER performance analysis of DSM in Imp-CSI ( $\sigma_e^2 = \frac{1}{SNR} = 0.01$ ) ( $m=1,3$ ) and DSM in P-CSI over Nakagami-m fading environment ( $m=1,2,3,4$ ) with $N_t = 4, N_r = 4$ , yielding $\eta = 8$ bpcu. . . . .	85
5.6	BER performance analysis of DSM and variants of SM schemes (ESM,QSM and SM) in P-CSI over Nakagami-m possesses non-uniform fading environment ( $m=4$ ) with $N_t = 4, N_r = 4$ , yielding $\eta = 8$ bpcu. . . . .	86
5.7	BER performance analysis of DSM schemes in Rayleigh, Rician and Nakagami-m fading environments comparison of ML and OB-MMSE with $N_t = 4, N_r = 4$ , yielding $\eta = 8$ bpcu. . . . .	86
5.8	BER performance analysis of DSM in P-CSI over Nakagami-m fading environment ( $m=1,2,3,4$ ) with $N_t = 8, N_r = 8$ , yielding $\eta = 10$ bpcu. . . . .	87
5.9	BER performance analysis of DSM in P-CSI over Nakagami-m fading environment ( $m=2,4$ ) comprising uniform and non-uniform phase distribution with $N_t = 8, N_r = 8$ , yielding $\eta = 10$ bpcu. . . . .	88
6.1	Gaussian constellations used for $4 \times 4$ MIMO system yielding $\eta= 8$ bpcu: The blue crosses represent $\{GF(17) \setminus \{0\}, \cdot\}$ , the red square and brown triangle represents the rotated $\{GF(5) \setminus \{0\}, \cdot\}$ signal constellations . . . . .	97

6.2	Gaussian constellations used for $4 \times 4$ MIMO system yielding $\eta= 9.5$ bpcu: The blue crosses represent $\{GF(17) \setminus \{0\}, \cdot\}$ , the red circle represents Eisenstein $\{GF(7) \setminus \{0\}, \cdot\}$ and magenta plus symbol indicates the subset of $\{GF(17) \setminus \{0\}, \cdot\}$ constellations. . . . .	101
6.3	Gaussian constellations used for $4 \times 4$ MIMO systems yielding $\eta= 10.3$ bpcu: The blue crosses represent $\{GF(17) \setminus \{0\}, \cdot\}$ , the red circle represents Eisenstein $\{GF(7) \setminus \{0\}, \cdot\}$ . . . . .	102
6.4	BER performance analysis of GESM and variants of SM schemes in a $4 \times 4$ MIMO system yielding $\eta = 8$ bpcu. . . . .	108
6.5	BER performance analysis of GESM and variants of SM schemes in a $4 \times 4$ MIMO system yielding $\eta = 10.3$ bpcu. (Exception: GESM brown line, represents secondary constellation extension producing 9.5 bpcu). . . . .	108
6.6	BER performance analysis of GESM and variants of SM schemes in a $8 \times 8$ MIMO systems yielding $\eta = 12.5$ bpcu. (Exception: GESM magenta line, represents secondary constellation extension producing 11.3 bpcu). . . . .	109
6.7	A comparison of achievable spectral efficiencies with variable number of transmit antennas, $N_t$ , and with $M = 16$ QAM and $F_{4+i}$ modulation for various SM systems. . . . .	110
7.1	The primary (red) and secondary (blue) constellations used in the proposed MSM . . . . .	118
7.2	Analytical upper bound on the performance of proposed MSM for spatially correlated (SC) channel with transmit antenna element spacing of $0.5\lambda$ and $0.5\lambda$ at the receiver. . . . .	121
7.3	BER performance of $4 \times 4$ MIMO systems with TX separation $=0.5\lambda$ and RX separation $=0.5\lambda$ yielding $\eta=8$ bpcu spectral efficiency, over a SC channel. . . . .	121
7.4	BER performance of $4 \times 4$ MIMO systems with TX separation $=0.1\lambda$ and RX separation $=0.5\lambda$ yielding $\eta=8$ bpcu spectral efficiency, over a Rayleigh SC channel. . . . .	122

7.5	BER performance of $4 \times 4$ MIMO systems with TX separation $=0.5\lambda$ and RX separation $=0.5\lambda$ yielding $\eta=8$ bpcu spectral efficiency, over a Rician fading SC channel with $K=3$ . . . . .	123
7.6	BER performance of $4 \times 4$ MIMO systems with TX separation $=0.1\lambda$ and RX separation $=0.5\lambda$ yielding $\eta=8,10,12$ bpcu spectral efficiency, over a Rayleigh SC channel. . . . .	124



## List of Tables

3.1	Mapping followed in ReSM for 4 bpcu employing QPSK Constellation	15
3.2	Transmit antenna selection	18
3.3	Active antenna requirement	18
3.4	USRP B210 specifications	30
3.5	Transmit frame structure used for channel estimation	31
3.6	Performance comparison of ReSM with variants of SM, TCSM in SC and Rician fading channels.	36
4.1	Values of $q, \pi, u$ and $v$	44
4.2	Values of $q', \Pi, b$ and $\beta$	45
4.3	Antenna Mapping	50
4.4	Gaussian Map exponent Table $G_{2+i}$ :	58
4.5	Eisenstein Map exponent table of $G_{3+2\rho}$ :	60
4.6	Gaussian Map exponent table of $G_{3+2i}$ :	62
4.7	Gaussian Map exponent table of $G_{4+i}$ :	64
6.1	$q, \Pi, a$ and $b$ values	94
6.2	$q', \Pi, u$ and $\beta$ values	94
6.3	ESM	95
6.4	Squared Minimum Euclidean distance of ESM and GESM	100
6.5	Maximum symbol energy of ESM and GESM	101
6.6	Receiver Complexity	107





# Chapter 1

## Introduction

### 1.1 Motivation for this Research work

In the era of modern wireless communications, the Multiple Input Multiple Output (MIMO) innovation has enabled the development of a large number of services (live video streaming, e-commerce applications, LTE to vehicular communications etc.). These applications require the underlying network to be highly spectrally efficient and the mobile platforms to be computationally capable and energy efficient. The MIMO paradigm has brought significant improvements in reliability and throughput of wireless systems when compared to the earlier Single Input Single Output (SISO) framework. To fulfill the ever increasing demand for higher information throughput, innovations in MIMO such as Spatial Multiplexing (SMX) and its various derivatives have been proposed. Space Time Codes (STC) have been synthesized with the goal of achieving improved reliability at a given throughput [Tarokh et al. (1998), Tarokh et al. (1999), Alamouti (1998)].

The motivation for this work started with the study of a high rate spectrally efficient Spatial Modulation (SM) scheme proposed by Mesleh et al. (2008). This was an important breakthrough in the design of Space Time (ST) techniques, which demonstrated that spectral efficiency along with energy efficiency could be simultaneously achieved by selecting only one antenna at a time out of the available antennas and assigning bits to the selected antenna. Thus, the notion of antenna selection bits and information bits was introduced. This technique allowed the designer to reduce the number of RF chains, improving the energy efficiency. Spectral efficiency was enhanced by commu-

nicating some information through the medium of antenna selection bits which are not physically communicated [Mesleh et al. (2008) Di Renzo et al. (2014)]. This scheme is amalgamated as a part of MIMO wireless communication system to expand the spectral efficiency and reliability. It also nullifies Inter Channel Interference (ICI) due to its inherent way of choosing only one antenna at a time during the process of transmission. Furthermore, ICI and inter antenna synchronization can be eliminated completely by activating a single RF chain at a time [Stavridis et al. (2012), Lee et al. (2005)] .

In Chapter 2 we give a brief description of System Models and Channel Models. Generalized MIMO system model and channel models including Rayleigh, Spatially Correlated (SC) Channel and Rician fading channel models have been discussed in this chapter. The causes of deterioration in SC channel conditions are explained by the use of Kronecker model. Similarly, Rician Fading channel model is described. The Nakagami-m fading channel and its detailed analysis is discussed in chapter 5.

In Chapter 3 we design modulation schemes specific to SC channel conditions and analyze the behavior of proposed modulation schemes under standard channel conditions. From literature we observe that the performance of all existing SM schemes deteriorate under SC fading channel situations. This is because of the inherent construction and single active antenna identification of SM. To combat the effect of SC, Trellis Coded Spatial Modulation (TCSM) was proposed by [Mesleh et al. (2010)]. It is well appreciated that in the case of smart phones and other hand held gadgets, multiple antenna positioning and placement within the small device footprint is always a challenging task. An increase in spectral efficiency by means of using higher order modulation schemes will results in the deterioration of BER performance.

Keeping in mind, the all important requirement of improving the reliability of information transfer, we have explored the idea of Space Time Block Codes (STBC) and their implementation for SM systems. During the period of literature survey, we became interested in the idea of the rank distance codes and their utilization in designing STBCs. [Sripati et al. (2004)]. A variety of Non-orthogonal STBCs can be designed (as shown in Chapter 4) by invoking the transform domain description of cyclic codes. This design and analysis is discussed in Chapter 4.

Chapter 5 outlines the need for achieving higher spectral efficiencies and impact of imperfect channel behavior on the performance of high rate spectrally efficient communication systems. Constructive schemes which yield a twofold increase in data rate compared to standard SM scheme have been devised [Yigit and Basar (2016)]. The Index Modulation (IM) based system can be used in MIMO and large MIMO schemes is known as Double Spatial Modulation (DSM) . The primary benefit of this approach is that it allows the activation of a couple of antennas which results in higher spectral performance. This scheme can allow a additional development in spectral efficiency from 10bps/Hz to 16bps/Hz (without increase in number of transmit antennas) which is a primary requirement in 5G wireless communication environment. Furthermore, an exhaustive study of DSM scheme under Nakagami-m fading environment with Perfect Channel State Information (P-CSI) and Imperfect Channel State Information (Imp-CSI) reveals the fact that the overall ABER performance of DSM scheme in Nakagami-m fading environment is superior to all the other competing schemes available in the literature.

Chapter 6 deals with the concept of two new signal designs for Enhanced Spatial Modulation (ESM) technique from Gaussian and Eisenstein integers known as Gaussian ESM (GESM), which leads to an improved spectral efficiency and performance. A more versatile and realistic structure is obtained by implementing non uniform constellations for a SM-MIMO framework. We have shown that the proposed GESM (both single stream and multi stream) schemes can be applied in general to any  $N_t \times N_r$  MIMO frameworks and it is quantified by the simulations for  $4 \times 4$  and  $8 \times 8$  systems with an analysis pertaining to union bound on ABEP.

Finally, Chapter 7 describes the idea of modified Multistream Spatial Modulation (MSM) specially designed for SC channel conditions. In this scheme, two antennas are made active all the time, mapping for antenna selection is judiciously adopted from primary and secondary constellation points. Secondary constellations are obtained through single geometric interpolation of the primary constellation points. Simulation results show that for a dedicated spectral efficiency and antenna combinations the proposed scheme produces an overall performance improvement as minimum as 4 dB at a ABER

of  $10^{-5}$  over all other conventional Spatial Modulation (SM) systems when evaluated over dense spatially correlated channels.

# Chapter 2

## Background

### 2.1 MIMO wireless communication systems

The persistent need for increasing high data rates in wireless communications has been driven to support a wide range of multimedia applications on mobile platforms. The most effective approach to address the need of higher spectral efficiency is the use of higher modulation schemes. However, higher order modulation schemes have the disadvantage of closer spacing between constellation points which can degrade BER performance. Diversity techniques such as antenna or frequency diversity resolves the issue pertaining to poor channel reliability. System exploiting antenna diversity with multiple transmit and receive antennas is termed as MIMO system. One of the impeccable advantage of MIMO Spatial Multiplexing (SMX) is the ability to provide enhanced spectral efficiency/ high data rates when compared to classical SISO systems. MIMO SMX has the potential to achieve higher data rates by utilizing multiple propagation paths and using them as an additional data pipes to carry information.

An energy efficient technique for MIMO wireless communications was first proposed in the paper [Mesleh et al. (2008)] and termed as Spatial Modulation (SM). In SM, only one transmit antenna (out of all available antennas) gets activated over a symbol interval. The data is divided into two categories, namely antenna selection bits and information bits. The antenna selection bits are used to choose the radiating antenna and the information bits are conveyed using appropriate modulation scheme such as Phase-Shift Keying (PSK) or Quadrature Amplitude Modulation (QAM) [Mesleh et al. (2008)]. In this era of limited spectrum availability, large number of users and

diverse applications, MIMO communication systems have to necessarily possess very high spectral efficiencies. One effective technique to improve spectral efficiency while retaining the single RF chain is to use spatial modulation (SM) scheme.

### 2.1.1 System Models

The basic and the orthodox configuration of wireless communication system is employing a single antenna at transmitter and single antenna at receiver working over a radio channel environment referred as a SISO system. Unlike SISO, MIMO systems employ more than one antenna at transmitter and receiver. In Figure 2.1, MIMO system model with  $N_t$  transmit antennas and  $N_r$  receive antennas is depicted.

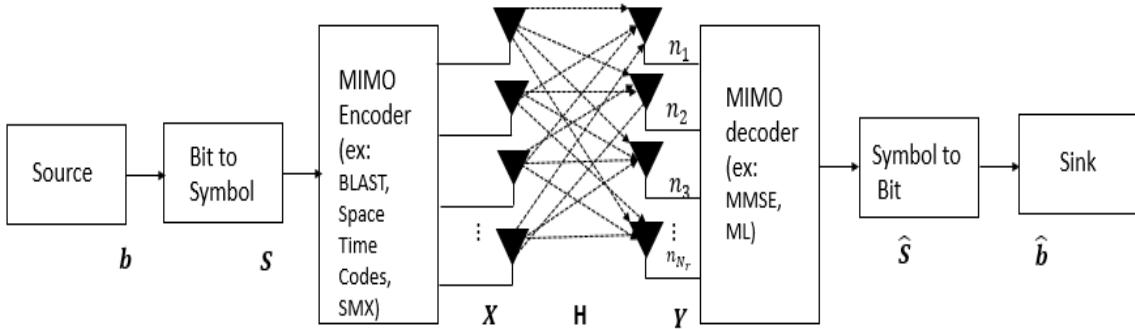


Figure 2.1 MIMO system model with  $N_t$  transmit antennas and  $N_r$  receive antennas [Mesleh (2007)]

In MIMO-SMX, independent streams of information are transmitted through multiple transmit antennas. For such a system with  $N_t$  transmit antennas spectral efficiency is given by  $N_t \times \log_2(M)$ , where  $M$  is the total number of available signal constellation symbols. The received signal can then be written as

$$\mathbf{Y} = \sqrt{\rho} \mathbf{H} \mathbf{X} + \mathbf{n} \quad (2.1)$$

The transmitted symbol vector  $\mathbf{X}$  of length  $N_t \times 1$  is represented as  $\mathbf{X} = [x_1, x_2, x_3, \dots, x_{N_t}]^T$ . Let  $N_r$  denote the number of receive antennas and  $\mathbf{H}$  represents the channel matrix with dimension  $N_r \times N_t$ , where  $\rho$  is the average SNR at each receive antenna,  $\mathbf{Y} = [y_1, y_2, y_3, \dots, y_{N_r}]^T$  denotes the received symbol vector of length  $N_r \times 1$ ,

$\mathbf{n} = [n_1, n_2, n_3, \dots, n_{N_r}]^T$  represents noise vector of length  $N_r \times 1$ . The entries of  $\mathbf{n}$  are sample values of independent and identically distributed (i.i.d) circularly symmetric complex Gaussian random variables with zero mean and unit variance.

### 2.1.2 Channel Models

A number of mathematical models have been proposed in literature to describe the behavior of channel perturbations introduced by the wireless channel operating over different frequencies in varied physical environments. Our primary interest is in channels which are most suitable for outdoor, indoor and real world scenarios. The set of channel models which describe channel behaviour include quasi static Rayleigh fading, Rician fading, Nakagami-m fading and spatially correlated (SC) channels with and without LoS components [Tzeremes and Christodoulou (2002), Panic et al. (2013)].

- **Rayleigh fading channel:** From [Younis (2014)], The Rayleigh distribution is often used to model multi-path fading with dominant Non line of Sight (NLoS) path, where the received signal is visualized as a sum of independent vectors with uniformly distributed phases. Thus, the entries of  $\mathbf{H}$  are modeled as complex, independent and identically distributed (i.i.d.) Gaussian random variables with zero mean and unit variance.
- **Rician fading channel:** From [Younis (2014)], The Rician distribution is used to model the fading signal amplitude in the presence of one strong LoS component and many weaker components. The entries of channel matrix  $\mathbf{H}$  are modeled as

$$\mathbf{H}_c = \sqrt{\frac{K}{1+K}} \bar{\mathbf{H}} + \sqrt{\frac{1}{1+K}} \mathbf{H} \quad (2.2)$$

In the above equation  $K$  is referred as Rician factor (typically  $K$  is chosen as 3 to mimic the behavior of indoor propagation channel model), the average power of the LoS component is given by  $K/(1+K)$ ,  $\bar{\mathbf{H}}$  is an all one matrix,  $1/(1+K)$  is the average power of the random component and  $\mathbf{H}$  is a  $N_r \times N_t$  matrix whose entries are modeled as circularly symmetric complex i.i.d Gaussian random variables with zero mean and unit variance.

- **Spatially Correlated fading channel:** The major parameters for the occurrence of spatial correlation in MIMO wireless communications are the distance of separation between the antenna elements and physical channel environment. The constraint of achieving required spacing between the antenna elements within a single array (either transmit or receive) is observed in modern hand-held devices. This leads to the inevitable demand of designing the nature of antenna array elements, which takes under consideration the effect of spatial correlation amongst the channel. The correlation between signals from any two antenna elements  $(m, n)$  within an array is determined as  $R_{(m,n)}$ . In this work we have used the clustered channel model as given in [Hedayat et al. (2005), Forenza et al. (2004)].

$$R_{(m,n)} = \frac{e^{j(D(m-n)\sin(\theta_0))}}{1 + \frac{\sigma_\theta^2}{2} [(D(m-n)\cos(\theta_0))]^2}; m, n \in \{1, 2, 3, \dots, N_t\} \quad (2.3)$$

Based on the distance of separation between the antenna elements in an array spatial correlation is considered in two ways: (a) If the separation is  $0.1 \lambda$  at the transmitter and  $0.5 \lambda$  at the receiver, the channel is considered to be highly correlated. (b) If the separation is  $0.5 \lambda$  at the transmitter and  $0.5 \lambda$  at the receiver, this situation resembles to moderately correlated channel. In equation (2.3),  $D = (2\pi d_a)/\lambda$  where  $d_a$  is the distance of separation between the antenna elements,  $\lambda$  is the wavelength at which the system works.  $\theta_0$  and  $\sigma_\theta$  are the Angle of Arrival (AoA) and Angular Spread (AS) respectively [Mesleh (2007); Simha et al. (2017)]. Using this equation, the transmit correlation and receive correlation matrices can be expressed as  $\mathbf{R}_{\text{TRAN}}, \mathbf{R}_{\text{REC}}$  and computed as shown in equations (2.5) and (2.6).

The SC channel is generated by using the following equation,

$$\mathbf{H}_c = \mathbf{R}_{\text{REC}}^{1/2} \mathbf{H} \mathbf{R}_{\text{TRAN}}^{1/2} \quad (2.4)$$



$$\mathbf{R}_{\text{TRAN}} = \begin{bmatrix} R_{(1,1)} & R_{(1,2)} & \cdots R_{(1,N_t)} \\ R_{(2,1)} & R_{(2,2)} & \cdots R_{(2,N_t)} \\ \vdots & \ddots & \vdots \\ R_{(N_t,1)} & R_{(N_t,2)} & \cdots R_{(N_t,N_t)} \end{bmatrix} \quad (2.5)$$

The transmit correlation matrix  $\mathbf{R}_{\text{TRAN}}$  contains information about the correlation between different antenna elements of the transmit array and the receive correlation matrix  $\mathbf{R}_{\text{REC}}$  specifies the correlation between various elements of the receive antenna array.

$$\mathbf{R}_{\text{REC}} = \begin{bmatrix} R_{(1,1)} & R_{(1,2)} & \cdots R_{(1,N_r)} \\ R_{(2,1)} & R_{(2,2)} & \cdots R_{(2,N_r)} \\ \vdots & \ddots & \vdots \\ R_{(N_r,1)} & R_{(N_r,2)} & \cdots R_{(N_r,N_r)} \end{bmatrix} \quad (2.6)$$

In order to compute  $\mathbf{R}_{\text{REC}}$ , the mean AoA is replaced by the mean angle of departure (AoD). Throughout our simulations we have considered the values of mean AoA, AS and mean AoD as indicated in [Forenza et al. (2004), Mesleh et al. (2008)].

For convenience of understanding and comparison, remaining system models, channel models and other conventional Spatial Modulation schemes are discussed in the relevant chapters of this thesis.

### 2.1.3 Summary

This chapters discusses the essential descriptions of channel models and system models. Spectrally Efficient and Energy Efficient schemes are designed in the forthcoming chapters which have recourse to the channel models described here in this section for the effective comparison.

- Generalized MIMO system model and channel models including: Rayleigh, Spatially Correlated (SC) Channel and Rician fading channel models have been discussed in this chapter.
- The predominant concern is the reduction in diversity gain for a MIMO system due to the use of SC channels.

In compact hand-held gadgets, installing over four transmit antennas operating within the same frequency band becomes a challenging task. This is primarily attributable to area constraints (considering this practical aspect), in the next chapter we describe the impact of channel correlation and the need for design of a modulation technique which can combat the effect of dense SC channel condition in case of lesser antenna spacing.

## Chapter 3

# Redesigned Spatial Modulation for Spatially Correlated channels

<sup>1</sup> In this chapter, a complete framework for the special case of Spatial Modulation entitled Redesigned Spatial Modulation (ReSM) under spatially correlated channel conditions has been proposed. ReSM scheme permits the use of more than one antenna at a time. Both single antenna as well as double antenna combinations can be excited. The choice of antenna selection depends upon the channel conditions. In ReSM scheme, a dynamic mapping of constellation symbols through antenna selection is adopted based on the channel induced perturbations. When evaluated over spatially correlated channel conditions, for a fixed spectral efficiency and number of transmit antennas, ReSM exhibits performance improvement of a minimum of 2 dB over all the standard SM schemes as well as Trellis Coded Spatial Modulation (TCSM). Additionally, a closed form expression for the upper bound on Pairwise Error Probability (PEP) for ReSM has been derived. This has been used to calculate the upper bound for the Average Bit Error Probability (ABEP) for spatially correlated channels. The results of Monte Carlo simulations are in good agreement with the predictions made by analytical results. The relative gains of all the comparison plots in this work are specified at a ABER of  $10^{-4}$ . To test the reliability in a strong LoS environment, an indoor ReSM scheme has been set up. BER plots comparing the performance of SM and ReSM in an indoor environment have been obtained. It has been shown that ReSM outperforms SM by about 7 dB in indoor environment.

---

<sup>1</sup>Goutham Simha G.D., et al. "Redesigned Spatial Modulation for Spatially Correlated Fading Channels", Springer: Wireless personal communications, Volume 97 Issue 4, pp 5003-5030 (2017)

### 3.1 Introduction

Wireless communication systems should have the ability to operate with severe constraints incumbent on two major limited resources, power and bandwidth. A variety of MIMO techniques were proposed in the early part of the twenty first century to boost spectral efficiency and/or reliability of communication. However, a disadvantage of these schemes is that they do not focus on all important issue of energy efficiency. In the year 2008, Mesleh et.al proposed a new scheme designated as Spatial Modulation (SM) for MIMO wireless communication systems [Mesleh et al. (2008)]. SM-MIMO technique was introduced to accomplish a trade-off between spectral efficiency and energy efficiency in MIMO wireless communication systems [Mesleh et al. (2008), Di Renzo et al. (2014)]. Various researchers have analyzed and investigated the performance of SM in all possible environments. After quantifying the benefits of SM, researchers have proposed variants of SM which aim to attain improved spectral efficiency without sacrificing energy efficiency. These techniques if deployed, can serve as replacements/alternatives to SMX in many applications. One of the techniques that has been employed to improve the performance of SM schemes is to activate more than one antennas at any given instant of time. A number of such schemes have been proposed in literature by Abdelhamid Younis et.al such as Generalized SM (GNSM) and Variable Generalized SM (VGSM) [Younis (2014)]. A more general approach termed as Improved Spatial Modulation (ISM) or Extended Spatial Modulation (EXSM) was proposed in 2012 by [Luna-Rivera and Gonzalez-Perez (2012)]. In 2014 Chien-Chun Cheng et.al presented another spectrally efficient method called Enhanced Spatial Modulation (ESM) for MIMO systems [Cheng et al. (2014), Cheng et al. (2015)]. In 2014, Mesleh gave an enhanced version of his original technique (SM) which could provide improved spectral efficiency and this was named as Quadrature Spatial Modulation (QSM) [Mesleh et al. (2015), Afana et al. (2015)]. It is generally observed that the performance of all SM schemes deteriorate under Spatially Correlated (SC) fading channel conditions. To combat the effect of SC, Trellis Coded Spatial Modulation (TCSM) was introduced by Mesleh et al. in [Mesleh et al. (2010), Mesleh et al. (2009)]. In TCSM,

the effect of correlation on the performance of SM can be minimized by segregating antennas into subsets. Antennas with large spatial separation are grouped in a subset while antennas with lesser spatial separation are placed in different subsets. A minimum of two transmit antennas are required to form the subsets. For a system with spectral efficiency of 4 bits per channel use (bpcu), it has been shown that TCSM  $4 \times 4$ , with hard decision Viterbi decoding and 8 QAM provides an improvement of  $\sim 2$ dB over uncoded SM  $4 \times 4$  system employing QPSK modulation in channels with appreciable correlation [Mesleh et al. (2010)]. Increasing the spectral efficiency in TCSM, requires an increase in the rate of the convolution code or the order of the modulation scheme.

Improved SM (ISM) [Luna-Rivera and Gonzalez-Perez (2012)] is another SM technique that is designed to employ variable number of transmit antennas. It provides an increase in spectral efficiency with a performance gain of  $\sim 2$ dB as compared to conventional SM when employed over uncorrelated channel environments. However, in the presence of channel correlation, a performance deterioration of  $\sim 2$ dB over SM is also observed. Inspired by the principles of TCSM and ISM, we have proposed a new scheme, named Redesigned Spatial Modulation (ReSM), for spatially correlated fading environments. This scheme has been designed to employ the concept of simultaneous transmission of different symbols via multiple collocated antennas. It also maximizes the Euclidean distance between active spatial bits which in turn serve to reduce the ambiguities in their recovery at the receiver end. The number of transmit antennas in ReSM must be a power of 2. The major advantage of ReSM compared with TCSM is that ReSM does not require any additional channel encoder/decoder (error correcting code). ReSM schemes combine well with the high end utilities and services provided by 4G systems. In SC fading environment, coded scheme (TCSM) perform better by about 3 dB as compared with uncoded SM schemes [Mesleh et al. (2009)]. We show that uncoded ReSM scheme can significantly outperform TCSM over SC channels (SNR gain over TCSM is  $\sim 3$  dB). In this work we have designed ReSM to ensure reliable transmission for spectral efficiency of 6 bpcu.

The specific contributions of this chapter are:

- Design and performance evaluation of ReSM, determination of suitability of ReSM in SC channel environments, derivation of a closed form expression for the PEP and an extension of this result to obtain an upper bound on the ABEP.
- Real time indoor measurements leading to determination of channel coefficients under close antenna spacing.

### 3.2 ReSM construction and Design

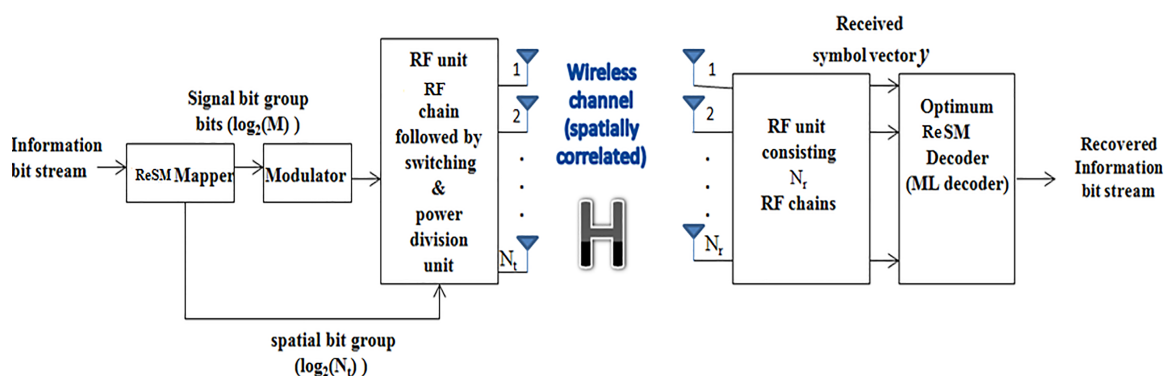


Figure 3.1 Block diagram of the proposed Redesigned Spatial Modulation system

The block schematic of the Redesigned Spatial Modulation (ReSM) system is shown in Figure 3.1. This scheme has been designed to operate efficiently in SC environments. The performance of the scheme is identical to that of SM when employed under conditions of zero channel correlation. The underlying idea of ReSM with QPSK modulation scheme is illustrated in Table. 3.1 and explained for 4 bpcu. The spectral efficiency can be enhanced to 6 bpcu using higher order modulation schemes. (Simulations and analyses are for 6 bpcu). Here we have considered the distance between two elements of transmitter array to be TX separation, similarly RX separation is the distance between two elements of receiver array [Babich and Lombardi (2000); Hoeher (1992)]. It should be noted that TX1, TX2 are tightly correlated, TX1, TX3 are less correlated and TX1, TX4 are least correlated due to their mutual spacing, this is true for other groups as well.

Table 3.1 Mapping followed in ReSM for 4 bpcu employing QPSK Constellation

Possible groups of $\log_2 M \cdot N_t$ (4 bpcu)	<b>TX1</b>	<b>TX2</b>	<b>TX3</b>	<b>TX4</b>
0000	$x1$			
0001	$x2$			
0010	$x3$			
0011	$x4$			
0100				$x1$
0101				$x2$
0110				$x3$
0111				$x4$
1000	$x1/\sqrt{2}$	$x2/\sqrt{2}$		
1001	$x2/\sqrt{2}$	$x3/\sqrt{2}$		
1010	$x3/\sqrt{2}$	$x4/\sqrt{2}$		
1011	$x4/\sqrt{2}$	$x1/\sqrt{2}$		
1100			$x1/\sqrt{2}$	$x2/\sqrt{2}$
1101			$x2/\sqrt{2}$	$x3/\sqrt{2}$
1110			$x3/\sqrt{2}$	$x4/\sqrt{2}$
1111			$x4/\sqrt{2}$	$x1/\sqrt{2}$

The mapping of signal constellation points to an antenna or antennas is solely based on the channel correlation values. Hence the given table is not static, instead it can be dynamically reassigned based on the channel conditions to improve the performance with an extra processing latency and feedback path. The assignment of different QPSK symbols  $x_1, x_2, x_3, x_4$  to various possible four bit sequences is specified. We see that corresponding to the sequences 0000, 0001, 0010, 0011, four distinct QPSK symbols are transmitted respectively from the 1st transmit antenna. The sequences 0100, 0101, 0110 and 0111 are communicated by transmitting four distinct QPSK symbols from transmit antenna number 4. Spatial separation between TX1 and TX4 is maximum and hence transmit channel 1 and transmit channel 4 are least correlated. This assignment of symbols to antennas is to facilitate easy identification of transmitting antenna at the receiver. Table. 3.1, reveals that sequences 1000, 1001, 1010, and 1011 are communicated by transmitting the adjacent QPSK symbols from antennas TX1 and TX2. Finally

the sequences 1100, 1101, 1110 and 1111 are communicated by transmitting the adjacent QPSK symbols from antennas TX3 and TX4. This assignment is designed to yield maximum Signal to Noise Ratio (SNR) even when the signals received at the antennas are correlated due to small antenna spacing. The output is represented in the form of a vector as given below

$$\mathbf{Y} = \sqrt{\beta\mathcal{O}} \mathbf{H}_c \mathbf{X} + \mathbf{n} \quad (3.1)$$

where  $\mathbf{Y} = [y_0, y_1, y_2, \dots, y_{N_r}]^T$  indicates the received symbol vector of length  $N_r \times 1$  further,  $x \in \mathbf{X}$  denotes a transmitted symbol vector of length  $N_t \times 1$ ,  $\mathbf{X}$  is the set of all possible transmit vectors for a given  $N_t$  and modulation order  $M$ .  $\mathbf{H}_c$  is a correlated channel matrix of dimension  $N_r \times N_t$ . The individual elements  $h_{ij} \in \mathbf{H}_c$  denote the channel gain from  $j^{th}$  transmit antenna to  $i^{th}$  receive antenna.  $\beta\mathcal{O}$  represents the average SNR at each receive antenna.  $\mathbf{n} = [n_0, n_1, n_2, \dots, n_{N_r}]^T$  denotes the noise vector of length  $N_r \times 1$ . The complex entries of  $\mathbf{n}$  are assumed to be circularly symmetric, independent and identically Gaussian distributed (i.i.d) with zero-mean and unit-variance. This distribution is represented by  $C \mathcal{N} (0, \sigma^2)$ . However, conventional SM schemes such as GNSM, VGSM, ISM chooses antenna sets in the pattern given by

$$\eta = \begin{pmatrix} N_t \\ 1 \end{pmatrix} + \begin{pmatrix} N_t \\ 2 \end{pmatrix} + \dots + \begin{pmatrix} N_t \\ N_t \end{pmatrix} \quad (3.2)$$

above three SM schemes does not impose any criteria for selecting the subsets. When spacing becomes dense i.e. the spacing between the antenna elements in transmit array is very small (correlated environment), gains of the individual channels obtained from adjacently placed transmit antennas are likely to be approximately equal as shown below:

$$h_{rp} \sim h_{r+1p}; \quad \forall r \in \{1, 2, \dots, N_r\}, p \in \{1, 2, \dots, N_t\} \quad (3.3)$$

where,  $h_{rp}$  represents channel gain from  $p^{th}$  transmit antenna to  $r^{th}$  receive antenna. As a consequence, there exists difficulty in determining the exact location of the transmit antenna that has radiated a given symbol at the receiving end. This leads to deterioration in the performance. In order to overcome the performance deterioration we have come up with a new strategy of antenna selection in ReSM.



### 3.2.1 Methodology of antenna selection algorithm in ReSM

The ReSM scheme has been designed to minimize possible ambiguities in antenna selection. This scheme achieves a spectral efficiency of  $(\log_2 M + \log_2 N_t)$  bpcu. Unlike other variants of SM, every spatial bit group in ReSM corresponds to a unique transmit antenna subset that comprises of 1 or 2 active transmit antennas. Whenever two transmit antennas are active, the transmitted symbol amplitude is scaled by  $1/\sqrt{2}$ . This ensures that the average power per transmitted symbol is same. Every spatial bit group in ReSM is identified by a unique transmit antenna subset and modulation symbol or symbols. We see that  $N_t$  distinct transmit antenna subsets need to be chosen amongst

the available  $\binom{N_t}{1} + \binom{N_t}{2}$  single and two element transmit antenna subsets.

In the following paragraph, we have described the criteria used for choosing the transmit antenna subsets. Amongst  $\binom{N_t}{1}$  single element subsets available,  $\frac{N_t}{2}$  subsets are chosen such that the selected single transmit antenna is sufficiently apart from

each other. The remaining  $\frac{N_t}{2}$  subsets are selected from  $\binom{N_t}{2}$  two element subsets.

For  $N_t = 4$ , active antenna assignment is illustrated in Table. 3.1. Antennas 1 and 4 (which has maximum spatial separation) are chosen when a single transmit antenna is selected for radiation. Antennas 2 and 3 will not be preferred for transmission to avoid ambiguity at the receiver due to correlation as explained above. The received symbol  $y_r$  for the single transmit antenna is given below

$$y_r = x_q h_i + n_r, \quad \text{for } i \in \{1, 2, \dots, N_t\}, q \in \{1, 2, \dots, M\} \quad (3.4)$$

Since the transmitting antenna can be identified distinctly by its AoA determination, there is no ambiguity about the transmitting antenna in this case. When two transmit antennas are active, the subsets chosen are either  $\{(1, 2) \text{ or } (3, 4)\}$ . The received symbols in these cases are respectively specified as follows,

$$y_r = \frac{x_q}{\sqrt{2}} h_{r_1} + \frac{x_{q+1}}{\sqrt{2}} h_{r_2} + n_r = \frac{1}{\sqrt{2}} (h_{r_1} x_q + h_{r_2} x_{q+1}) + n_r, \text{ where } h_{r_1} = h_{r_2} \quad (3.5)$$

$h_{r_1} = h_{r_2}$  due to the assumption of close antenna spacing. Therefore, equation (3.6) can be re-written as

$$y_r = \frac{h_{r_1}}{\sqrt{2}}(x_q + x_{q+1}) + n_r, \quad (3.6)$$

Similarly,

$$y_r = \frac{x_q}{\sqrt{2}}h_{r_3} + \frac{x_{q+1}}{\sqrt{2}}h_{r_4} + n_r = \frac{1}{\sqrt{2}}(h_{r_3}x_1 + h_{r_4}x_2) + n_r, \text{ where } h_{r_3} = h_{r_4} \quad (3.7)$$

Therefore, equation(3.7) can be written as

$$y_r = \frac{h_{r_3}}{\sqrt{2}}(x_q + x_{q+1}) + n_r \quad (3.8)$$

$h_{r_3} = h_{r_4}$  due to the assumption of close antenna spacing.

This scheme can be readily extended to higher modulation orders, antenna combinations and antenna requirement for all the modulation schemes as stated below in Tables 3.2 and Table 3.3.

Table 3.2 Transmit antenna selection

Number of transmit antennas (" $N_t$ ")available	<b>2</b>	<b>4</b>	<b>8</b>
Number of bits mapped to spatial domain (" $\log_2 N_t$ ")	<b>1</b>	<b>2</b>	<b>3</b>
Enumeration of transmit antenna subsets chosen as per proposed ReSM scheme	<b>{1}, {1,2}</b>	<b>{1},{4}, {1,2},{3,4}</b>	<b>{1},{3},{5},{7}, {1,2},{3,4},{5,6},{7,8}</b>

Table 3.3 Active antenna requirement

	SM	GNSM	VGSM	ISM/EXSM	ESM	QSM	<b>ReSM</b>
Min	1	$N_t$	2	1	1	1	<b>1</b>
Max	1	$N_t$	$N_t$	$N_t$	2	2	<b>2</b>

### 3.2.2 Optimal Maximum Likelihood detection criterion:

Optimal Maximum Likelihood (ML) detection strategy for conventional SM as described in [Jeganathan et al. (2008)] has been adopted for demodulation of SM and

all its variants. The ML estimates are provided by

$$\hat{\mathbf{X}}_{ML} = [\hat{j}_{ML}, \hat{q}_{ML}] = \arg \min_{j,q} \|Y - H_c X\|^2 \quad (3.9)$$

$$\hat{\mathbf{X}}_{ML} = [\hat{j}_{ML}, \hat{q}_{ML}] = \arg \min_{j,q} \sqrt{\delta\mathcal{P}} \|g_{jq}\|^2 - 2\text{Re}\{\mathbf{Y}^H g_{jq}\} \quad (3.10)$$

where,  $g_{jq} = h_j x_q$ ,  $1 \leq j \leq N_t$ ,  $1 \leq q \leq M$ ,  $M$  is the modulation order,  $\mathbf{Y}^H$  is the Hermitian of  $\mathbf{Y}$ .  $\hat{j}_{ML}$ ,  $\hat{q}_{ML}$  are estimates of the estimated active transmit antenna index and the radiated spatial signal constellation symbol respectively.  $\hat{j}_{ML}$  is an integer while  $\hat{q}_{ML}$  is an estimated constellation point. The performance evaluation of the system is quantified using analytical upper bound and Monte Carlo simulations. ML decoder provides a significant enhancement in Bit Error Rate (BER) performance over sub-optimal MRRC detection method as showed in [Jeganathan et al. (2008)].

### 3.3 Analytical Treatment for ReSM

To verify the accuracy of Monte Carlo simulations performed for the proposed ReSM and acquire a proper understanding into its characteristics under SC channels and measured indoor channel, bounds on the PEP are considered in this section. It is assumed that Perfect Channel State Information (P-CSI) is available at the receiver and optimum ML decoding method is used. Following [Younis (2014)], the Average Pairwise Error Probability (APEP) can be found using the union bound [Hedayat et al. (2005), Proakis (1998), Van Zelst and Hammerschmidt (2002)] and ABER for the proposed ReSM system can be approximated by

$$ABER_{ReSM} \leq \frac{1}{2\eta} \sum_{n_t, s_t} \sum_{n, s} \frac{N(x_{n_t, s_t}, x_{n, s})}{\eta} E_H \{PEP\} \quad (3.11)$$

In this equation,  $n_t$  is the number of active transmit antennas,  $s_t$  is the transmitted symbol,  $\eta$  is the spectral efficiency,  $N(x_{n_t, s_t}, x_{n, s})$  is the total number of bits in error  $x_{n_t, s_t}, x_{n, s}$ ,  $E_H \{\cdot\}$  is the expectation of the PEP across the channel  $\mathbf{H}$ . The PEP is given by

$$PEP(\mathbf{X} \rightarrow \hat{\mathbf{X}}) = P_r(\|\mathbf{y} - \mathbf{H}_c x_{n_t, s_t}\|^2 > \|\mathbf{y} - \mathbf{H}_c x_{n_t, s}\|^2 | \mathbf{H}) \quad (3.12)$$

$$= Q\left(\sqrt{\frac{\|\mathbf{H}_c \mathfrak{z}\|^2}{2\sigma_n^2}}\right) \quad (3.13)$$

here,  $\mathfrak{z} = x_{n_t, s_t} - x_{n_t, s}$ . By using Craig's formula for the Gaussian  $Q(\cdot)$  function

$$Q(x) = \frac{1}{\pi} \int_0^{\frac{\pi}{2}} \exp\left(\frac{-x^2}{2\sin^2\theta}\right) d\theta \quad (3.14)$$

$$= \frac{1}{\pi} \int_0^{\frac{\pi}{2}} \exp\left(\frac{-\varphi \|\mathbf{H}_c \mathfrak{z}\|_F^2}{2\sin^2\theta}\right) d\theta \quad (3.15)$$

where,  $\varphi = 1/2\sigma_n^2$ . Taking the expectation and using the MGF based approach presented in [Simon and Alouini (2005)] we can write the above equation as

$$E_H\{PEP\} = \frac{1}{\pi} \int_0^{\frac{\pi}{2}} \Phi\left(-\frac{1}{4\sigma_n^2 \sin^2\theta}\right) d\theta \quad (3.16)$$

$\Phi(\cdot)$  is the Moment Generating Function (MGF) of the random variable  $\|\mathbf{H}_c \mathfrak{z}\|^2$ .

$$\begin{aligned} \|\mathbf{H}_c \mathfrak{z}\|_F^2 &= \text{tr}(\mathbf{H}_c \mathfrak{z} \mathfrak{z}^H \mathbf{H}_c^H) \\ &= \text{vec}(\mathbf{H}_c^H)^H (I_{N_r} \otimes \mathfrak{z} \mathfrak{z}^H) \text{vec}(\mathbf{H}_c^H) \\ &= \text{vec}(\mathbf{H}^H)^H R_s^{\frac{H}{2}} (I_{N_r} \otimes \mathfrak{z} \mathfrak{z}^H) \text{vec}(\mathbf{H}^H) R_s^{\frac{1}{2}} \end{aligned} \quad (3.17)$$

where  $\text{tr}(\cdot)$  is the trace function.  $I_n$  is an  $n \times n$  identity matrix.  $R_s = R_{REC} \otimes R_{TRAN}$  is the covariance matrix for  $\text{vec}(\mathbf{H}^H)$ . We wish to evaluate MGF of the above random variable which has a positive semidefinite quadratic form comprising of Gaussian vectors  $\text{vec}(\mathbf{H}^H)$ .

From [Younis (2014)] it is clear that any i.i.d. Gaussian random variable with mean  $\mathbf{v}$  and Hermitian matrix  $\mathfrak{h}$ . The MGF then can be written as

$$\Phi(s) = \frac{\exp\left(s \mathbf{v}^H \mathfrak{h} (I - s \mathcal{L}_v \mathfrak{h})^{-1} \mathbf{H}\right)}{|I - s \mathcal{L}_v \mathfrak{h}|} \quad (3.18)$$

$\mathcal{L}_H$  is the covariance matrix of  $\mathbf{H}$ .

$$\Phi(s) = \frac{\exp\left(s \times \text{vec}(\mathbf{H}^H)^H \hat{\Gamma} (I_{N_r N_t} - s \mathcal{L}_{\mathcal{H}} \hat{\Gamma})^{-1} \text{vec}(\mathbf{H}^H)\right)}{|I - s \mathcal{L}_{\mathcal{H}} \hat{\Gamma}|} \quad (3.19)$$

$I_n$  is an  $n \times n$  identity matrix,  $\text{vec}(\mathbf{H})$  is the column of matrix stacked into a column

vector.  $\hat{\Gamma} = R_{REC} \otimes (\mathfrak{Z}\mathfrak{Z}^H R_{TRAN})$ ,  $\mathcal{L}_H$  is the covariance matrix,  $\mathbf{H}$  is the mean matrix,  $\otimes$  is the Kronecker product and  $(\cdot)^H$  is the Hermitian.

Making use of the Chernoff bound, PEP then can be written as,

$$PEP(\mathbf{X} \rightarrow \hat{\mathbf{X}}) \leq \frac{1}{2\pi} \frac{\exp\left(-\frac{1}{4\sigma_n^2} \text{vec}(\check{\mathbf{H}}^H)^H \hat{\Gamma} \left(I_{N_r N_t} + \frac{1}{4\sigma_n^2} \mathcal{L}_H \hat{\Gamma}\right)^{-1} \text{vec}(\check{\mathbf{H}}^H)\right)}{\left|I_{N_r N_t} + \frac{1}{4\sigma_n^2} \mathcal{L}_H \hat{\Gamma}\right|} \quad (3.20)$$

$(\cdot)^H$  is the Hermitian and  $I_n$  is an  $n \times n$  identity matrix.

Finally the upper bound is given by

$$ABER_{ReSM} \leq \frac{1}{2\eta} \sum_{n_t, s_t} \sum_{n, s} \frac{N(x_{n_t, s_t}, x_{n, s})}{\eta} \times \frac{1}{2\pi} \frac{\exp\left(-\frac{1}{4\sigma_n^2} \text{vec}(\check{\mathbf{H}}^H)^H \hat{\Gamma} \left(I_{N_r N_t} + \frac{1}{4\sigma_n^2} \mathcal{L}_H \hat{\Gamma}\right)^{-1} \text{vec}(\check{\mathbf{H}}^H)\right)}{\left|I_{N_r N_t} + \frac{1}{4\sigma_n^2} \mathcal{L}_H \hat{\Gamma}\right|} \quad (3.21)$$

The channel matrix  $\mathbf{H}$  is realized using the same procedure described in [Van Zelst and Hammerschmidt (2002), Mesleh (2007), Paulraj and Papadias (1997)]. This allows the behavior of the channel to be identical to that of the standard 3GPP model for SC fading channels. The mean matrix and the covariance matrix are entirely dependent on the type of the channel used and the channel matrix for different fading scenarios. It is given as follows:

Equation (3.20) is an upper bound for both Rayleigh fading as well as Rician fading as indicated in [Younis (2014)]. The mean matrix  $\check{\mathbf{H}} = 0_{N_r \times N_t}$ , the covariance matrix  $\mathcal{L}_H = I_{N_r \cdot N_t}$  for Rayleigh fading channel.

For Rician fading mean matrix is defined as  $\check{\mathbf{H}} = \sqrt{\frac{K}{1+K}} \times 1_{N_r \times N_t}$  and covariance matrix is given as  $\mathcal{L}_H = \sqrt{\frac{1}{1+K}} \times I_{N_r \cdot N_t}$ .  $K$  represents the Rician factor.  $K = 3$  (5 dB).

### 3.4 Receiver Computational Complexity Comparison

In this section, the receiver complexity of ReSM-ML is compared with all other conventional SM schemes for the same spectral efficiency. Following [Younis (2014)] the computational complexity of SM-ML is given as,

$$C_{SM-ML} = 8N_r 2_{SM}^\eta \quad (3.22)$$

where the ML detector searches through the whole search space. The computational complexity of GNSM-ML and VGSM-ML are identical [Younis (2014)]. The result is reproduced here for convenience and comparison.

$$C_{GNSM-ML} = 6N_r 2^{\eta}_{GNSM}, \quad C_{VGSM-ML} = 6N_r 2^{\eta} \quad (3.23)$$

thus we see that  $C_{GNSM-ML} = C_{VGSM-ML}$ .

In the following paragraph, we have computed the computational complexity of ISM/EXSM systems. Let us consider an ISM system with  $N_t = 4, N_r = 4, \eta = 6$  bpcu. Since these systems are characterized by  $\eta=6$  bpcu, the total number of available antenna combinations are 64. There are  $\binom{4}{1} \times 4$  possible single antenna combinations

and  $\binom{4}{2} \times 2 \times 4$  two antenna combinations. Different symbols can be transmitted from multiple activated antennas. When only one antenna is active, the transmit antenna can transmit one out of the four possible symbols based on the input bit pattern hence  $N_t \times M$  possible combinations exist. The remaining combinations numbering  $2^{\eta} - 2^{\log_2(N_t \times M)}$  are accomplished through two active antenna arrangements. For single active antenna combination, the complexity of the system is given by

$$C_{ISM-ML(1)} = 8N_r 2^{\log_2(N_t \times M)}_{ISM} \quad (3.24)$$

$$C_{ISM-ML(2)} = 12N_r \left( 2^{\eta} - 2^{\log_2(N_t \times M)} \right) \quad (3.25)$$

The maximum number of computational steps required per transmitted symbol is

$$C_{ISM-ML(2)} = 12N_r \left( 2^{\eta} - 2^{\log_2(N_t \times M)} \right) \quad (3.26)$$

Further, for QSM systems the complexity of QSM-ML scheme as given in [Mesleh

et al. (2015)] is quantified by

$$C_{QSM-ML} = 8N_r 2^{\eta}_{QSM} \quad (3.27)$$

### 3.4.1 Computational Complexity of the Proposed ReSM

We will now determine the receiver computational complexity of the proposed ReSM scheme. Consider the above example for  $N_t = 4, N_r = 4, \eta = 6$  bpcu and choosing  $M=16$  QAM. Let us determine the number of computations required to estimate  $\|\mathbf{Y} - \mathbf{H}\hat{\mathbf{X}}\|_F^2$  where,  $\mathbf{H}$  is the  $N_r \times N_t$  complex channel matrix,  $\hat{\mathbf{X}}$  is the  $N_t \times 1$  complex transmitted matrix,  $\mathbf{Y} - \mathbf{H}\hat{\mathbf{X}}$  is the  $N_r \times 1$  complex received matrix, multiplication of  $\mathbf{H}$  by  $(\hat{\mathbf{X}})$  requires  $N_t$  complex multiplications. Each complex multiplication in turn requires four real multiplications. Therefore each row give rise to  $4 \cdot N_t$  real multiplications. Since  $\mathbf{H}$  has  $N_r$  rows, total number of real multiplications required to evaluate  $\mathbf{H}\hat{\mathbf{X}}$  is given by  $4 \cdot N_t \cdot N_r$ .

$$|\mathbf{Y} - \mathbf{H}\hat{\mathbf{X}}|^2 = (\mathbf{Y} - \mathbf{H}\hat{\mathbf{X}})^H (\mathbf{Y} - \mathbf{H}\hat{\mathbf{X}}) \quad (3.28)$$

Here total number of multiplications (real) involved in computing  $|\mathbf{Y} - \mathbf{H}\hat{\mathbf{X}}|^2$  is equal to  $4 \cdot (N_t + 1) \cdot N_r$ .

The above analysis is for one transmit vector  $\hat{\mathbf{X}}$  there exists  $2^\eta$  possible combinations of vector  $\hat{\mathbf{X}}$ . Therefore total computational complexity is  $4 \cdot (N_t + 1) \cdot N_r \cdot 2^\eta$ .

First  $\binom{16}{1}$  symbols are transmitted through the transmitting antenna 1 and the same symbols are transmitted through transmitting antenna 4, constituting to the total of  $\binom{16}{1} \times 2$  combinations. Therefore the computational complexity of ReSM-ML detector for single active antenna combination is given by  $8N_r 2^{\eta-1}$ . For two active transmit

antennas, transmitting antenna 1 and 2 combined has  $\binom{16}{1}$  combinations and the next

$\binom{16}{1}$  combinations are pervaded by antennas 3 and 4. Hence the computational complexity when transmitting two different symbols from two antennas can then be written as  $12N_r2^{\eta-1}$ . Apparently all combinations of single active and two active antenna constitutes to total of 64 groupings. The maximum number of computational steps required per transmitted symbol is shown in (3.27) and plotted in Figure 3.2.

$$C_{ReSM} = 12N_r2^{\eta-1} \quad (3.29)$$

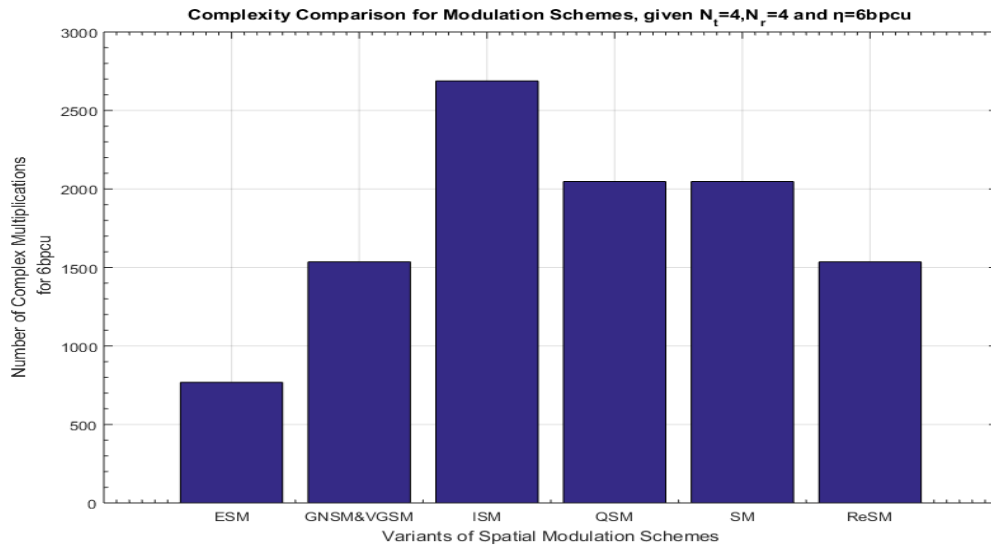


Figure 3.2 Block diagram of the proposed Redesigned Spatial Modulation system

### 3.5 Simulation Results

This subsection is devoted to a description of the performance of ReSM and the comparison of these results with conventional SM under various channel conditions. Monte Carlo simulations have been carried out with a minimum of  $10^6$  channel realizations. The ABER values are plotted against SNR. A Rician  $K$  factor equal to 3 has been



assumed in all simulations pertaining to the Rician fading environment. As per 3GPP standards, channel correlation is observed when antenna separation is  $0.1 \lambda$  at the transmitter and  $0.5 \lambda$  at the receiver. These results specify the performance obtained under 4G/LTE channel scenario as per 3GPP standards [Lee et al. (2016)]. Further, we witness denser correlation environment when antenna separation at the receiver reduces to  $0.1 \lambda$ . The performance of all variants of SM (SM, GNSM, VGSM, ISM/EXSM, ESM, QSM and TCSM) have been compared against ReSM under conditions of equal spectral efficiency (4 bpcu and 6 bpcu). Later, to determine typical channel coefficients for indoor communication, a  $2 \times 2$  MIMO system was set up in the laboratory using USRP B210. The channel coefficients obtained by these measurements correspond to Rician fading in the presence of spatial correlation brought about by close antenna spacing. Our study indicates that ReSM scheme provides an improvement of approximately 7 dB over conventional SM system in indoor environment with antenna spacing of  $0.1 \lambda$  at the transmitter and  $0.5 \lambda$  at the receiver [Hottinen et al. (2004), Group et al.].

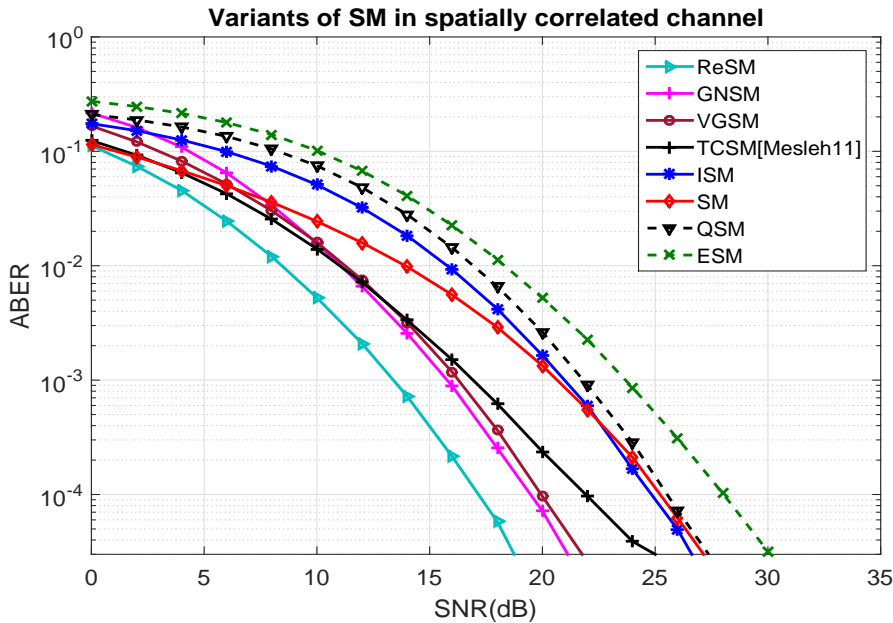


Figure 3.3 BER performance of  $4 \times 4$  systems with TX separation  $=0.1 \lambda$  and RX separation  $=0.5 \lambda$  yielding  $\eta = 6$  bpcu spectral efficiency, in a SC channel.

In Figure 3.3, it is seen that ReSM outperforms all the other variants of SM. The environment under consideration is the typical mobile scenario with 3GPP specification

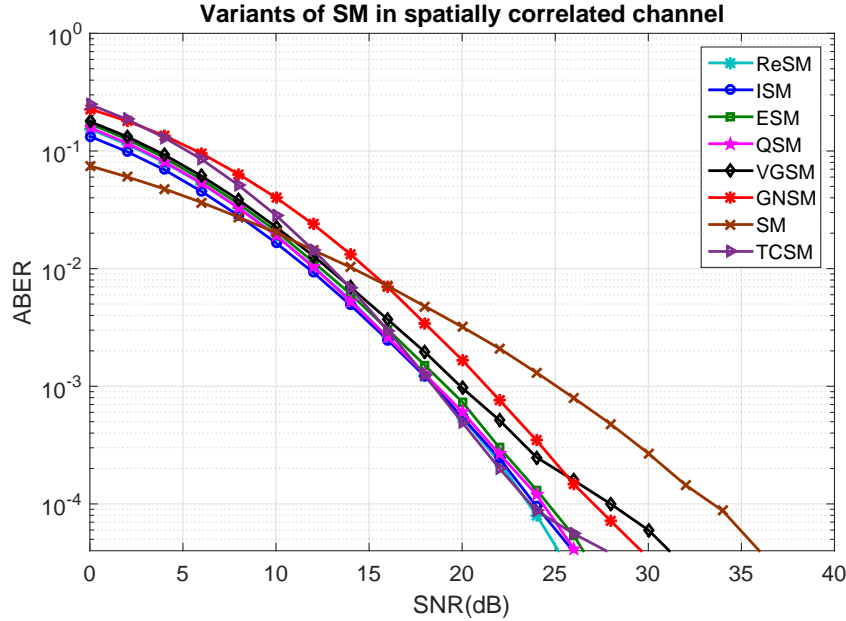


Figure 3.4 BER performance of  $4 \times 4$  systems with TX separation  $=0.1\lambda$  and RX separation  $=0.3\lambda$  yielding  $\eta = 6$  bpcu spectral efficiency, in a SC channel.

designed for 4G/LTE [Lee et al. (2016)]. Here the transmitter separation (TX separation) is  $0.1\lambda$  and receiver separation (RX separation) is  $0.5\lambda$ . These comparisons have been carried out at ABER of  $10^{-4}$ . ReSM offers a performance improvement over GNSM, VGSM schemes by  $\sim 3$  dB, TCSM by  $\sim 5$  dB, and almost 7 dB over ISM, SM, QSM systems and an improvement of about  $\sim 10$  dB in comparison with ESM systems.

A smaller change in the antenna separation at the receiver (RX separation  $=0.3\lambda$ ) [Goldsmith (2005), Bossert (1999), Kim et al. (2004)] causes change in performance of all the competing schemes due to higher spatial correlation.

This is depicted in Figure 3.4. We observe that even under these changed conditions, the performance of ReSM is superior to all the other schemes. ReSM offers a performance improvement over ISM, QSM, TCSM schemes by  $\sim 0.5$  dB in higher SNR regime,  $\sim 3.4$  dB over GNSM, VGSM and an improvement of  $\sim 10$  dB over SM system.

In Figure 3.5, it is seen that a further reduction in the receiver antenna spacing (RX separation  $=0.1\lambda$ ) leads to dense spatial correlation resulting a significant change in performance of all the SM schemes. The comparison in Figure 3.5 shows that ReSM

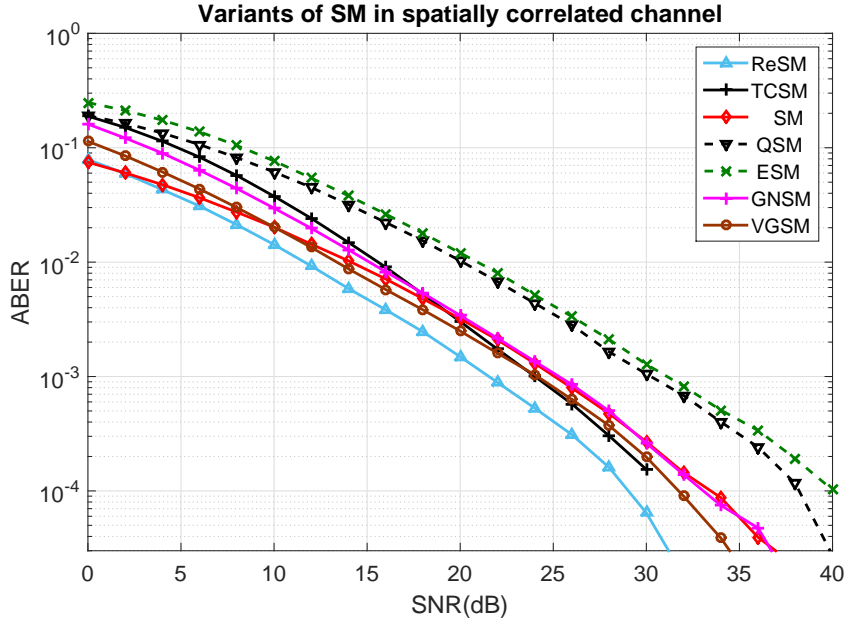


Figure 3.5 BER performance of  $4 \times 4$  systems with TX separation  $=0.1\lambda$  and RX separation  $=0.1\lambda$  yielding  $\eta = 6$  bpcu spectral efficiency, in a SC channel.

outperforms by  $\sim 2$  dB, 2.5 dB, 3.5 dB, 3.6 dB, 9 dB, 11 dB over TCSM, VGSM, GNSM, SM, QSM and ESM schemes respectively.

It has been observed that some configurations for  $2 \times 4$  systems which produces a spectral efficiency of  $\eta = 4$  bpcu cannot be constructed because of its impediments in choosing constellation points and antenna groupings. From Figure 3.6, it is seen that for dense spatial correlated channel conditions ReSM offers a performance improvement of  $\sim 1$  dB, 2 dB, 2 dB, 2.5 dB over VGSM, GNSM, ISM and SM schemes respectively.

Figure 3.7 illustrates the relative performance of  $4 \times 4$  systems yielding  $\eta = 6$  bpcu in a Rician fading channel with  $K=3$ . We see that the performance of ReSM is superior to SM, TCSM schemes by about  $\sim 2$  dB. The  $\sim 0.8$  dB advantage associated with VGSM and QSM arises from the fact that both antennas in VGSM are transmitting the same symbol and QSM uses lower order modulation scheme. This makes antenna identification easier and minimizes the errors arising from antenna misidentification in strong LoS environment. We also see that the plots corresponding to ReSM and VGSM converge at SNR value of 20 dB.

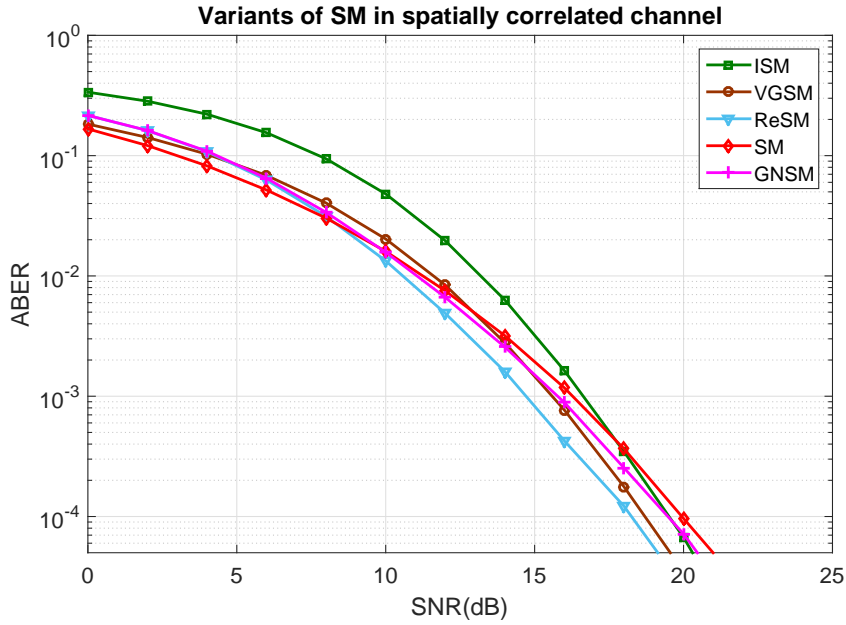


Figure 3.6 BER performance of  $2 \times 4$  systems with TX separation  $=0.1\lambda$  and RX separation  $=0.1\lambda$  yielding  $\eta = 4$  bpcu spectral efficiency, in a SC channel.

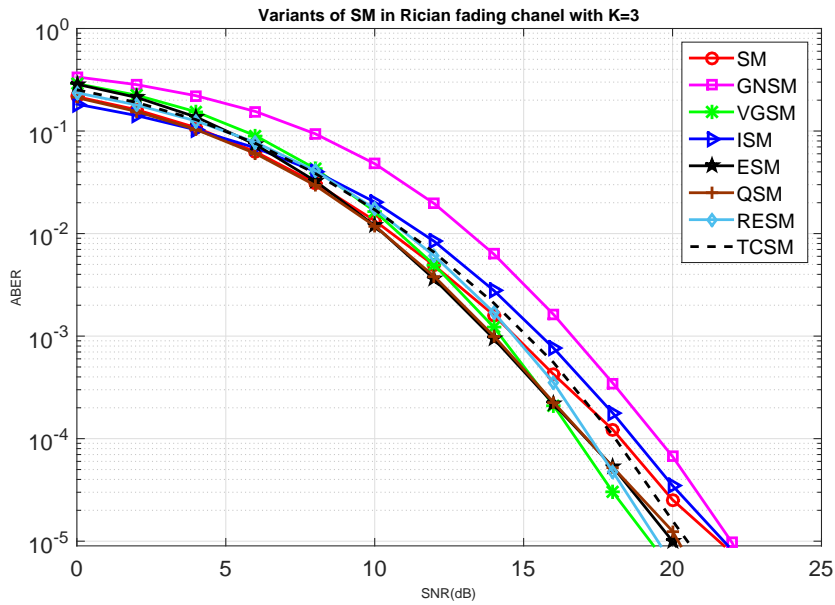


Figure 3.7 BER performance of  $4 \times 4$  systems with TX separation  $=0.1\lambda$  and RX separation  $=0.5\lambda$  yielding  $\eta = 6$  bpcu spectral efficiency, in a Rician fading channel with  $K=3$ .

ABEP of the ReSM scheme is mathematically analyzed for MIMO configuration involving  $4 \times 4$  system producing 6 bpcu. The performance of ReSM according to (3.19)

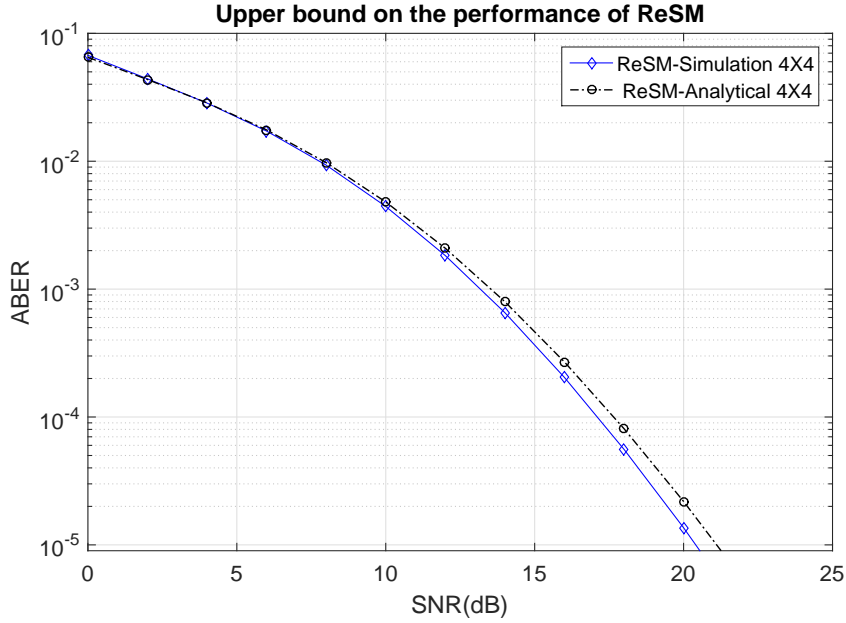


Figure 3.8 BER performance of  $4 \times 4$  systems with TX separation  $=0.1\lambda$  and RX separation  $=0.5\lambda$  yielding  $\eta =6$  bpcu spectral efficiency, in a Rician fading channel with  $K=3$ .

has been compared with the performance obtained under Monte Carlo simulations, this has been demonstrated in Figure 3.8. Close correspondence between the two plots is observed.

### 3.6 Real time Measurements

#### 3.6.1 A detailed procedure for channel estimation using USRP B210

To determine typical channel coefficients for indoor communication [Adachi et al. (1986), Pedersen et al. (1998), Serafimovski et al. (2013)], a  $2 \times 2$  MIMO system was set up in the laboratory by using USRP B210. It has an inbuilt RF front-end and open re-programmable FPGA that controls signal processing and other applications. The specifications of USRP B210 are shown in Table.3.4.

For an indoor environment, the minimum channel coherence time is measured to be approximately 20ms as given in [MacLeod et al. (2005), Spencer et al. (2000), Erceg (2004); Lee (1973)]. It's an unavoidable need to carry out the estimation of channel gains corresponding to all transmit antennas within a time period, which is lesser than

Table 3.4 USRP B210 specifications

RF coverage	70 MHz to 6 GHz
ADC/DAC	12 bit with a maximum sampling rate of 61.44MS/s
FPGA	Xilinx Spartan 6 XC6SLX150
MIMO capability	$2 \times 2$ fully coherent
Supported bandwidths	56 MHz of instantaneous, Bandwidth for $1 \times 1$ and 30.72MHz for $2 \times 2$ .
RF Power Output	>10dBm (single channel)
Receive Noise Figure	<8dB
APIs(Application Peripheral Interface)	GNU Radio, C++, Python

the channel coherence time. To estimate the channel coefficients individually from the respective transmit antennas, we have made use of a transmit frame length comprising of 690 symbols. The 160 symbols out of 690 are used for frame synchronization and the rest 512 symbols (pilot symbols) are used to estimate the channel behavior. Peak detection technique is employed to achieve synchronization. For synchronization, a sequence of 16 pulses with maximum power each separated by 9 zeros is used. The total of 512 symbols in the transmit frame of which first 256 symbols constitute to pilot 1 are transmitted from first active transmit antenna, during this period the second transmit antenna is deactivated. Similarly the rest 256 symbols constituting to pilot 2 are transmitted from second active transmit antenna while the first antenna is switched off. In order to distinguish between two frames 18 zero valued symbols are padded at the start of every frame. The most challenging aspect of this hardware realization is to have maximum SNR with minimum ISI (Inter symbol Interference). Up sampling and pulse shaping (matched filtering) are employed to achieve these two essential requirements. Every frame is sampled with an up sampling ratio of 2 and it is passed through a root raised cosine (RRC) filter with 32 taps and an excess bandwidth factor of at least 0.35. This process is accomplished by the use of GNU radio software framework. In Table 3.5, we have demonstrated the transmit frame structure for USRP B210 which is used

to estimate the channel coefficients

Table 3.5 Transmit frame structure used for channel estimation

18 zero valued symbols	160 Synchronization pulses	Pilot 1 (256 symbols)	Pilot 2 (256 symbols)
------------------------	----------------------------	--------------------------	--------------------------

In co-ordinance with the transmitting end, at the receiver, every received frame in baseband is appropriately down sampled and later passed through RRC filter having the same specifications. For every filtered frame that is received, the receiver peaks are searched, this is done by considering certain threshold which in this case is 70 % of the maximum value of the received vector. The received vector is allowed for further evaluation only if the number of peaks found to be 16 each followed by 9 zeros. The received pilot symbols arriving after the peak detection are used for channel estimation and the respective channel gains  $h_{11}, h_{12}, h_{21}$  and  $h_{22}$  are evaluated using Least Square (LS) channel estimation principle. Pilot 1 is used to estimate the channel gains for  $h_{11}, h_{21}$ .  $h_{11}$  is the channel coefficient for receive antenna 1 from transmit antenna 1 and  $h_{21}$  is the channel coefficient for receive antenna 2 from transmit antenna 1. Similarly pilot 2 is used to estimate channel gains pertaining to  $h_{12}, h_{22}$ . The spatial correlation of two transmit/receive antennas in an indoor laboratory environment has been analyzed in the presence of local scatterers and by varying the mutual distance between the two transmit antennas as well as receive antennas. Three set of channel measurements have been performed for distance of separation  $\lambda, 0.5\lambda$  and  $0.1\lambda$  between transmit array/receive array. The operating frequency is selected as 2 GHz, corresponding to it the antenna separations are  $1\lambda=15$  cm,  $0.5\lambda=7.5$  cm and  $0.1\lambda=1.5$  cm. To estimate the channel coefficients  $h_{11}, h_{12}, h_{21}$ , and  $h_{22}$  approximately  $10^7$  samples are processed [Constantine et al. (2005); Duman and Ghayeb (2008)].

The channel correlation values for the TX1 and TX2 are computed using the relation given below.

$$h_{(mag_{ratio})}(n) = |h_{11}(n)|/|h_{12}(n)|; \quad \forall n \quad (3.30)$$

$$h_{(angle_{diff})}(n) = \angle(h_{11}(n)) - \angle(h_{12}(n)); \forall n \quad (3.31)$$

where,  $|h|$  represents magnitude of  $h(n)$ ,  $\angle h$  represents phase value of  $h$  and  $n$  represents discrete time instance. Figures 3.9 and 3.10 show the histograms of  $h_{(mag_{ratio})}$  values and  $h_{(angle_{diff})}$  values computed for antenna separations of  $1 \lambda$ ,  $0.5 \lambda$  and  $0.1 \lambda$  respectively. Figure 3.9 shows, the histogram of the magnitude plot for different values of  $\lambda$ . It is observed that as the element separation of transmit array are reduced to  $0.1 \lambda$ , the histogram peak shift towards 1 showing a close correlation between TX1 and TX2. Similarly from Figure 3.10, it is clear that the histogram peak of angular plot tend towards zero as the antenna distance decreases. This indicates that lesser the antenna separation closer are the values of channel coefficients .

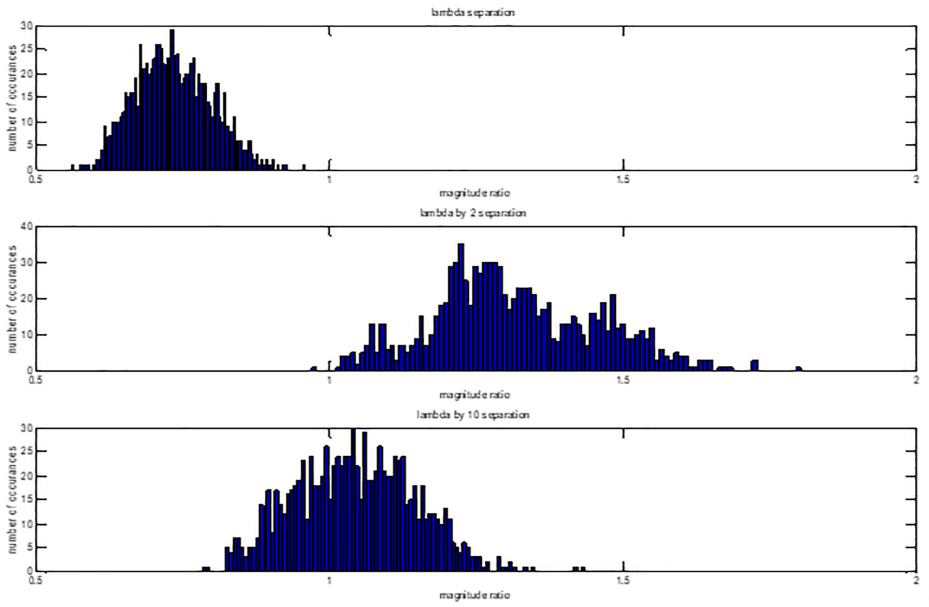


Figure 3.9 Histograms of  $h_{(mag_{ratio})}$  values computed for transmit/receive antenna separation of  $1\lambda$ ,  $0.5\lambda$  and  $0.1\lambda$  .

Figure 3.11, shows close resemblance between Rician distribution and measured indoor environment in terms of PDF and CDF plots. This proves that the laboratory set up for a  $2 \times 2$  MIMO system is a demonstration of Rician fading channel.



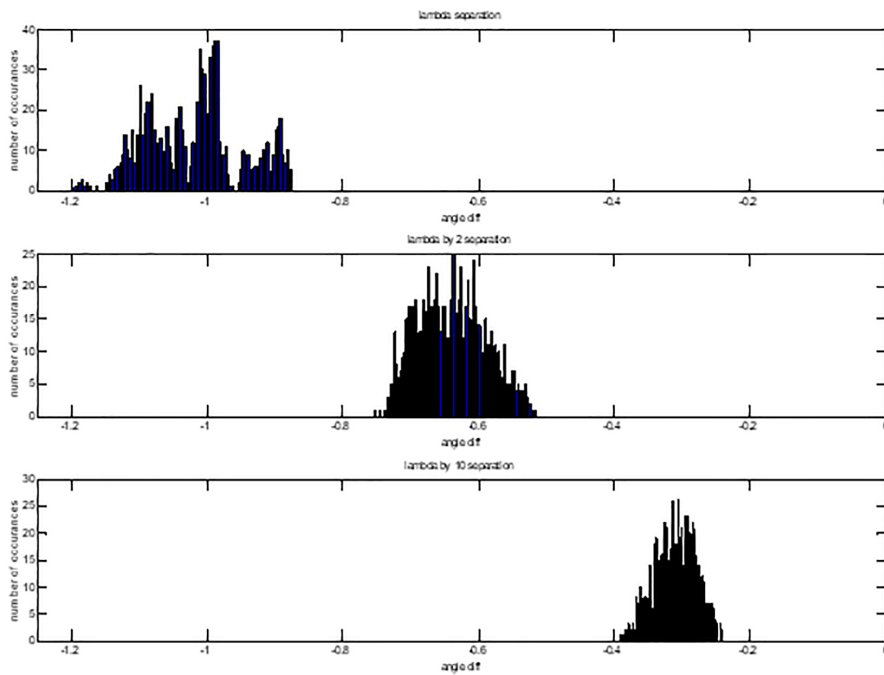


Figure 3.10 Histograms of  $h_{(angle_{diff})}$  values computed for transmit/receive antenna separation of  $1\lambda$ ,  $0.5\lambda$  and  $0.1\lambda$ .

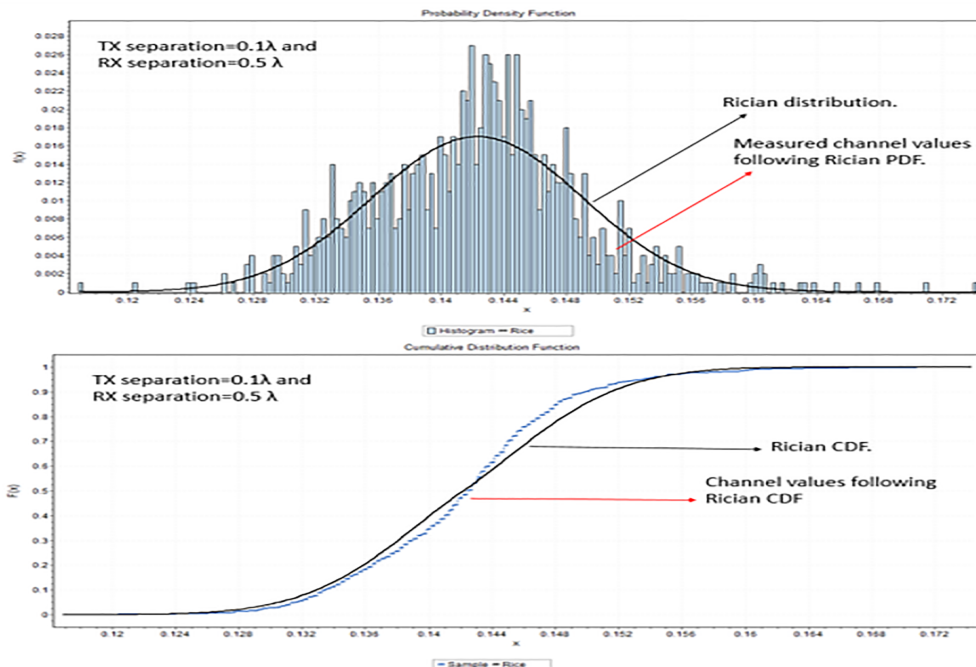


Figure 3.11 Comparison of PDF-CDF between Rician and measured indoor channel with TX separation= $0.1\lambda$ , RX separation= $0.5\lambda$ .

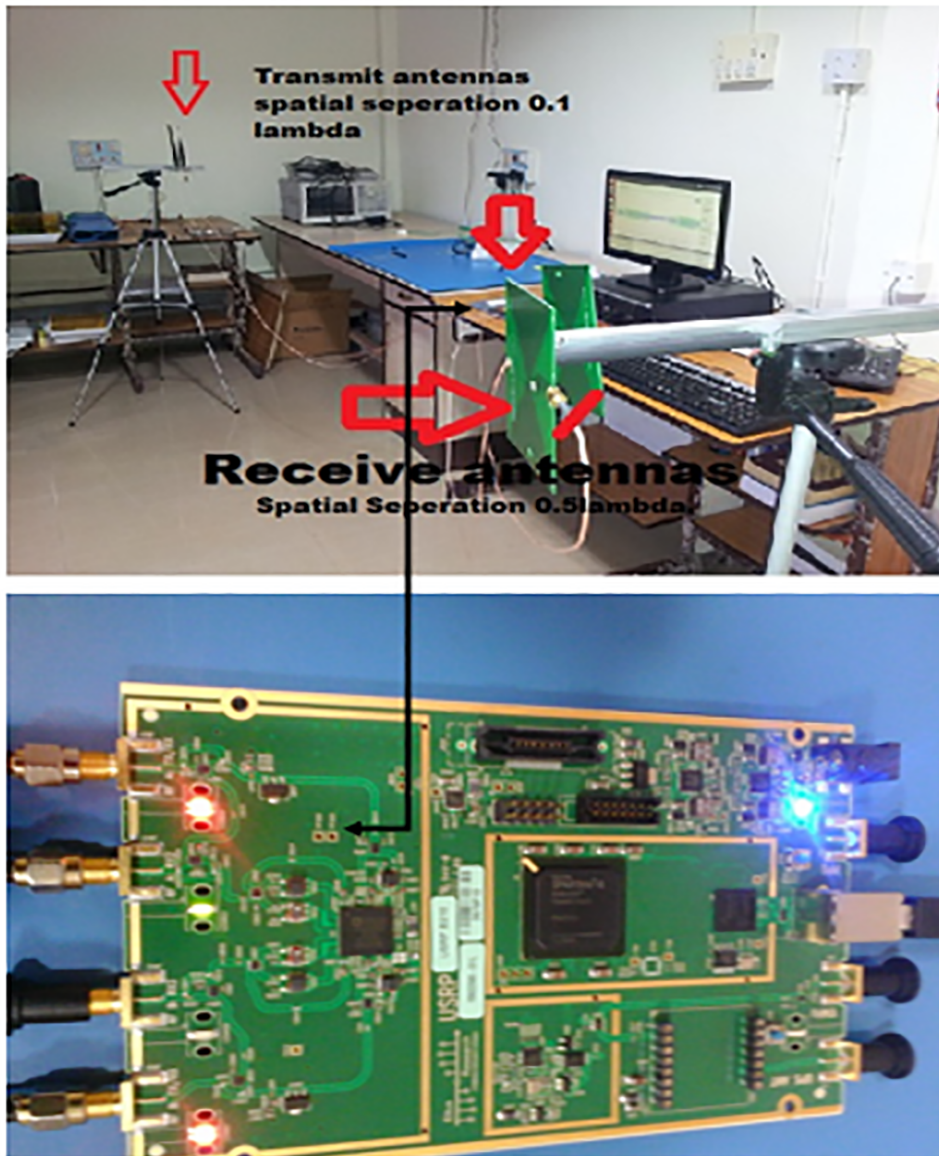


Figure 3.12 Real measurements of  $2 \times 2$  MIMO systems with a total distance TX-RX separation of 3 meters TX separation  $=0.1\lambda$  and RX separation  $=0.5\lambda$  yielding  $\eta=4$  bpcu spectral efficiency operating in an indoor environment.

Figure 3.12, shows the setup used in the laboratory to determine the values of channel coefficients from USRP B210 ( $2 \times 2$  MIMO). Figure 3.13, quantifies the performance of ReSM and SM for indoor environment with transmit antenna spacing of  $0.1\lambda$  and receive antenna spacing of  $0.5\lambda$  (TX-RX separation is 3 meters). It is seen that ReSM scheme outperforms SM by approximately 7 dB. A comparison of results is specified in Table 3.6. It is evident from the simulation plots that ReSM offers supe-

rior performance as compared to all the other competing schemes specifically in spatial correlated channel conditions.

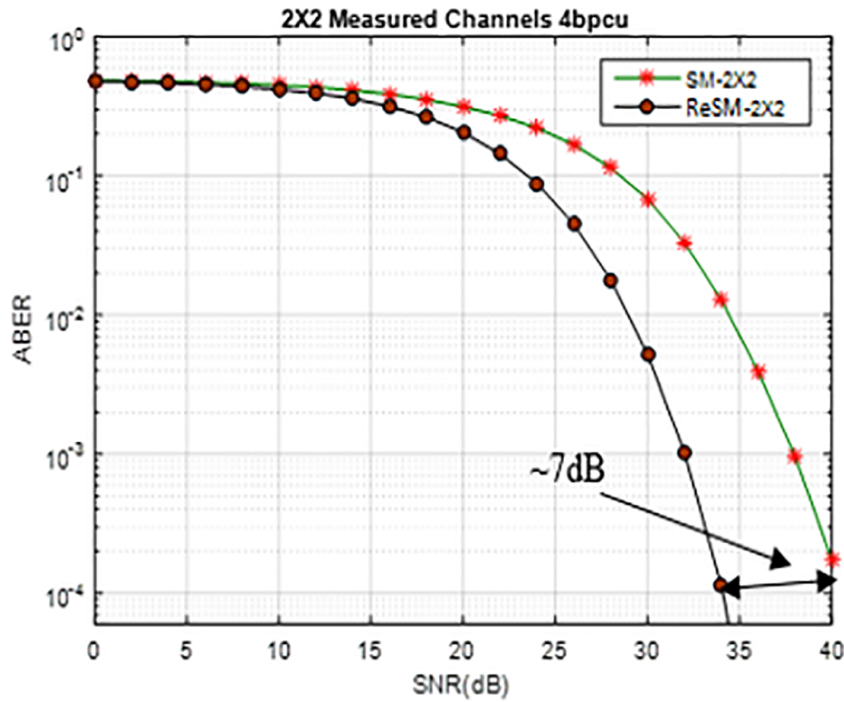


Figure 3.13 Performance results of SM  $2 \times 2$  and ReSM  $2 \times 2$  under SC channel with channel coefficients obtained by USRP B210 at TX-RX separation of 3 meters. TX separation= $0.1\lambda$ , RX separation= $0.5\lambda$  yielding  $\eta=4$  bpcu.

### 3.7 Summary

ReSM is a special case of SM scheme designed to support reliable communication in SC channels exhibiting flat fading. The major advantage of ReSM is the absence of complex encoder/decoder when compared with TCSM, it also provides BER advantage of  $\sim 4$  dB. Additionally, a minimum of 3 dB BER improvement is also observed over all other SM variants. The only exception is seen in Rician fading environment where VGSM gives a small performance improvement of  $\sim 0.5$  dB over ReSM for  $\eta=6$  bpcu. These performance gains are obtained without any additional burden of computational complexity. The ABER values obtained by exact closed form computations were

Table 3.6 Performance comparison of ReSM with variants of SM, TCSM in SC and Rician fading channels.

MIMO scheme	$N_t, N_r$	$\eta$ spectral efficiency	Required SNR at a ABER of $10^{-4}$ in dB
ReSM (SC)	4,4	6	$\sim 17$
TCSM (SC)	4,4	6	$\sim 21$
GNSM (SC)	4,4	6	$\sim 20$
VGSM (SC)	4,4	6	$\sim 20$
ISM(SC)	4,4	6	$\sim 24$
SM (SC)	4,4	6	$\sim 24$
ESM(SC)	4,4	6	$\sim 27$
QSM (SC)	4,4	6	$\sim 26$
ReSM,(Rice $K=3$ )	4,4	6	$\sim 17.1$
TCSM,(Rice $K=3$ )	4,4	6	$\sim 19$

compared with Monte Carlo simulations and similarity between them was observed. Further, a typical real time indoor channel environment was set up using USRP B210 and channel measurements were carried out. This data was used to evaluate the performance of ReSM and SM schemes for indoor environments and ReSM outperforms conventional SM by  $\sim 7$  dB. Therefore, ReSM scheme can be advantageously employed in portable hand held devices, where antenna spacing is a major issue and battery power is limited.

Further, in order to improve the reliability of data transfer we have explored the concept of Space Time Block Codes and its implementation for SM Systems. During this process we became interested in the rank distance properties of  $n$ -length cyclic codes over  $GF(q^m)$ , by utilizing the concept of Galois Field Fourier Transforms. This will be explained in the next chapter.

## Chapter 4

# Full Rank Non Orthogonal STBC design for SM-MIMO Systems from Cyclic codes: A Complete Framework.

<sup>1</sup> In this chapter, we present a novel Non Orthogonal Space Time Block Coded Spatial Modulation scheme (NSTBC-SM) for MIMO systems. A generalized procedure for designing NSTBC-SM schemes for any number of transmit antennas ( $N_t$ ) has been devised. For spectral efficiencies of 4,5,6 bpcu and two active transmit antenna ( $N_a$ ) configuration, a coding gain of at least 2.2 dB over varied STBC-SM schemes is observed. An analytical upper bound on the Average Bit Error Probability (ABEP) for the proposed scheme has been derived and substantiated using Monte Carlo simulations. Finally, the computational complexity of the decoding scheme has been estimated.

### 4.1 Introduction

Since SM is a single-RF MIMO architecture which exploits the spatial domain to convey information bits, this scheme can be a powerful tool to achieve power efficiencies as well as spectral efficiency [Mesleh et al. (2008), Di Renzo et al. (2014)]. Another important aspect of MIMO wireless communication lies in improving the reliability of information transfer over harsh fading environments. This can be achieved by making use of Space Time Block Codes (STBC). Various Researchers have extended the fundamental SM scheme by blending SM with STBCs in a MIMO design. Such designs

---

<sup>1</sup>Goutham Simha G.D. et.al, (Unpublished)

have an advantage that the loss in rate brought about by the use of channel code can be compensated by the application of SM. [Basar et al. (2011)] introduced the notion of coded SM by incorporating the Alamouti code to multiple antenna SM schemes. These schemes have been referred to as STBC-SM in literature. Since Alamouti code possesses orthogonality, low complexity ML decoder with phase rotation was proposed. STBC-SM exhibits a reduction in the spectral efficiency when compared with conventional SM schemes. The limitation of Alamouti scheme is that it provides a spectral efficiency of one symbol per time interval. To overcome this drawback, high rate STBC-SM technique with cyclic structure preserving transmit antenna diversity was proposed by [Li and Wang (2014)]. In order to enhance the performance of SM-MIMO systems under conditions of channel variation, an Adaptive Spatial Modulation technique for wireless MIMO systems was proposed by [Yang et al. (2011)]. In spite of the augmentation of channel coding and spatial diversity, the performance of SM-MIMO systems is poor in environments possessing dense channel correlation. [Le et al. (2014)], proposed a Spatially Modulated Orthogonal Space Time Block Code (SM-OSTBC) design which is a high-rate, high performance and low-complexity MIMO transmission scheme. SM-OSTBC scheme performs better than STBC-SM by exploiting the idea of linear dispersion representation and the orthogonality of the Alamouti STBC which paves the way towards a low-complexity ML decoder designs. In order to improve the throughput and enhance the reliability of SM, [Wang et al. (2014)] have proposed a high-rate STBC-SM derived from  $(n, k)$  error correcting codes. After a thorough study followed by extensive simulations, we have been able to appreciate the improvements and limitation associated with these schemes. This has motivated us to propose Non Orthogonal Space Time Block Coded Spatial Modulation (NSTBC-SM) which yields improved performance when compared with conventional STBC-SM, GNSM , VGSM , QSM , ESM and SM.

The major contributions of this work can be outlined as follows:

- Following [Sripati and Rajan (2003)], we have synthesized several full rank STBC designs from Non binary cyclic codes over  $GF(q^2)$ .
- A novel NSTBC-SM MIMO transmission scheme using Gaussian integer [Huber

(1994b)] map and Eisenstein integer map [K.Huber (1994)] (for setting up a rank preserving map between symbols from a finite field and symbols from a complex number field) has been proposed. Unlike conventional STBC-SM, in this technique each column of the codeword is radiated using different transmit antenna pairs selected using antenna selection symbols.

- The proposed technique is generalized for any number of transmit antennas (only two antennas are actively radiating at any given instant is considered in our work). Cyclic codes over extension fields of size  $4b + 1$  or  $6b + 1$  for  $b = 1, 2, 3, \dots$  have been chosen to meet the requirements of Gaussian or Eisenstein map.
- A closed form expression for the ABEP and an estimation of the decoding complexity have been derived. This allows us to determine an upper bound on the performance of NSTBC-SM schemes.

## 4.2 Design of Non Orthogonal Full Rank Space Time Block Coded Spatial Modulation (NSTBC-SM)

### 4.2.1 Transform Domain description of cyclic codes

In this section we present the concept of Galois Field Fourier Transform (GFFT) and its application to obtain cyclic codes of length  $n$  over  $GF(q^m)$ , whose codewords are full rank  $(m \times n)$  matrices over  $GF(q)$  which are used to construct full rank STBCs.

### 4.2.2 Cyclotomic coset

The cyclotomic cosets modulo  $n$  with respect to  $GF(q)$  is a partitioning of the integers into sets. Let  $I_n = 0, 1, 2, \dots, n - 1$ , for any  $f \in I_n$  and for any divisor  $d$  of  $m$  the  $q^d$  cyclotomic coset of  $f \bmod n$  is a set defined by

$$[f]^d = \{i \in I_n | f = iq^{dt} \bmod n \text{ for some } t \geq 0\} \quad (4.1)$$

Cardinality of the above set is given by  $e_f^{(d)}$ . When  $(d = 1)$ , we denote the  $q$ -cyclotomic coset of  $f \bmod n$  by  $[f]$  and its cardinality by  $e_f$ .

### 4.2.3 Galois Field Fourier Transforms (GFFT)

Let  $\alpha$  be an element of order  $n$  in  $GF(q^m)$ . The Galois Field Fourier Transform (GFFT) of an  $n$ -tuple  $\mathbf{a}$  over the finite field  $GF(q)$  of characteristic  $p$  is defined to be the vector  $\mathbf{A}=(A_0, A_1 \cdots A_{n-1}) \in GF(q^m)^n$  and is given by

$$A_j = \sum_{i=0}^{n-1} \alpha^{ij} a_i, \quad j = 0, 1, 2, \dots, n-1. \quad (4.2)$$

The Inverse Galois Field Fourier Transform (IGFFT) is defined as

$$a_i = \frac{1}{n \bmod p} \sum_{j=0}^{n-1} \alpha^{-ij} A_j, \quad i = 0, 1, 2, \dots, n-1. \quad (4.3)$$

The vectors  $\mathbf{a}$  and  $\mathbf{A}$  are the time domain and its transform domain representations respectively.

The GFFT defined in (4.2) is a  $GF(q^m)$  linear map satisfying the following two properties.

- **Property 1:** (*Conjugacy Constraint*): Following [Sripati and Rajan (2003)],  $\mathbf{A} \in GF(q^m)^n$  is the GFFT of some vector  $\mathbf{a} \in GF(q)^n$  if and only if

$$A_{jq^{m \bmod n}} = A_j^{q^m} \forall j \in [0, n-1]. \quad (4.4)$$

- **Property 2:** (*Cyclic Shift Property*): If  $\mathbf{A}=\text{GFFT}(\mathbf{a})$ ,  $b \in GF(q)^n$  such that  $b_i = a_{i-1 \bmod n} \forall i \in [0, n-1]$  and  $\mathbf{B}=\text{GFFT}(b)$ , then  $B_j = \alpha^j A_j, \forall j \in [0, n-1]$

From property 2 for linear cyclic codes,  $A_j$  takes values from  $\{0\}$  or  $GF(q^{e_j^{(m)}})$ . Hence cyclic code can be considered as a set of inverse GFFT vectors of all the vectors of a subspace of  $\text{GFFT}(GF(q)^n) \in GF(q^m)^n$ . Here, transform components in  $[j]^m$  of every vector take on only the zero vector or all the values of  $GF(q^{e_j^{(m)}})$  and transform components in disjoint  $[j_1]^m$  and  $[j_2]^m$  take values independently.

Cyclic/RS codes with specified minimum distance properties can be designed by specifying nonzero components in the transform domain [Wicker (1995), Moon (2005), Blahut (1983)] and employing the IGFFT to determine the time domain components. In [Sripati and Rajan (2003)] a constructive technique for deriving  $n$  length cyclic codes over  $GF(q^m)$  whose codewords are full rank  $(m \times n)$  matrices over  $GF(q)$  has been



described. We have employed this description to determine full rank designs for Space Time Block Codes.

#### 4.2.4 Characterization of cyclic codes for Rank metric

Definition of rank metric:

Let  $\mathbf{a}=\{a_i : i = 0 \text{ to } n-1\} \in GF(q^m)$  can be written as  $(m \times n)$  matrix over  $GF(q)$  as shown below.

$$\begin{bmatrix} a_{0,0} & a_{0,1} & a_{0,2} & a_{0,3} & \dots & a_{0,n-1} \\ a_{1,0} & a_{1,1} & a_{1,2} & a_{1,3} & \dots & a_{1,n-1} \\ a_{2,0} & a_{2,1} & a_{2,2} & a_{2,3} & \dots & a_{2,n-1} \\ \vdots & \vdots & \vdots & \vdots & \ddots & \vdots \\ a_{m-1,0} & a_{m-1,1} & a_{m-1,2} & a_{m-1,3} & \dots & a_{m-1,n-1} \end{bmatrix}$$

The rank of vector  $\mathbf{a}$  over  $GF(q)$  is defined as the rank of the above matrix. Given a description of the code  $C$  in the transform domain we try to construct cyclic codes of length  $n$  over  $GF(q^m)$ , with rank distance  $m$  [Sripati and Rajan (2003), Gabidulin (1985)].

**Theorem 4.1** : If  $C$  is a cyclic code of length  $n|q^m - 1$  over  $GF(q^m)$  such that it has one free transform domain component  $A_{jq^s} \in A_{[j]}, (|[j]| = e_j, 0 \leq s \leq e_j - 1)$ . Then  $Rank_q(C) = e_j$  [Sripati et al. (2004)].  $e_j$  is the size of the  $q$ -cyclotomic coset containing  $jq^s$ .

**Proof** : From (4.3), with  $A_{jq^s}$  as the only free transform domain component, it is evident that the time domain component  $a_i$  can be represented as,

$$\mathbf{a}_i = A_{jq^s} \alpha^{-ijq^s}$$

(The scale factor  $1/(n \bmod p)$  is ignored as it does not affect the rank). Hence the vector  $\mathbf{a}$  comprising of  $a_i, 0 \leq i \leq n-1$  can be represented as,

$$\mathbf{a} = (A_{jq^s}, A_{jq^s} \alpha^{-jq^s}, A_{jq^s} \alpha^{-2jq^s}, \dots, A_{jq^s} \alpha^{-(n-1)jq^s})$$

Representing each element of  $\mathbf{a}$  as an  $m$ -tuple over the base field  $GF(q)$  we obtain,

$$\mathbf{a} = \begin{bmatrix} A_{0,0} & A_{0,1} & A_{0,2} & \cdots & A_{0,n-1} \\ A_{1,0} & A_{1,1} & A_{1,2} & \cdots & A_{1,n-1} \\ A_{2,0} & A_{2,1} & A_{2,2} & \cdots & A_{2,n-1} \\ \vdots & \vdots & \vdots & \ddots & \vdots \\ A_{m-1,0} & A_{m-1,1} & A_{m-1,2} & \cdots & A_{m-1,n-1} \end{bmatrix} \quad (4.5)$$

Every  $(m \times n)$  matrix  $\mathbf{a}$  (a codeword of the  $n$ - length cyclic code) obtained in this manner is a full rank matrix over  $GF(q)$ .

Following [ Sripati et al. (2004)],

**Corollary :** If  $C$  is a cyclic code of length  $n|q^m - 1$  over  $GF(q^m)$  with free transform domain component  $A_{jq^s}$  and all other transform domain components constrained to zero. For any non-zero codeword

$\mathbf{a} = (a_0, a_1, \dots, a_{e_j-1}, a_{e_j}, \dots, a_{n-1}) \in C$ , then the entries  $(a_0, a_1, \dots, a_{e_j-1})$  are linearly independent and the entries  $(a_{e_j}, a_{e_j+1}, \dots, a_{n-1})$  can be expressed as the linear combination of  $(a_0, a_1, \dots, a_{e_j-1})$ .

**Proof :** From the definition of IGFFT we write

$$\mathbf{a} = (A_{jq^s}, A_{jq^s} \alpha^{-jq^s}, A_{jq^s} \alpha^{-2jq^s}, \dots, A_{jq^s} \alpha^{-(n-1)jq^s})$$

$$\mathbf{a} = (A_{jq^s}, \alpha^{-jq^s} A_{jq^s}, \alpha^{-2jq^s} A_{jq^s}, \dots, \alpha^{-(e_j-1)jq^s} A_{jq^s},$$

$\alpha^{-(e_j)jq^s} A_{jq^s}, \dots, \alpha^{-(n-1)jq^s} A_{jq^s})$  For the sake of analysis and simplicity, the above equation can be re-written as

$$\mathbf{a} = A_{jq^s} (1, \alpha^{-jq^s}, \alpha^{-2jq^s}, \dots, \alpha^{-(e_j-1)jq^s}, \alpha^{-(e_j)jq^s}, \dots, \alpha^{-(n-1)jq^s}).$$

Let  $\mathbf{S} = (1, \alpha^{-jq^s}, \alpha^{-2jq^s}, \dots, \alpha^{-(e_j-1)jq^s}, \alpha^{-(e_j)jq^s}, \dots, \alpha^{-(n-1)jq^s})$  Since,  $A_{jq^s}$  is non-zero  $Rank_q(\mathbf{a}) = Rank_q(\mathbf{S})$ . We will show that the elements of  $\mathbf{S}'$  are linearly independent where,  $\mathbf{S}' = \{1, \alpha^{-jq^s}, \alpha^{-2jq^s}, \dots, \alpha^{-(e_j-1)jq^s}\}$  and that,  $\{\alpha^{-(e_j)jq^s}, \dots, \alpha^{-(n-1)jq^s}\}$  can be expressed as the linear combination of the elements of  $\mathbf{S}'$ . To prove this assertion, let us assume on the contrary that the elements of  $\mathbf{S}'$  are linearly dependent. Then there exists coefficients  $c_0, c_1, \dots, c_{e_j-1} \in GF(q)$  not all  $c_i = 0$  such that  $\sum_{i=0}^{e_j-1} c_i \alpha^{-ijq^s} = 0$

This implies that  $\alpha^{-jq^s}$  is a root of a polynomial of degree  $e_j-1$  over  $GF(q)$ . But  $\alpha_{[-jq^s]} = \{\alpha^{-jq^s}, \alpha^{-2jq^s}, \dots, \alpha^{-(e_j-1)jq^s}\}$  corresponds to the  $q$ -cyclcotoxic coset  $[-jq^s]$

also of cardinality  $e_j$ . This proves that minimal polynomial of  $\alpha^{-jq^s}$  is of degree  $e_j$ . This contradicts our assumption that the elements of  $\mathbf{S}'$  are linearly dependent. Using the fact that the minimal polynomial of  $\alpha^{-jq^s}$  is of degree  $e_j$ , it is straight forward to show that the other elements of  $\mathbf{S}$  can be expressed as linear combinations of  $\mathbf{S}'$ . Hence  $Rank_q(C) = e_j$ .

#### 4.2.5 Cyclic Codes as STBC

For communication over wireless channel the codeword symbols have been traditionally mapped (bijective map) onto points in complex constellations (QAM/PSK). Since the symbols are over field  $GF(q)$  there is a requirement for a map which connects these symbols to the symbols of complex plane. In [Huber (1994b), K. Huber (1994)] code construction over Gaussian integers and Eisenstein-Jacobi integers have been discussed.

In 2003, [Lusina et al. (2003)] has proposed a rank preserving map between finite fields of cardinality of the form  $4b + 1$  where,  $b$  is an integer. Let  $q$  be a prime number of the form  $4b + 1$  where  $b \geq 1$ . By definition a Gaussian integer  $\omega$  is a complex number defined as  $\omega = x + iy$ ;  $x, y \in \mathbb{Z}, i = \sqrt{-1}$ . From number theory, it is known that every prime number  $q \equiv 1 \pmod{4}$  can be written as  $q = (u + iv) \times (u - iv) = u^2 - v^2$ . The number  $\pi = u + iv$  is known as the Gaussian prime number where  $u, v \in \mathbb{Z}$ . Let  $\pi' = u - iv$ . The calculation modulo  $\pi$  is defined as  $Z_i = i \pmod{\pi} = i - \lfloor \frac{i\pi'}{\pi} \rfloor \pi$  for  $i = 0, 1, 2, \dots, q - 1$  where  $\lfloor \cdot \rfloor$  performs the operation of rounding to the nearest Gaussian integer. Lusina et.al. have proved that the Gaussian integer modulo  $\pi$  form a field, represented as shown.

$$G_\pi = \{Z_0 = 0, Z_1 = 1, \dots, Z_{q-1}\} \quad (4.6)$$

Such that the map  $\zeta : GF(q) \Rightarrow G_\pi$  given by  $Z_i$  is isomorphic. Therefore the map between code words from a linear cyclic code over  $GF(q^m)$ , which are  $(m \times n)$  matrices over  $GF(q)$ , and  $(m \times n)$  matrices over the complex Gaussian field, is rank preserving. Table. 4.1 provide values of  $\pi, u$  and  $v$  for primes  $q \equiv 1 \pmod{4}$  ( $q = 5, 13, 17$ )

A second map called the Eisenstein map was defined by [K. Huber (1994)]. It is shown that the set of complex numbers obtained using Eisenstein integer forms a field. Let  $q'$  be a prime of the form  $q' = 6b + 1$  i.e  $q' = 7; 13; 19 \dots$ . By defini-

Table 4.1 Values of  $q, \pi, u$  and  $v$

$q$	$\pi$	$u$	$v$
5	$2+i$	-1	$1+i$
13	$3+2i$	-2	$1+2i$
17	$4+i$	-2	$2+i$

tion, a Eisenstein-Jacobi (EJ) integer  $\omega$  is a complex number defined as  $\omega = b + \rho\beta$  where  $\rho = (-1 + i\sqrt{3})/2$ , which comprises of real and rho parts. Primes of the form  $q' \equiv 1 \pmod{6}$  can then be written as  $q' = b^2 + 3\beta^2$ . These primes are product of two conjugate Eisenstein-Jacobi integers  $q' = b^2 + 3\beta^2 = \Pi\Pi^*$ . The number  $\Pi$  is defined as  $b + \beta + \rho \cdot 2\beta$  and  $\Pi^* = b + \beta + \rho^2 \cdot 2\beta$  is the conjugate of  $\Pi$ . Let

$$\xi(i) = i\Pi \triangleq i - \left[ \left( \frac{i\Pi}{i\Pi^*} \right) \right] \Pi \text{ for } i = 0, 1, 2 \dots q' - 1 \quad (4.7)$$

here  $[\cdot]$  (denotes the rounding operation) closest to EJ number which is defined such that the norm of  $\xi$  is as small as possible. Let  $J_\Pi$  be defined as,

$$J_\Pi = \{\xi_0 = 0, \xi_1 = 1, \xi_2 \dots \dots, \xi_{q'-1}\} \quad (4.8)$$

$J_\Pi$  is the residue class of  $J \pmod{\Pi}$  where, the modulo function is defined according to (4.8). Huber has shown that the set  $J_\Pi$  given by (4.8) is a complex field over  $GF(\Pi)$  [K.Huber (1994)]. From [Lusina et al. (2003)] it follows that the Eisenstein map is bijective similar to Gaussian map. The transformed codewords over the complex Eisenstein field preserve the full rank property [Puchinger et al. (2016)].

The elements of the map described in [Lusina et al. (2003)] can be viewed as the points in a complex plane. In this work we will employ these points in a two dimensional complex plane as elements of signal constellation. Therefore the map between codewords from a linear code over  $GF(q^m)$ , which are  $(m \times n)$  matrices over  $GF(q)$ , and  $(m \times n)$  matrices over the complex Gaussian integer field and Eisenstein field, is rank preserving. Table 4.2 gives values of  $\Pi, b, \beta$  for primes  $q' \equiv 1 \pmod{6}$  ( $q' = 7; 13; 19 \dots$ ). Designs for full rank STBCs can be derived by use of the above rank preserving maps for a suitable values of  $q$ . The code word matrices of these STBCs are allowed to take on values from a signal set matched to  $GF(q)$ . Such designs can be proposed for any linear code.

Table 4.2 Values of  $q'$ ,  $\Pi$ ,  $b$  and  $\beta$

$q'$	$\Pi$	$b$	$\beta$
7	$3+2\rho$	2	1
13	$3+4\rho$	1	2
19	$5+2\rho$	4	1

### 4.3 Non Orthogonal Full Rank Space Time Block Coded Spatial Modulation (NSTBC-SM)

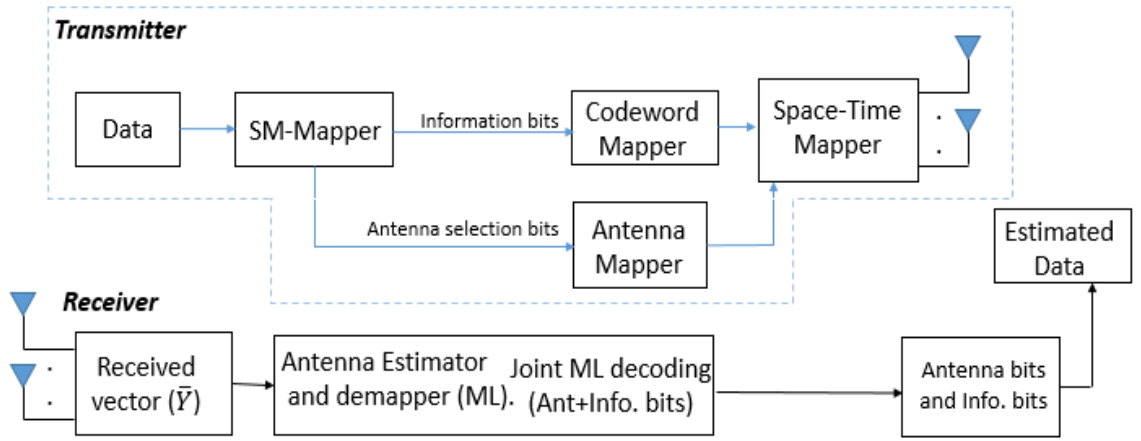


Figure 4.1 Block diagram for NSTBC-SM system

The block diagram of the NSTBC-SM scheme is shown in Figure 4.1. The SM mapper demultiplexes the source data into information bits and antenna selection bits. The number of information bits and/or antenna selection bits depends on the number of transmit antennas  $N_t$ , desired spectral efficiency ( $\eta$ ) and Galois Field  $GF(q^m)$ . Let us consider the case when  $m$  transmit antennas of the transmit antenna array are active at any given time. Theorem 4.1 outlines a procedure that can be used to construct cyclic codes over  $GF(q^m)$  which is viewed as  $(m \times n)$  matrices of full rank over  $GF(q)$ .

Using Corollary the  $(m \times n)$  matrices are reduced to full rank preserving  $(m \times m)$  matrices over  $GF(q)$  as shown below.

$$\underbrace{(10101\dots)} \longrightarrow \begin{bmatrix} A_{0,0} & A_{0,1} & A_{0,2} & \dots & A_{0,m-1} \\ A_{1,0} & A_{1,1} & A_{1,2} & \dots & A_{1,m-1} \\ A_{2,0} & A_{2,1} & A_{2,2} & \dots & A_{2,m-1} \\ \vdots & \vdots & \vdots & \ddots & \vdots \\ \vdots & \vdots & \vdots & \dots & \vdots \\ A_{m-1,0} & A_{m-1,1} & A_{m-1,2} & \dots & A_{m-1,m-1} \end{bmatrix} \quad (4.9)$$

By employing the rank preserving Gaussian integer map or Eisenstein map these matrices can be converted to full rank matrices over complex number field. Using the proposed STBC constructions the codeword mapper maps  $(\lfloor \log_2(q^m) \rfloor)$  binary information bearing symbols into suitable codewords with Gaussian integers or Eisenstein-Jacobi integers as conceptually indicated in (4.10).

$$X_{SM} = \begin{bmatrix} \mathfrak{F}(A_{0,0}) & \mathfrak{F}(A_{0,1}) & \mathfrak{F}(A_{0,2}) & \dots & \mathfrak{F}(A_{0,m-1}) \\ \mathfrak{F}(A_{1,0}) & \mathfrak{F}(A_{1,1}) & \mathfrak{F}(A_{1,2}) & \dots & \mathfrak{F}(A_{1,m-1}) \\ \mathfrak{F}(A_{2,0}) & \mathfrak{F}(A_{2,1}) & \mathfrak{F}(A_{2,2}) & \dots & \mathfrak{F}(A_{2,m-1}) \\ \vdots & \vdots & \vdots & \ddots & \vdots \\ \mathfrak{F}(A_{m-1,0}) & \mathfrak{F}(A_{m-1,1}) & \mathfrak{F}(A_{m-1,2}) & \dots & \mathfrak{F}(A_{m-1,m-1}) \end{bmatrix} \quad (4.10)$$

where,  $\mathfrak{F}$  is either  $\zeta$  or  $\xi$  depending upon the Gaussian or Eisenstein map that is selected. The antenna mapper selects  $\log_2(\Psi)$  bits and maps them to the active antenna pair. Based on the antenna pair the space time mapper assigns the symbols of codeword to active antennas, thus forming the STBC of size  $N_t \times n$  as shown below ( $m \leq N_t$ ).

It can be seen that unlike STBC-SM, in which all columns of the codeword are transmitted using same antenna pair, in the proposed method each column is transmitted using different antenna pairs. This essentially increases the transmitted information bits, and at the receiver can infer from the knowledge of active antennas. This scheme

improves the spectral efficiency using antenna selection.

Since traditional STBC-SM deployments usually employ two active antennas [Basar et al. (2011)], we have also used only two antennas in this work though NSTBC-SM schemes with any number of active transmit antennas can be designed.

$$\hat{X}_{SM} = \begin{bmatrix} \mathfrak{F}(A_{0,0}) & \mathfrak{F}(A_{0,1}) & \mathfrak{F}(A_{0,2}) & \dots & 0 \\ \mathfrak{F}(A_{1,0}) & \mathfrak{F}(A_{1,1}) & 0 & \dots & \mathfrak{F}(A_{0,m-1}) \\ 0 & 0 & 0 & \dots & \mathfrak{F}(A_{1,m-1}) \\ 0 & 0 & \mathfrak{F}(A_{1,2}) & \dots & 0 \\ \vdots & \vdots & \vdots & \dots & \vdots \\ 0 & 0 & 0 & \dots & 0 \end{bmatrix} \quad (4.11)$$

---

**Algorithm 1** *Generalized Algorithm for NSTBC – SM :*

---

- 1: Input:  $\mathbb{M}$
  - 2: Output:  $T$
  - 3: **Step.1:** Consider  $\mathbb{M}_{info} = (M_0, M_1, \dots, M_{\lfloor \log_2(q^m) \rfloor})$ .
  - 4:  $Index = bin2dec(\mathbb{M}_{info})$ .
  - 5: Obtain  $X = \phi(C)$  by defining the appropriate Rank preserving map.
  - 6: **Step.2** Define a map  $\phi : \mathbb{M}_{info} \rightarrow \mathfrak{F}(C)$ .
  - 7: **Step.3:** Antenna selection.
  - 8: Consider  $\mathbb{M}_{ant} = (M_{\lfloor \log_2(q^m) \rfloor + 1}, \dots, M_{\lfloor \log_2(q^m) \rfloor + n \cdot \log_2(\Psi) - 1})$  bits.
  - 9: Obtain:  $\hat{X}_{SM}$
- 

The encoding procedure of NSTBC-SM scheme is given in Algorithm 1. Initial bits are considered as message bits and are mapped to a rank preserved codeword matrix using the codeword mapper as shown in Step 1 . Consider, the next bits as  $M_{ant}$ . For each column of the codeword the active antenna index is chosen using a map defined in Step.2. Later, the matrix elements of  $\mathfrak{F}(C)$  are transmitted through the corresponding active antenna indices and  $\hat{X}_{SM}$  is obtained.

Example 1, describes the NSTBC-SM construction over  $GF(5^2)$ .

**Example 1 :** For a spectral efficiency of  $\eta = 4$ , let  $N_t = 4$  and  $q = 5$ . The length  $n$  of a cyclic code is chosen such that  $n|q^m - 1$ . In this case  $3|5^m - 1$ , for  $m = 2$ . The value of  $m$  determines the number of information bits assigned to the codeword.

Thus using Theorem 4.1 we have constructed  $2 \times 3$  codeword matrices over  $GF(5^2)$  of the form,

$$\begin{bmatrix} A_{0,0} & A_{0,1} & A_{0,2} \\ A_{1,0} & A_{1,1} & A_{1,2} \end{bmatrix} \quad (4.12)$$

where,  $(A_{i,j}) \in GF(q = 5)$ ,  $0 \leq i \leq 1$ ,  $0 \leq j \leq 2$ .

Using Corollary and rank preserving map  $\xi : GF(5) \rightarrow GF(2+i)$ , the above matrix in (4.12) is reduced to

$$\begin{bmatrix} \mathfrak{F}(A_{0,0}) & \mathfrak{F}(A_{0,1}) \\ \mathfrak{F}(A_{1,0}) & \mathfrak{F}(A_{1,1}) \end{bmatrix} \quad (4.13)$$

Now the incoming data is divided into two streams: the information sequence stream and the antenna selection stream.

**Note:** In Spatial Modulation, symbol 0 represents the inactive state of antenna. In order to avoid ambiguity between the symbol 0 of the codeword and 0 representing the inactive antenna, the codeword symbol 0 is mapped to a nonzero prime number which is chosen to be the Gaussian integer or Eisenstein-Jacobi integer used to construct the complex field (Symbol 0 is mapped to  $G_{2+i}$ ,  $G_{3+2\rho}$ ,  $G_{3+2i}$ ,  $G_{4+i}$  for different maps which yield different spectral efficiencies).

A pictorial representation of a NSTBC-SM transmission scheme is illustrated in Figure 4.2. Figure explains the antenna selection for the antenna bit sequence (00, antenna index (1,4)). Similarly the next set of antenna selection bits follow as shown in Table. 4.3.

Information is usually encoded in binary form. We are using a shortened (2,1) cyclic code over  $GF(5^2)$  with  $5^2 = 25$  codewords. Length of the information sequence to be encoded is such that the number of distinct message sequences is less than or equal to  $5^2$ . The length of information sequence here is chosen to be four bits as  $4 = (\lfloor \log_2 4^2 \rfloor)$ .



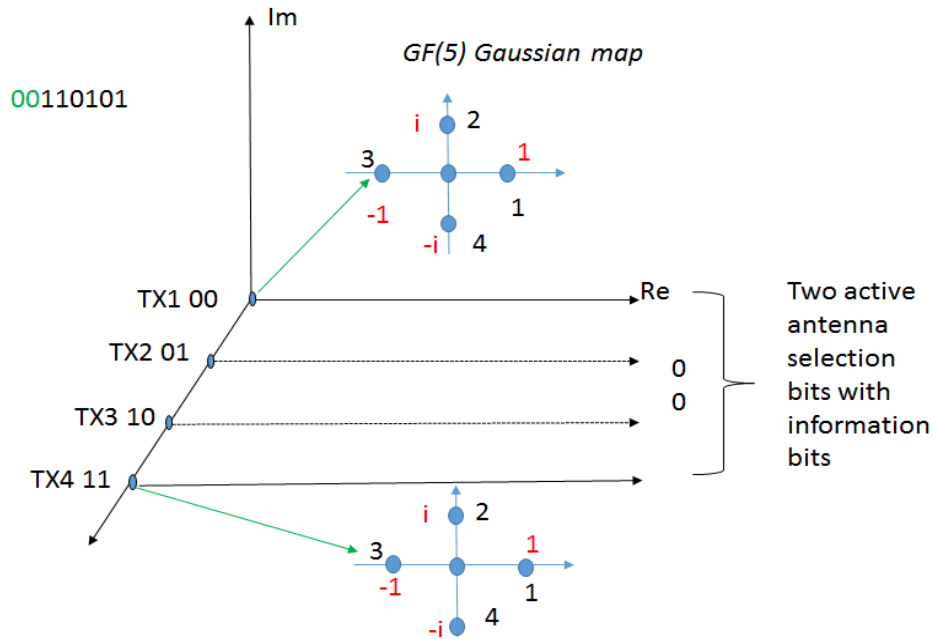


Figure 4.2 Illustration of Antenna selection (corresponding to first time slot as shown in (4.14). Symbol 0 is mapped to  $G_{2+i}$ ,  $G_{3+2\rho}$ ,  $G_{3+2i}$ ,  $G_{4+i}$  for different maps which yield different spectral efficiencies.)

Every distinct length 4 bit information sequence is mapped onto a unique shortened codeword of the  $(2,1)$  cyclic code over  $GF(5^2)$ .

The next  $(n \cdot \log_2 \Psi)$  bits after the information sequence is considered as antenna selection sequence stream. In this example we have chosen the antenna selection sequence to be 0001. From Table. 4.3, it can be inferred that the active antenna sequence is  $[(1,4),(1,3)]$ . Thus, in the first time slot, antennas 1 and 4 are activated, in the second time slot antennas 1 and 3 are activated. Finally the space time mapper forms an STBC codeword as shown below.

$$\begin{bmatrix} \mathfrak{F}(A_{00}) & \mathfrak{F}(A_{01}) \\ 0 & 0 \\ 0 & \mathfrak{F}(A_{11}) \\ \mathfrak{F}(A_{10}) & 0 \end{bmatrix} \quad (4.14)$$

Table 4.3 Antenna Mapping

Input Bit stream	Active antenna combination
00	(1,4)
01	(1,3)
10	(1,2)
11	(2,3)

The Table 4.3 is used to generate spectral efficiencies of 4,5,6 bpcu.

(From Table 4.3, it is shown that 4 bpcu can be obtained by constructing NSTBC-SM over  $GF(5)$ , 4.5 bpcu over  $GF(7)$ , 5 bpcu over  $GF(13)$ , 6 bpcu over  $GF(17)$ ).

### 4.3.1 Spectral Efficiency Calculation for NSTBC-SM

For a length  $n$  codeword over  $GF(q^m)$  and antenna selection bits  $\log_2(\Psi)$ , the spectral efficiency (bits per channel usage) is given by:

$$\eta = \log_2(\Psi) + \left( \frac{\lfloor \log_2(q^m) \rfloor}{n} \right) \quad (4.15)$$

### 4.3.2 ML decoder for the proposed NSTBC-SM

This subsection, gives a detailed description and formulation of the ML decoder for the proposed NSTBC-SM scheme. The output of the MIMO channel is given by

$$\mathbf{Y} = \mathbf{H}\mathbf{X} + \mathbf{n} \quad (4.16)$$

where,  $\mathbf{X}$  is the transmitted vector of size  $N_t \times 1$  communicated over a given time slot,  $\mathbf{H}$  is the channel matrix of size  $N_r \times N_t$  which depends on the channel distribution.  $\mathbf{n}$  is a column vector of circularly symmetric complex Gaussian random numbers (independent and identically distributed ( $C \mathcal{N}(0, 1)$ )).

The optimal receiver shown in Figure 4.1 has a single stage decoder. Assuming perfect CSI at the receiver the antenna index and the information pertaining to STBC is inferred using the following equation

$$(\widehat{l}_t \widehat{S}_q)_{ML} = \arg \min \|\mathbf{Y} - \mathbf{H}\widehat{\mathbf{X}}\|^2 \forall l_t, S_q \quad (4.17)$$

where,  $\widehat{l}_t$  is the estimated antenna index of the received vector and  $\widehat{S}_q$  is the estimated

transmission symbols. Since there are  $\binom{N_t}{2}$  possible antenna combinations the transmitted codeword vector can be any one of the total number of possible combinations given by

$$\binom{N_t}{2} \times q^2 \quad (4.18)$$

Later, a 4 bpcu NSTBC-SM design employing a shortened cyclic code of length 2 cyclic code over  $GF(5^2)$  which uses the Gaussian map is presented. The second example also quantifies the complexity of search required for ML decoding at the receiver.

---

**Algorithm 2** *Decoding Algorithm for NSTBC – SM :*

---

- 1: Input:  $\mathbf{Y}$
  - 2: Output:  $\hat{\mathbf{M}}$
  - 3: **Step.1:** for  $\mathbf{t} = \mathbf{1} : \mathbf{m}$
  - 4: Consider  $Y$ . Compute  $(\hat{\ell}, \hat{X})_{ML} = \arg \min_{X \neq \hat{X}} \|Y - H\hat{X}\|_F^2 \forall \hat{X} \in X$
  - 5: **Step.2:** Estimate Antenna Selection bits and Information bits from  $\hat{X}_{SM}$ .
- 

Unlike conventional SM-ML decoding strategy, the proposed Algorithm 2 has two steps. **Step.1** employs joint ML detection of antenna selection symbols and codeword symbols, **Step.2** is used to obtain the information bits from the estimated codeword. Finally, the decoded information is obtained by the augmentation of estimated information sequence and antenna selection sequence.

From Example 4.1 there are  $\binom{4}{2} = 6$  transmit antenna combinations. Let the symbols conveyed in the first time slot be  $c_{00}$  and  $c_{10}$ . The transmitted vector possibilities are as shown.

$$\mathbf{X} = \begin{bmatrix} c_{00} \\ c_{10} \\ 0 \\ 0 \end{bmatrix} \text{ or } \begin{bmatrix} 0 \\ c_{00} \\ c_{10} \\ 0 \end{bmatrix} \text{ or } \begin{bmatrix} c_{00} \\ 0 \\ c_{10} \\ 0 \end{bmatrix} \text{ or } \begin{bmatrix} c_{00} \\ 0 \\ 0 \\ c_{10} \end{bmatrix} \quad (4.19)$$

Each symbol is an element from field  $GF(5)$ . Thus, antenna selection possibilities can have either  $c_{00}$  and  $c_{10}$  in the field  $GF(5)$ . This results in  $5 \times 5 \times 4 = 100$  total number of transmit vector combinations over one time slot for one antenna selection.

This gives the fact that each time when vector  $\mathbf{Y}$  is received, ML decoder searches the whole space i.e. all 100 possible vectors to decide the estimated transmitted vector  $\hat{\mathbf{X}}$ . Antenna selection bits are then decoded based on the positions of zeros in the estimated vector  $\hat{\mathbf{X}}$ . To recover the information bits the estimates are buffered until the whole codeword is formed. Hence it is necessary to receive the remaining  $(m-1)\hat{\mathbf{Y}}$  columns which are used to decode the information bits. It can be inferred from the above analysis that the mathematical complexity of the decoder is high in comparison with STBC-SM. However due to parallel processing architectures and efficient search algorithms, both the decoder stages can work in parallel, thus reducing the time taken to decode the information.

#### 4.4 NSTBC-SM Analytical Performance

In this section, we introduce the error performance of the NSTBC-SM system. In order to substantiate the exactness of Monte Carlo simulations executed in the proposed scheme, an analytical upper bound on the Average Bit Error Probability (ABEP) has been derived. A theoretical upper bound on the ABEP of SM systems can be given by [Younis (2014), Proakis (1998), Gesbert et al. (2003)].

The upper bound can be given by union bound as shown below,

$$ABER_{NSTBC-SM} = \frac{1}{2^{\lfloor C_2^{N_t} \log_2(q^2) \rfloor}} \sum_{i=1}^{2^{\lfloor C_2^{N_t} \log_2(q^2) \rfloor}} \sum_{j=1}^{2^{\lfloor C_2^{N_t} \log_2(q^2) \rfloor}} \frac{N(X_{SM} - \hat{X}_{SM})}{2\eta} E_H(P(X_{SM} \rightarrow \hat{X}_{SM})) \quad (4.20)$$

Here,  $E_H (P (X_{SM} \rightarrow \hat{X}_{SM}))$  is the average pairwise error probability obtained by averaging pairwise error probability (PEP)  $P (X_{SM} \rightarrow \hat{X}_{SM})$  over the channel matrix  $\mathbf{H}$ .

The upper bound can be given by union bound as shown below,

$$P(X_{SM} \rightarrow \hat{X}_{SM}) = Pr(\|y - H_c X_{SM}\|^2 > \|y - H_c \hat{X}_{SM}\|^2 | H) \quad (4.21)$$

Following [Basar et al. (2012)], the average PEP can be equated to Marcum-Q function (Craig's formula), and is be given by

$$E_H (P (X_{SM} \rightarrow \hat{X}_{SM})) = \frac{1}{\pi} \int_0^{\pi/2} \left( \frac{\sin^2 \theta}{\sin^2 \theta + c} \right)^{N_r} d\theta \quad (4.22)$$

We will now show that the above integral can be equated to  $J_m(c)$ , where  $c = \frac{\lambda_{i,j} E_s}{4N_0}$ .

Let us consider,

$$J_m(a, b) \triangleq \frac{a^m}{\Gamma(m)} \int_0^\infty e^{-at} t^{m-1} \left( \frac{1}{\pi} \int_0^{\pi/2} e^{-\frac{bt}{2\sin^2 \theta}} d\theta \right) dt \quad (4.23)$$

Interchanging the order of integration and simplifying equation (4.23) we get

$$J_m(a, b) \cong \frac{a^m}{\pi \Gamma(m)} \int_0^{\pi/2} \int_0^\infty t^{m-1} e^{-\left(a + \frac{b}{2\sin^2 \theta}\right) t} dt d\theta \quad (4.24)$$

We know that by definition the Gamma function is given by,

$$\Gamma(m) = \alpha^m \int_0^\infty t^{m-1} e^{-\alpha t} dt \quad (4.25)$$

letting  $\alpha = \left(a + \frac{b}{2\sin^2 \theta}\right)$  in equation (4.24) we get

$$\Gamma(m) = \left(a + \frac{b}{2\sin^2 \theta}\right)^m \int_0^\infty t^{m-1} e^{-\left(a + \frac{b}{2\sin^2 \theta}\right) t} dt d\theta \quad (4.26)$$

From equations (4.26) and (4.25) we can re-write equation (4.24) as

$$J_m(a, b) \cong \frac{a^m}{\pi \Gamma(m)} \int_0^{\pi/2} \frac{\Gamma(m)}{\left(a + \frac{b}{2\sin^2 \theta}\right)^m} d\theta = \frac{a^m}{\pi} \int_0^{\pi/2} \frac{1}{a^m \left(1 + \frac{b}{2\sin^2 \theta}\right)^m} d\theta \quad (4.27)$$

$$J_m(a, b) \cong \frac{1}{\pi} \int_0^{\pi/2} \left( \frac{1}{\left(1 + \frac{c}{\sin^2 \theta}\right)} \right)^m d\theta = \frac{1}{\pi} \int_0^{\pi/2} \left( \frac{\sin^2 \theta}{(\sin^2 \theta + c)} \right)^m d\theta \quad (4.28)$$

where  $c = \frac{b}{2a}$

From equation (4.24) and (4.28) we see that if  $c = \frac{b}{2a} = \frac{\lambda_{i,j}E_s}{4N_0}$  and  $m = N_r$  equation (4.24) can be written as

$$\frac{1}{\pi} \int_0^{\pi/2} \left( \frac{\sin^2 \theta}{(\sin^2 \theta + c)} \right)^m d\theta = J_{N_r} \left( \frac{\lambda_{i,j}E_s}{4N_0} \right) \quad (4.29)$$

Finally, we know that  $J_m(c)$  has a closed form expression given by

$$J_m(c) = \frac{1}{2} \left[ 1 - \mu(c) \sum_{k=0}^{N_r-1} \binom{2k}{k} \left( \frac{1 - \mu^2(c)}{4} \right)^k \right] \quad (4.30)$$

Hence, equation (4.28) can be written as

$$J_m \left( \frac{\lambda_{i,j}E_s}{4N_0} \right) = \frac{1}{2} \left[ 1 - \mu \left( \frac{\lambda_{i,j}E_s}{4N_0} \right) \sum_{k=0}^{N_r-1} \binom{2k}{k} \left( \frac{1 - \mu^2 \left( \frac{\lambda_{i,j}E_s}{4N_0} \right)}{4} \right)^k \right] \quad (4.31)$$

A simplified upper bound:

Equation (4.31), provides an upper limit on probability of error of the proposed NSTBC-SM. A more simple equation of ABER can be obtained by considering the nature of  $\sin^2 \theta$ . Since  $\sin \theta$  is a monotonically increasing function of  $\theta$  in the interval  $(0, \pi/2)$ , an upper bound on its integral in the interval  $(0, \phi)$ ,  $\phi \leq \pi/2$  can be found by setting  $\sin \theta = \sin \phi$ . Thus we get

$$\frac{1}{\pi} \int_0^{\phi} \left( \frac{\sin^2 \theta}{\sin^2 \theta + c} \right)^{N_r} d\theta \leq \frac{\phi}{\pi} \left( \frac{\sin^2 \phi}{\sin^2 \phi + c} \right)^{N_r} \quad (4.32)$$

for  $\phi = \pi/2$  the upper bound can be represented as shown in (4.32).

$$\frac{1}{\pi} \int_0^{\pi/2} \left( \frac{\sin^2 \theta}{\sin^2 \theta + c} \right)^{N_r} d\theta \leq \frac{1}{2(1+c)^{N_r}} \quad (4.33)$$

where,  $c = b/2a = (\lambda E_s)/(2N_0)$

Thus union bound on ABER can now be given by,

$$ABER_{NSTBC-SM} \leq \frac{1}{2 \left[ (c_2^{N_r})^2 \log_2(q^2) \right]} \sum_{i=1}^2 \left[ (c_2^{N_r})^2 \log_2(q^2) \right] \sum_{j=1}^2 \left[ (c_2^{N_r})^2 \log_2(q^2) \right] \frac{N(X_{SM} - \hat{X}_{SM})}{4\eta} \frac{1}{2(1+c)^{N_r}} \quad (4.34)$$

The proposed NSTBC is of dimension  $2 \times 2$  resulting in two non-zero Eigen values for the term  $(X_{SM} - \hat{X}_{SM})^H (X_{SM} - \hat{X}_{SM})$ . Hence for two non-zero Eigen values the upper bound is obtained by making an association with a closed-form result obtained by [Simon and Alouini (2005)]. The Average PEP is now given by

$$E_H(P(X_{SM} \rightarrow \hat{X}_{SM})) = \frac{1}{\pi} \int_0^{\pi/2} \left( \frac{1}{1 + \frac{\rho \lambda_{i,j1}}{4 \sin^2 \theta}} \right)^{N_r} \left( \frac{1}{1 + \frac{\rho \lambda_{i,j2}}{4 \sin^2 \theta}} \right)^{N_r} d\theta \quad (4.35)$$

Where  $\lambda_{i,j1}$  and  $\lambda_{i,j2}$  are the Eigen values of the distance matrix  $(X_{SM} - \hat{X}_{SM})^H (X_{SM} - \hat{X}_{SM})$ . We know that  $0 < \sin^2 \theta < 1$  which implies

$$\left( \frac{\sin^2 \theta}{\sin^2 \theta + c1} \right) \leq \frac{\sin^2 \theta}{c1} \quad (4.36)$$

$$\frac{1}{\pi} \int_0^{\pi/2} \left( \frac{\sin^2 \theta}{\sin^2 \theta + c1} \right)^{N_r} \left( \frac{\sin^2 \theta}{\sin^2 \theta + c2} \right)^{N_r} d\theta = \frac{1}{\pi} \int_0^{\pi/2} \left( \frac{\sin^2 \theta}{c1} \right)^{N_r} \left( \frac{\sin^2 \theta}{c2} \right)^{N_r} d\theta \quad (4.37)$$

$$= \frac{1}{c1^{N_r} c2^{N_r}} \int_0^{\pi/2} (\sin^2 \theta)^{2N_r} d\theta \quad (4.38)$$

From [Simon and Alouini (2005)] we know that,

$\frac{1}{\pi} \int_0^{\pi/2} \left( \frac{\sin^2 \theta}{\sin^2 \theta + c1} \right)^m d\theta$  has a closed form expression given by,

$$\frac{1}{\pi} \int_0^{\pi/2} \left( \frac{\sin^2 \theta}{\sin^2 \theta + c1} \right)^m d\theta \leq \frac{C_m^{2m}}{2^{2m+1} c^m} \quad (4.39)$$

and considering  $c=1$ ,

$$\int_0^{\pi/2} (\sin^2 \theta)^{2N_r} \leq \frac{\binom{2(2N_r)}{N_r}}{2^{2(2N_r)+1} 1^{N_r}} = \frac{\binom{4N_r}{2N_r}}{2^{4N_r+1}} \quad (4.40)$$

Therefore,

$$\frac{1}{c1^{N_r} c2^{N_r}} \int_0^{\pi/2} (\sin^2 \theta)^{2N_r} d\theta \leq \frac{1}{c1^{N_r} c2^{N_r}} \frac{\binom{4N_r}{2N_r}}{2^{4N_r+1}} \quad (4.41)$$

In this work we have considered the number of receive antennas to be 4, irrespective of the underlying NSTBC. Hence,

$$\frac{1}{c1^{N_r}c2^{N_r}} \int_0^{\frac{\pi}{2}} (\sin^2\theta)^{2N_r} d\theta \leq \frac{1}{c1^{N_r}c2^{N_r}} \frac{\left(C_{2N_r}^{(4N_r)}\right)}{2^{4N_r+1}} = \frac{1}{c1^4c2^4} \frac{\left(C_8^{16}\right)}{2^{17}} \quad (4.42)$$

Finally, from (4.20) we write

$$ABER_{NSTBC-SM} = \frac{1}{2^{\lfloor C_2^{N_t} \log_2(q^2) \rfloor}} \sum_{i=1}^{2^{\lfloor C_2^{N_t} \log_2(q^2) \rfloor}} \sum_{j=1}^{2^{\lfloor C_2^{N_t} \log_2(q^2) \rfloor}} \frac{N(X_{SM} - \hat{X}_{SM})}{2\eta} \frac{1}{c1^{N_r}c2^{N_r}} \frac{\left(C_{2N_r}^{(4N_r)}\right)}{2^{4N_r+1}} \quad (4.43)$$

## 4.5 Computational Complexity Analysis

In this section, we discuss the computational complexity of the proposed scheme in terms of number of real multiplications required. Let us determine the number of computations required to estimate  $|\mathbf{Y} - \mathbf{H}\hat{\mathbf{X}}|^2$  where,  $\mathbf{H}$  is the  $N_r \times N_t$  complex channel matrix,  $\hat{\mathbf{X}}$  is the  $N_t \times 1$  complex transmitted matrix,  $\mathbf{Y} - \mathbf{H}\hat{\mathbf{X}}$  is  $N_r \times 1$  complex receive matrix.

Since only two antennas are active at a time, multiplication of  $\mathbf{H} \cdot \hat{\mathbf{X}}$  requires  $2N_r$  complex multiplications.

$$|\mathbf{Y} - \mathbf{H}\hat{\mathbf{X}}|^2 = (\mathbf{Y} - \mathbf{H}\hat{\mathbf{X}})^H (\mathbf{Y} - \mathbf{H}\hat{\mathbf{X}})$$

The computational complexity step by step calculation is in accordance with the one explained in Section 3.4.1. In general, the computational complexity is  $cM^2$ , where  $c$  is the total number of codewords and  $M$  is the modulation index. [Basar et al. (2011)]. This is directly incorporated to our NSTBC-SM scheme, where the total number of codewords is  $q^m$  and modulation index is  $q$ .

## 4.6 Simulation Results and Performance Analysis

In this section we present the simulation results for NSTBC-SM system and make comparisons with STBC-SM [Basar et al. (2011)] and SM systems for a spectral efficiency of 4 and 5 bpcu. Further, the proposed system is compared with all conventional systems described in the literature such as STBC-SM, SM, QO-STBC, Srinath-STBC, SM-OSTBC and other SM schemes for a spectral efficiency of 6 bpcu under Rayleigh and Rician fading environments. Finally, the performance of the proposed scheme is evaluated over a spatially correlated fading channel environment.



We assume that  $N_t = N_r = 4$  and that the channel is characterized as exhibiting quasi static frequency flat fading. The Monte Carlo simulations are carried under the assumption that perfect channel state information is available at the receiver. Performance comparisons of all schemes are made at an ABER of  $10^{-5}$ .

#### 4.6.1 Performance Analysis under Rayleigh Channel conditions

In Spatial Modulation, symbol 0 represents the inactive state of antenna. In order to avoid ambiguity between the symbol 0 of the codeword and 0 representing the inactive antenna, the codeword symbol 0 is mapped to a nonzero prime number which is chosen to be the Gaussian integer or Eisenstein-Jacobi integer used to construct the complex field. In case of symbols from  $GF(5)$  the codeword symbol 0 in  $GF(5)$  is mapped to  $2 + i \equiv 0 \pmod{2 + i}$  in  $G_{2+i}$ , the codeword symbol 0 in  $GF(7)$  is mapped to  $3 + 2\rho \equiv 0 \pmod{3 + 2\rho}$  in  $G_{3+2\rho}$ , similarly codeword symbol 0 in  $GF(13)$  is mapped to  $3 + 2i \equiv 0 \pmod{3 + 2i}$  in  $G_{3+2i}$ , and codeword symbol 0 in  $GF(17)$  is mapped to  $4 + i \equiv 0 \pmod{4 + i}$  in  $G_{4+i}$ .

#### 4.6.2 STBC construction for 4 bpcu

Since  $N_t = 4$  and only two antennas are active at any given time, the total number of active antenna combinations is  $\binom{4}{2} = 6$ . We consider only 4 combinations as shown in Table 4.3. A spectral efficiency of  $\eta=4$  bpcu can be achieved by employing a cyclic code of length 3 over  $GF(5^2)$ . The average spectral efficiency is  $\log_2(4) + \frac{4}{2} = 4$  bpcu. Theorem 4.1 and Corollary specifies the encoding Algorithm 1 for determining full rank codeword matrices of order  $2 \times 2$  over  $GF(5)$ . We have employed this encoding algorithm to determine the codeword matrices of the cyclic code. The last  $(n - m = 3 - 2 = 1)$  columns of every codeword matrix are eliminated resulting in a codeword matrix specified as  $2 \times 2$  full rank matrix over  $GF(5)$ . These matrices have to be mapped into equivalent matrices over the complex number field. Since  $q = 5$  the mapping is done by employing rank preserving Gaussian integer map [Lusina et al. (2003)].

Table 4.4 Gaussian Map exponent Table  $G_{2+i}$ :

$s$	$\alpha^s$	$s$	$\alpha^s$
0	$2+i$	3	$-1$
1	$1$	4	$-i$
2	$i$		

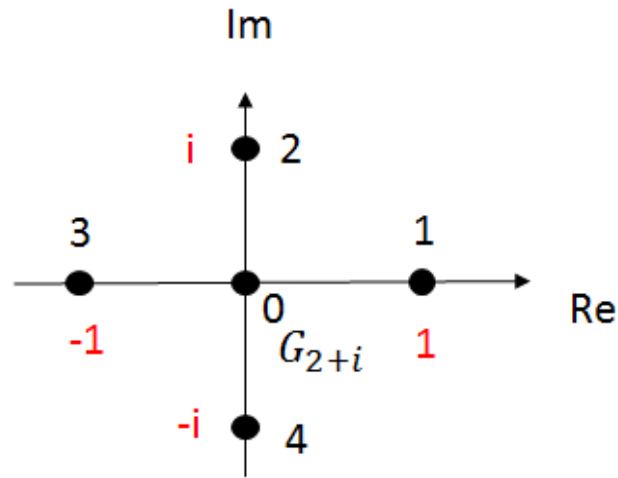


Figure 4.3 Gaussian Map Signal Constellation for  $G_{2+i}$

The mapping table and constellation diagram for  $G_{2+i}$  is given below.

In Figure 4.5 we present the BER performance of the NSTBC-SM over  $GF(5)$  and  $GF(7)$  for a spectral efficiency  $\eta=4, 4.5$  bpcu respectively. The figure also presents the ABEP upper bound curves of the proposed scheme evaluated using (4.43). It is observed that simulation results approach the derived upper bound for higher SNR values. It can be noted that the bound presented is not very tight. This is due to the fact that the decoding is two stage with the first stage decoding antenna index. The ABEP in the antenna index can be obtained by approximating the first term in (4.43) using analysis provided in [Younis (2014)]. The second term in (4.43) is observed to have negligible contribution to the overall ABEP at higher SNR regime.

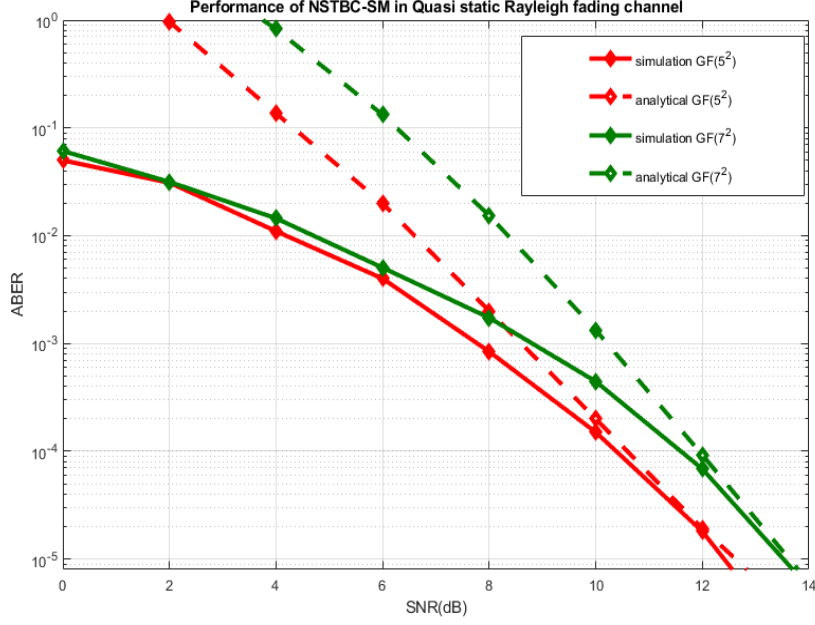


Figure 4.4 BER performance at 4 bpcu, for NSTBC-SM, with theoretical upper bounds

### 4.6.3 STBC construction for 4.5 bpcu using Eisenstein map

Since  $N_t = 4$ , and only two antennas are active at any given time, the total number of active antenna combinations is  $\binom{4}{2} = 6$ . We consider only 4 combinations as shown in Table 4.5. A spectral efficiency of  $\eta=4.5$  bpcu can be achieved by employing a cyclic code of length 4 over  $GF(7^2)$ . The average spectral efficiency is  $\log_2(4) + \frac{5}{2} = 4.5$  bpcu. Theorem 4.1 and Corollary specifies the encoding algorithm for determining full rank codeword matrices of order  $(2 \times 2)$  over  $GF(7)$ . We have employed this encoding algorithm to determine the codeword matrices of the cyclic code. Since  $q = 7$  the mapping is done by employing rank preserving Eisenstein map given by [K.Huber (1994)].

In Figure 4.7, we have presented the BER plots for NSTBC-SM with  $N_t = 4$ , over  $GF(5^2)$ , STBC-SM with  $N_t = 4$ , and 8-QAM as the modulation scheme and SM characterized by  $N_t = 4$ , and QPSK as the modulation scheme. It is observed that the perfor-

Table 4.5 Eisenstein Map exponent table of  $G_{3+2\rho}$ :

s	$\alpha^s$	s	$\alpha^s$
0	$3+2\rho$	4	-1
1	1	5	$-1-\rho$
2	$1+\rho$	6	$-\rho$
3	$\rho$		

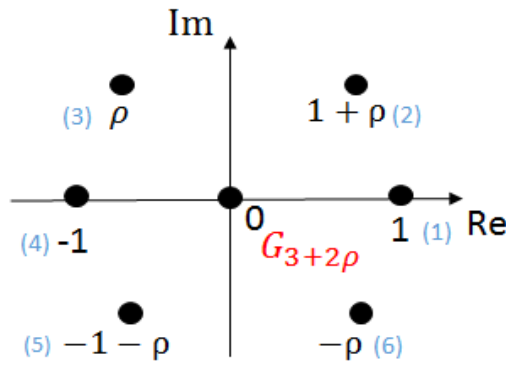


Figure 4.5 Eisenstein Map Signal Constellation for  $G_{3+2\rho}$

mance improvement of NSTBC-SM is  $\sim 2.3$  dB as compared to STBC-SM and  $\sim 4.3$  dB as compared to SM system. As a second example we have considered NSTBC-SM scheme employing a one dimensional non binary cyclic code over  $GF(7^2)$ . The Eisenstein map has been employed as it is a rank preserving map. This system is characterized by  $\eta = 4.5$  bpcu. We see that the proposed NSTBC-SM scheme provides a coding gain of  $\sim 1.5$  dB over STBC-SM scheme and  $\sim 3.6$  dB when compared to SM system.

#### 4.6.4 STBC construction for 5.5 bpcu using Gaussian map

These constructions are characterized by  $N_t = 4$  and only two antennas remain active at any given time. The total number of active antenna combinations is  $\binom{4}{2} = 6$ . A spectral efficiency of  $\eta = 5.5$  bpcu can be achieved by employing a one dimensional cyclic

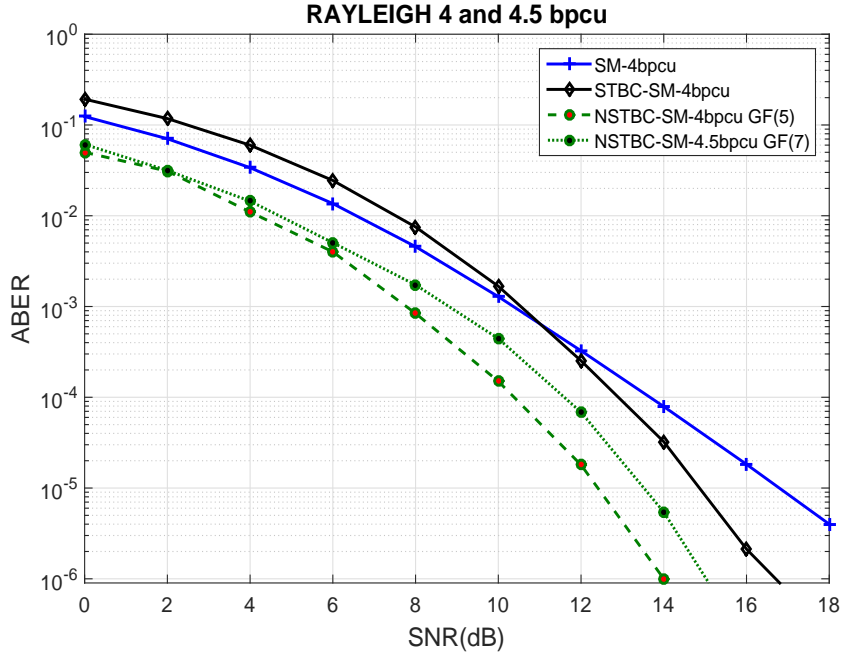


Figure 4.6 BER performance at 4 and 4.5 bpcu, for NSTBC-SM, STBC-SM, and SM in a Rayleigh Channel

code of length 7 over  $GF(13^2)$ . The average spectral efficiency is  $\log_2(4) + \frac{7}{2} = 5.5$  bpcu. Theorem 4.1 specifies the encoding algorithm for determining full rank codeword matrices of order  $2 \times 7$  over  $GF(13)$ . Using Corollary we have shortened the codeword matrices to  $(2 \times 2)$ . These matrices have to be mapped into equivalent matrices over the complex number field. Since  $q = 13$  the mapping is done by employing rank preserving Gaussian integer map [Lusina et al. (2003)]. Since the size of the codeword is  $13^2$  the number of bits that can be assigned to each codeword is  $\lfloor \log_2(13^2) \rfloor = 7$ . Hence information bit length is 7 and antenna selection average bit length is 4 for codeword of length 2.

In Figure 4.9 the performance of NSTBC-SM with  $N_t=4$ , over  $G_{(3+2i)}$  yielding a spectral efficiency of  $\eta=5.5$  bpcu is compared with the performance of STBC-SM with  $N_t=4$  and 16 QAM, SM with  $N_t=4$  and 8-QAM, both of which yield a spectral efficiency  $\eta=5$ . It is observed that NSTBC-SM provides a coding gain of 2.2 dB, 4.7

Table 4.6 Gaussian Map exponent table of  $G_{3+2i}$ :

$s$	$\alpha^s$	$s$	$\alpha^s$
0	$3+2i$	7	-1
1	1	8	$-1-i$
2	$1+i$	9	$-2i$
3	$2i$	10	$i$
4	$-i$	11	$-1+i$
5	$1-i$	12	-2
6	2		

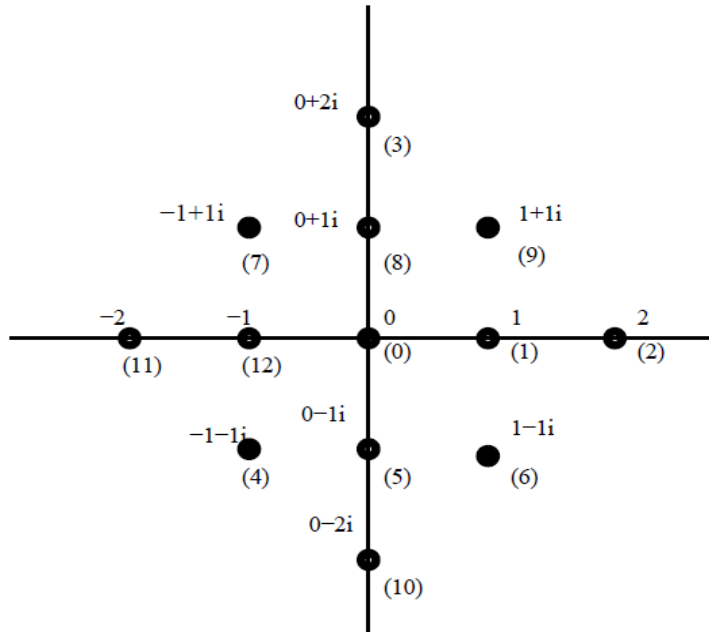


Figure 4.7 Gaussian Map Signal Constellation for  $G_{3+2i}$

dB over STBC-SM and SM system respectively.

#### 4.6.5 STBC construction for 6 bpcu using Gaussian map

These constructions are characterized by  $N_t = 4$  and only two antennas remain active at any given time. The total number of active antenna combinations is  $\binom{4}{2} = 6$ . A spectral efficiency of  $\eta = 6$  bpcu can be achieved by considering only 4 active combinations

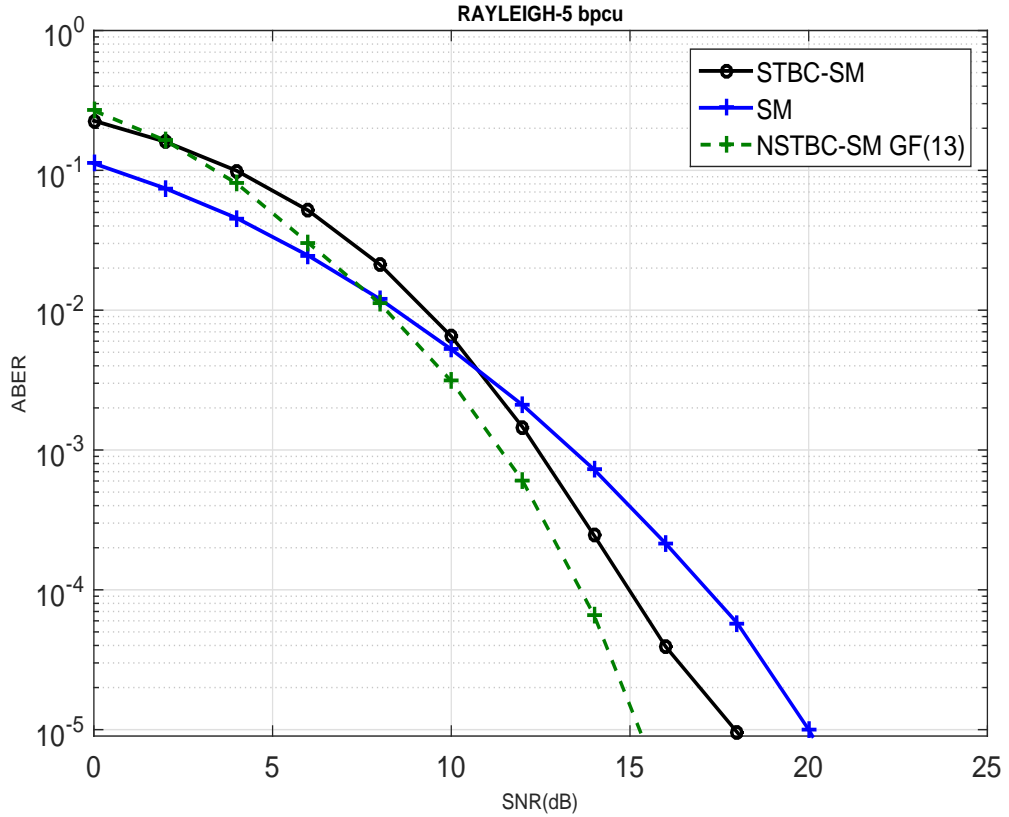


Figure 4.8 BER performance at 5 and 5.5 bpcu, exception for NSTBC-SM  $\eta=5.5$  bpcu, STBC-SM ( $\eta=5$ ), and SM ( $\eta=5$ ) over Rayleigh fading Channel.

and employing a one dimensional cyclic code of length 3 over  $GF(17^2)$ . The average spectral efficiency is  $\log_2(4) + \frac{8}{2} = 6$  bpcu . Theorem 4.1 and Corollary specifies the encoding algorithm for determining full rank codeword matrices of order  $(2 \times 2)$  over  $GF(17)$ . Since  $q = 17$  the mapping is done by employing rank preserving Gaussian integer map [Lusina et al. (2003)] . Since the size of the codeword is  $(17^2)$  the number of bits that can be assigned to each codeword is  $\lfloor \log_2(17^2) \rfloor = 8$ . Hence information bit length is 8 and antenna selection average bit length is 3 for the shortened codeword of length 2.

We initially present the ABER performance analysis of the proposed NSTBC-SM scheme with over  $GF(5^2)$ ,  $GF(7^2)$  and  $GF(17^2)$ . As a source of relative importance,

Table 4.7 Gaussian Map exponent table of  $G_{4+i}$ :

$s$	$\alpha^s$	$s$	$\alpha^s$	$s$	$\alpha^s$	$s$	$\alpha^s$
0	$4+i$	5	$i$	10	$-1-i$	15	2
1	1	6	$-1+i$	11	$-2i$	16	$-2+i$
2	$1+i$	7	-2	12	$1+2i$		
3	$2i$	8	$2-i$	13	$-i$		
4	$-1-2i$	9	-1	14	$1-i$		

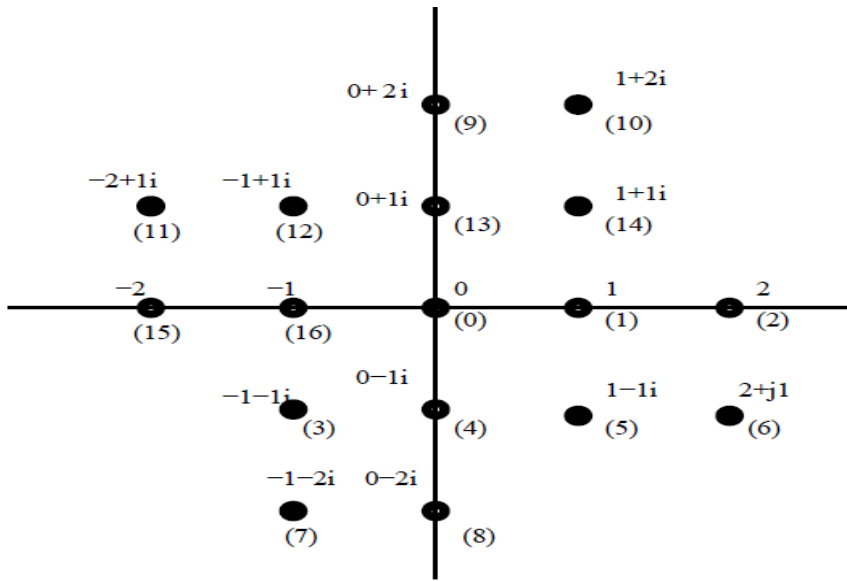


Figure 4.9 Gaussian Map Signal Constellation for  $G_{4+i}$

ABEP upper bound curves of the NSTBC-SM are synthesized and evaluated from (4.43) are depicted in Figure 4.11. The derived upper bound is very tight for higher SNR and is used to analyze the behavior of error that exists for different values of  $q$  in an NSTBC-SM scheme.

Figure 4.12 shows the comparison of ABER of the proposed NSTBC-SM scheme with STBC-SM [Basar et al. (2011)] (both  $(4 \times 4)$  and  $(8 \times 4)$  systems), Srinath STBC [Srinath and Rajan (2009)], SM-OSTBC, QOSTBC [Le et al. (2014)] and conventional SM schemes, all frameworks are designed to give a spectral efficiency of 6 bpcu. The conventional STBCs like Srinath-STBC, SM-OSTBC, QOSTBC and SM schemes use 16 QAM, STBC-SM  $(4 \times 4)$  uses 32 QAM and STBC-SM  $(8 \times 4)$  uses 16 QAM con-



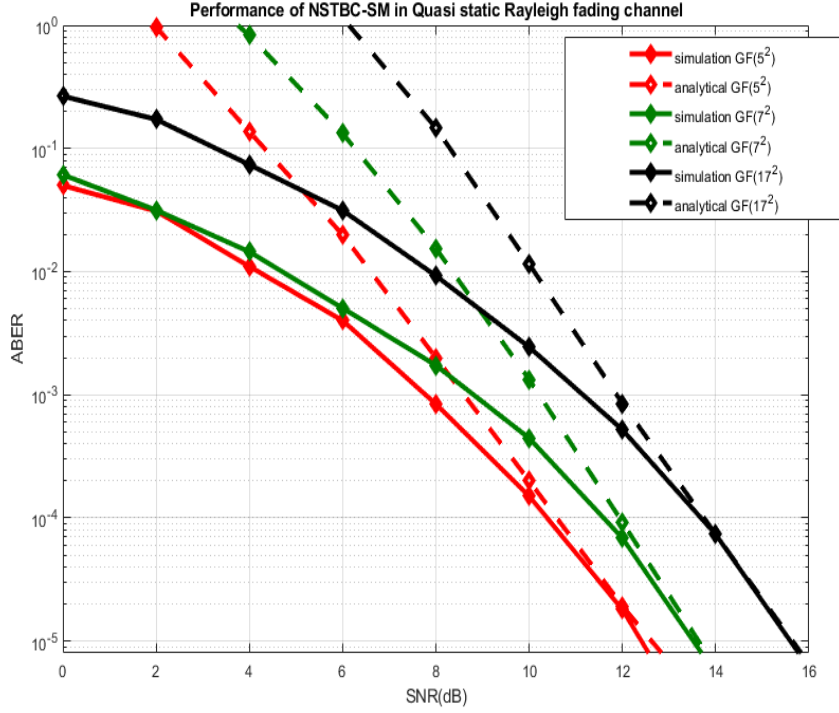


Figure 4.10 Analytical and simulated ABER performance of NSTBC-SM.

figurations to achieve the above spectral efficiency. It is observed that a coding gain of 1.2 dB, 2 dB, 2 dB, 4 dB, 5.1 dB and 6.2 dB over Srinath-STBC, SM-OSTBC, STBC-SM ( $8 \times 4$ ), STBC-SM ( $4 \times 4$ ), SM and QOSTBC systems is achieved respectively. The presence of error correcting structure in the proposed NSTBC scheme leads to the improvement in ABER performance over conventional STBC systems.

#### 4.6.6 Performance Analysis Under Rician Channel Conditions:

It is expected that similar performance trend follows under Rician channel conditions. However to prove our claim we present the performance analysis of the proposed scheme under Rician channel conditions for 6 bpcu.

To achieve  $\eta = 6$  bpcu we have constructed codewords of length 4 over  $GF(17^2)$  as explained in the previous section.

In Figure 4.13: BER plots for NSTBC-SM with  $N_t = 4$ , over  $G_{4+i}$ , STBC-SM employing  $N_t = 4$  and 32 QAM, SM system  $N_t = 4$  and 16 QAM, GNSM system  $N_t = 4$

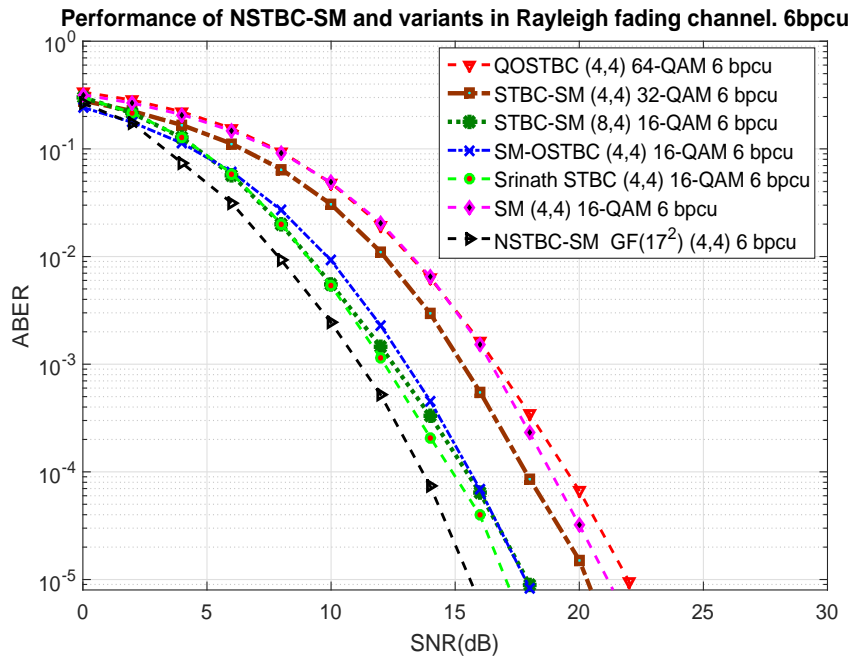


Figure 4.11 ABER performance comparison of various schemes with NSTBC-SM achieving  $\eta = 6$  bpcu with  $N_t = 4$ ,  $N_r = 4$  and  $N_a=2$ .

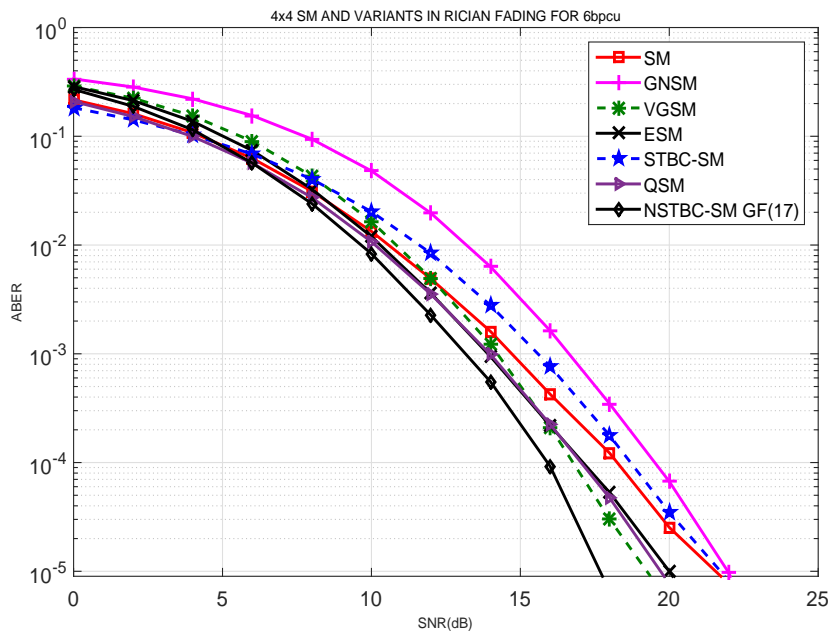


Figure 4.12 BER performance at 6 bpcu for NSTBC-SM, STBC-SM, VGSM, GNSM, ESM, QSM and SM in a Rician fading Channel with  $K=3$ .

and 16 QAM, VGSM system with  $N_t = 4$  and 8 QAM, QSM system with  $N_t = 4$  and QPSK and finally ESM system with  $N_t = 4$  and QPSK is considered to produce a spectral efficiency of 6 bpcu. Rician Fading channel with ( $K = 3$ ). Proposed NSTBC-SM clearly shows superior performance as compared to all the conventional SM schemes. It is observed that NSTBC-SM offers very high coding gains of 1.7 dB, 2.0 dB, 2.3 dB, 4 dB, 4.3 dB, 4.7 dB over VGSM, QSM, ESM, SM, STBC-SM and GNSM systems respectively.

#### **4.6.7 Performance Analysis Under Spatially Correlated Channel Conditions**

[Mesleh et al. (2010),Basar et al. (2011)] have studied the performance of Trellis coded spatial modulation (TCSM) and STBC-SM respectively for  $\eta = 6$  over spatially correlated channels. We have synthesized a NSTBC-SM design with  $\eta = 6$  for use over spatially correlated channels. The performance of NSTBC-SM has been compared with the results published in [Basar et al. (2011), Mesleh et al. (2010)]. In Figure 4.13, the performance of NSTBC-SM with  $N_t = 4$ , over  $G_{4+i}$ , STBC-SM with  $N_t = 4$ , and 32 QAM and SM with  $N_t = 4$ , and 16 QAM has been compared. It is observed that NSTBC-SM shows improvement of 1 dB in lower SNR regime (8 dB to 18 dB). The performance of NSTBC-SM and STBC-SM converge at a SNR of 22 dB. It is also seen that NSTBC-SM shows an improvement of  $\sim 5$  dB over SM systems in spatially correlated environments.

#### **4.7 Summary**

In this second contributory work, a novel Nonorthogonal Space time Block Coded spatial modulation has been proposed as an improvement over conventional SM-MIMO transmission scheme and their variants such as STBC-SM, SM and GNSM, VGSM, QSM and ESM schemes. Comparisons have been carried out over Rayleigh fading, Rician fading and spatially correlated fading environments. An improvement in spectral efficiency is obtained by judiciously associating certain data bits with antenna indices. The transmit diversity order is retained to be 2 for comparison with schemes described in literature. The proposed scheme has the advantage that it can be generalized to any

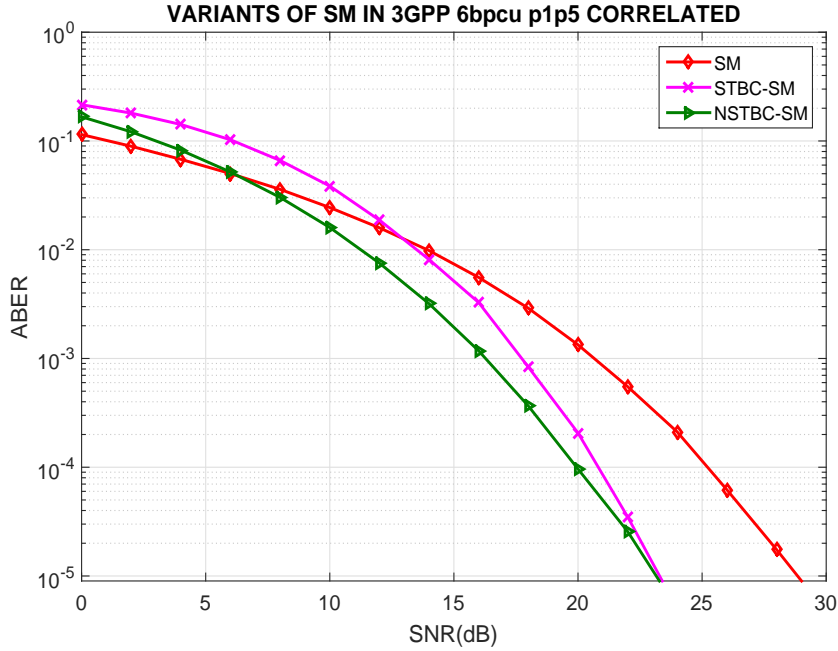


Figure 4.13 BER performance at 6 bits/s/Hz for NSTBC-SM, STBC-SM, and SM in a quasi-static flat channel Spatially Correlated channel with a inter antenna separation  $0.1\lambda$  at the TX and  $0.5\lambda$  at the RX.

number of antennas, and any transmit diversity orders. Our schemes exhibit coding gains superior to those described in literature for comparable spectral efficiencies. We have derived an upper bound on the performance of these codes and have carried out analysis of the computational complexity involved in decoding. The proposed NSTBC-SM scheme offers coding gains ranging from  $\sim 1.2$  dB to 2.8 dB over STBC-SM and  $\sim 4$  dB over SM systems. In conclusion, we feel that the proposed NSTBC-SM scheme can be effectively employed in the design of high-rate spectrally efficient MIMO wireless communication systems such as LTE, LTE Advanced and WiMAX. In addition, the proposed NSTBC-SM scheme is also superior in performance to competing schemes over spatially correlated environments.

The next contributory chapter in the thesis analyzes the effect of Imperfect channel state information on the performance of the designed scheme. The motivation behind this work started with the idea of analyzing the performance deterioration of conventional SM systems in the presence of varied channel state information.

## Chapter 5

# A Comprehensive Framework for Double Spatial Modulation Under Imperfect Channel State Information

<sup>1</sup> The essential requirement for a 5G wireless communication system is the realization of energy efficient as well as spectrally efficient modulation schemes. Double Spatial Modulation (DSM) is a recently proposed high rate Index Modulation (IM) scheme, designed for use in Multiple Input Multiple Output (MIMO) wireless systems. The aim of this scheme is to increase the spectral efficiency of conventional Spatial Modulation (SM) systems while keeping the energy efficiency intact. In this work, the impact of imperfect channel knowledge on the performance of DSM system under Rayleigh, Rician and Nakagami-m fading channels has been quantified. Later, a low complexity decoder for the DSM scheme has been analyzed using Ordered Block Minimum Mean Square Error (OB-MMSE) criterion. Its performance under varied fading environments have been quantified via Monte Carlo simulations. Finally, a closed form expression for the Pairwise Error Probability (PEP) for a DSM scheme under conditions of perfect and imperfect channel state information has been derived. This is employed to calculate the upper bound on the Average Bit Error Probability (ABEP) over aforementioned fading channels. It is observed that, under perfect and imperfect channel conditions DSM outperforms all the other variants of SM by at least 2 dB at an Average Bit Error Ratio (ABER) of  $10^{-5}$ . Tightness of the derived upper bound is illustrated by Monte Carlo

---

<sup>1</sup>Goutham Simha G.D., et al., A comprehensive framework for Double Spatial Modulation under imperfect channel state information, Volume 25 Part-2 pp 519-526, Physical Communication (2017) Elsevier.

simulation results.

## 5.1 Introduction

Considering the exigent objectives for next generation 5G wireless communication systems, researchers have propounded intelligent and novel physical layer modulation techniques. To extend the spectral efficiency in SM-MIMO systems Younis et.al, came up with the idea of Generalized Spatial Modulation (GNSM) in which the number of active antennas is increased to two [Younis (2014)]. The primary limitation of this scheme when compared with conventional SM is its requirement of more than one RF chain. SM systems enable a logarithmic improvement in the multiplexing gain with an increase in the number of antennas. A new technique was proposed by Mesleh et.al, known as the Quadrature Spatial Modulation (QSM) which retains the structural features of conventional SM systems, while providing an improvement in spectral efficiency [Mesleh et al. (2015)]. In order to improve the performance over conventional SM systems, a Euclidean distance based Enhanced Spatial Modulation (ESM) was developed by Cheng et.al, in this technique active antenna combinations vary as one or two. The ESM technique uses primary constellation points if one antenna is active and employs secondary constellation if two antennas become active. In order to associate identical number of antenna bits with every antenna combination, a number of bits associated with secondary constellation is half of the number of bits involved in primary. (16 QAM, 4 QAM), (4 QAM,BPSK) are some specific examples of primary and secondary constellations [Cheng et al. (2015)]. It has been shown with proper analytical reasoning that QSM systems outperform SM systems in almost all uncorrelated fading environments under conditions of identical spectral efficiency and antenna number [Mesleh and Ikki (2015)]. Younis et.al proposed a performance study of QSM systems over Nakagami-m fading channels which enumerates the advantages of QSM systems over SM systems in different non uniform Nakagami-m fading channels [Younis et al. (2016)]. In order to have a twofold increase in spectral efficiency as compared to traditional SM scheme, Zehra and Basar proposed a high rate IM scheme for use in MIMO and large MIMO systems which is designated as Double Spatial Modulation (DSM) [Yigit and Basar (2016)]. The primary advantage of this technique is that it allows the activation of more

than one antenna which leads to higher spectral efficiency. This scheme can allow an improvement in spectral efficiency from 10 bpcu to 16 bpcu, which is a requirement in 5G wireless communication environment. In DSM scheme, the first bit splitter splits the incoming data bits into two SM streams. The upper SM configuration processes bits provided to it in the conventional manner. Bits fed to the lower block are processed by an SM stream which employs an optimally rotated signal constellation of identical size. This has been done exclusively to improve the ease of detection [Yigit and Basar (2016)]. ML decoding is optimum, but has the disadvantage of requiring a large number of computations. Yue Xiao et.al proposed a low complexity decoding technique known as the OB-MMSE, which achieves near ML execution with eighty percent reduction in computational complexity [Xiao et al. (2014)]. The primary focus and the contributions of this chapter are broadly classified as follows:

- To propose a framework for the contemporary high rate index modulated DSM scheme under conditions of perfect and imperfect channel information over Rayleigh, Rician and Nakagami-m fading channels.
- For any MIMO system, a more adaptable and pragmatic framework can be obtained by implementing non-uniform phase distribution of Nakagami-m channel as given in [Yacoub (2009)]. A special case study of the DSM scheme under Nakagami-m fading environment with Perfect Channel State Information (P-CSI) and Imperfect Channel State Information (Imp-CSI) is described and simulated. This is to quantify the performance of DSM scheme in Nakagami-m fading environment under conditions of non-uniform phase distribution for different values of m.
- To design and evaluate the performance of a low complexity OB-MMSE signal detector for a DSM system over ML detection.

## 5.2 System and Channel Model

The system model of a DSM (high rate index modulated) scheme is shown in Figure 5.1 [Yigit and Basar (2016)]. The system under consideration is in the form of  $N_t \times$

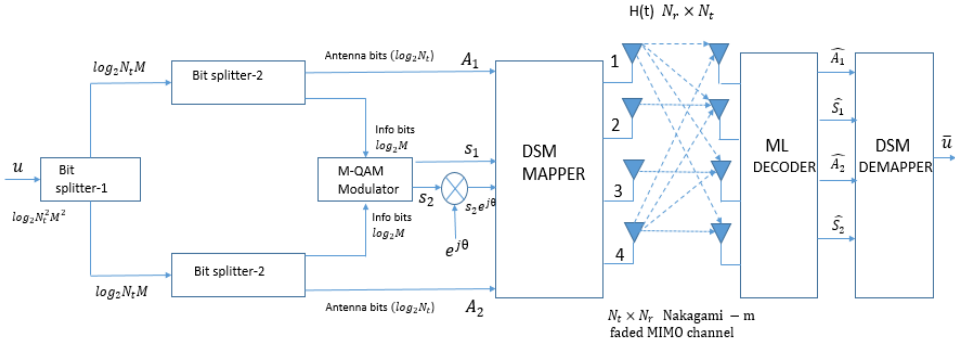


Figure 5.1 Block diagram for DSM system [Yigit and Basar (2016)]

$N_r$  MIMO arrangement where,  $N_t$  denotes the number of transmit antennas,  $N_r$  is the number of receive antennas and  $M$  is the constellation order. The spectral efficiency of this scheme is defined to be  $\log_2(N_t^2 M^2)$  bpcu. Let us consider that  $\log_2(N_t^2 M^2)$  bits are to be transmitted. Bit splitter-1 arrangement divides these bits into two equal halves. Each stream contains  $\log_2(N_t M)$  bits. From this arrangement, it is apparent that DSM can be viewed as two individual SM systems working in tandem. Later, bit splitter-2 splits the data symbols into information bearing bits and antenna indexing bits. At this stage, the  $\log_2(M)$  bits constitute to information bits and  $\log_2(N_t)$  bits represent antenna selection bits respectively. It can be inferred from Figure 5.1 that, the first information symbol  $S_1$  is directly radiated from the transmit antenna indexed as  $A_1$ . The second information symbol  $S_2$  is rotated by an optimum angle  $\theta$  (which depends upon the constellation) prior to transmission over the second active transmit antenna, indexed as  $A_2$ . To minimize bit error rate, the optimized rotation angle  $\theta$  has been determined for commonly used MQAM constellations [Yigit and Basar (2016)]. The transmission vector  $\mathbf{s} \in \mathbb{C}^{N_t \times 1}$  is of the form

$$\mathbf{S} = [\mathbf{0} \cdots \underbrace{S_1}_{A_1} \cdots \mathbf{0} \cdots \underbrace{S_2 e^{j\theta}}_{A_2} \cdots \mathbf{0} \cdots \mathbf{0}]^T \quad (5.1)$$

vector  $\mathbf{s}$  is transmitted over a frequency flat MIMO channel of size  $N_r$ . Let  $\mathbf{H}$  be a  $N_r \times N_t$  channel matrix,  $\mathbf{n}$  is a column vector containing circularly symmetric complex Gaussian number as elements  $C \mathcal{N}(0, \sigma^2)$ . The elements of  $\mathbf{n}$  are assumed to be independent and identically distributed (i.i.d).

The received signal can be characterized by



$$\mathbf{Y} = \mathbf{H} \mathbf{S} + \mathbf{n}; \quad y = h_{A_1} S_1 + h_{A_2} S_2 e^{j\theta} + \mathbf{n} \quad (5.2)$$

where,  $\mathbf{Y}$  is a  $\mathbb{C}^{N_r \times 1}$  matrix,  $\mathbf{n} \in \mathbb{C}^{N_r \times 1}$ ,  $h_{A_1} S_1$  and  $h_{A_2} S_2$  indicate the respective column vectors.

The performance analysis of spectrally efficient DSM scheme over Rayleigh, Rician and Nakagami-m fading channels with P-CSI and Imp-CSI is analytically derived and quantified. Later, as a special case we have studied the characteristics of DSM scheme under Nakagami-m fading environment for uniform and non-uniform distribution. The following subsections describe the channel models for various fading environments.

### 5.2.1 Rayleigh and Rician Fading Channels

The channel matrix is constructed as given in [Koca and Sari (2012), Younis (2014), Duman and Ghayeb (2008)]. Realization of both Rayleigh and Rician fading channels in uncorrelated and correlated scenarios is presented.

$$\mathbf{H}_c = \mathbf{R}_{\text{REC}}^{1/2} \cdot \mathbf{H} \cdot \mathbf{R}_{\text{TRAN}}^{1/2} \quad (5.3)$$

As shown in equation (2.2) the entries of the Rician channel matrix  $\mathbf{H}$  are modeled as given in [Younis (2014), Koca and Sari (2012)]

$$\mathbf{H}_{c(\text{Rician})} = \sqrt{\frac{K}{1+K}} \bar{\mathbf{H}} + \sqrt{\frac{1}{1+K}} \mathbf{H} \quad (5.4)$$

For a Rician fading channel the mean matrix is expressed as

$$\bar{\mathbf{H}} = \sqrt{\frac{K}{1+K}} \times \mathbf{1}_{N_r \times N_t} \quad (5.5)$$

where,  $K$  denotes the Rician factor,  $K/(1+K)$  constitutes to average power of the LoS component,  $\bar{\mathbf{H}}$  is the mean matrix and is defined as matrix of all ones,  $1/(1+K)$  is the average power of the random component and  $\mathbf{H}$  is a Rayleigh  $N_r \times N_t$  matrix whose entries are complex i.i.d Gaussian random variables with zero mean and unit variance.

### 5.2.2 Nakagami-m Fading Channels

As mentioned in the Introduction, various researchers have analyzed the performance of several MIMO schemes under Nakagami-m fading environment by considering the assumption that phase distribution is uniform. For a Nakagami fading the special case

of uniform distribution is obtained when  $m=1$ . Under this condition, the Nakagami distribution is identical to the Rayleigh distribution. Similarly when  $m= \infty$ , Nakagami fading reduces to the non-fading Additive White Gaussian Noise (AWGN) environment. It resembles Hoyt distribution (also known as Nakagami- $q$  distribution) when the value of  $m$  is less than 1 [Younis (2014)].

The behavior of Nakagami- $m$  distribution is mainly used to describe channels perturbed by mild to severe fading. In this work, we investigate the performance of DSM scheme over more realistic non-uniform phase distributed Nakagami- $m$  fading channel [Younis (2014), Younis et al. (2016), Yacoub (2009)].

The channel matrix for Nakagami- $m$  fading is formulated using [Younis (2014)]

$$h_{r,t} = \sqrt{\sum_{i=1}^m |\mathbb{Z}_i^R|^2} + j\sqrt{\sum_{i=1}^m |\mathbb{Z}_i^I|^2} \quad (5.6)$$

$\mathbb{Z}_i^R, \mathbb{Z}_i^I$  are circularly symmetric i.i.d Gaussian random variables with zero mean and variance is equal to  $\sigma_{\mathbb{Z}}^2 = 1/(2m)$  and  $m$  is the Nakagami parameter.

The envelope of the Nakagami- $m$  fading channel is described as shown in (5.6).

$$p(\varpi) = \frac{2m^m \varpi^{2m-1}}{\Gamma(m)} e^{-m\varpi^2} \quad (5.7)$$

where,  $\Gamma(\cdot)$  is the Gamma function and  $\varpi$  is a random variable.

Additionally, we define PDF of the phase according to real time investigations as demonstrated in [Yacoub (2009)]

$$p(\phi) = \frac{\Gamma(m) |\sin(2\phi)|^{m-1}}{2^m \Gamma^2(\frac{m}{2})}. \quad (5.8)$$

where,  $\phi$  is the phase corresponding to Nakagami- $m$  distribution. Our major interest is to analyze and quantify the performance of DSM scheme with P-CSI and Imp-CSI. This channel model is in accordance with that shown in [Mesleh and Ikki (2015)]. Here we have considered estimate of the channel  $\mathbf{H}$  to be  $\hat{\mathbf{H}}$  and that the elements of  $\mathbf{H}$  and  $\hat{\mathbf{H}}$  both are jointly ergodic and stationary Gaussian random processes. Moreover, we expect that the estimate of the channel  $\hat{\mathbf{H}}$  and estimation error  $\mathbf{E}$  are orthogonal to each other and can be written analytically as

$$\mathbf{H} = \hat{\mathbf{H}} + \mathbf{E} \quad (5.9)$$

here,  $\mathbf{E}$  is defined to be complex Gaussian with zero mean and variance  $\sigma_e^2$ . Note that  $\sigma_e^2$  is the variance parameter that subjugates the condition of channel estimation.

### 5.2.3 Optimal ML and Suboptimal OB-MMSE decoding strategies for DSM

In this section, two decoding strategies have been employed namely optimal ML and suboptimal OB-MMSE detection which is used to reduce the complexity of search space.

### 5.2.4 Optimal ML detection

ML detection is used to distinguish the symbols and to achieve a optimal BER performance for the considered DSM scheme. The antenna indices ( $A_1, A_2$ ) and information symbols ( $S_1, S_2$ ) which were transmitted from the combination of active antennas are detected at the receiver side. Joint estimation of these antenna indices and MQAM information symbols are estimated over an exhaustive ML search metric of  $N_t^2 M^2$ .

$$[\hat{S}_1, \hat{S}_2, \hat{A}_1, \hat{A}_2] = \arg \min_{S_1, S_2, A_1, A_2} \left\| \mathbf{Y} - (h_{A_1} S_1 + h_{A_2} S_2 e^{j\theta}) \right\|^2 \quad (5.10)$$

### 5.2.5 Suboptimal OB-MMSE detection

Although ML produces the optimal solution for decoding or detection, nevertheless the complexity of ML system increases exponentially with the increase in number of transmit antennas. This hinders its implementation in practical systems. Yue Xiao et.al. proposed a low complexity decoder scheme which has a stable trade-off between complexity and the error performance [Xiao et al. (2014)].

A low complexity OB-MMSE algorithm for use in DSM systems is presented in this section. Following [Xiao et al. (2014)], complete algorithm is explained below. The received vector is first processed to determine the Transmit Antenna Combinations (TACs). Pseudo-inverse of each channel has been computed to evaluate  $z$ .

Let  $\mathbf{Y}$  denote the received vector,  $\mathbf{H}$  denotes the channel matrix,  $N_t$  denote the total number of transmit antennas,  $N_a$  denote the number of active antennas. For a DSM scheme the number of active antennas is equal to one or two.  $I = (I_1, I_2, I_3 \dots I_N)$  is the set of  $N_a$  active transmit antenna combinations in the  $i^{th}$  TAC,  $V_{th} = 2N_R\sigma^2$  is the threshold value. OB-MMSE is an ordering algorithm firstly developed to sort the transmit antenna combinations (TACs). The Pseudo-inverse [best approximate solution] of each channel column is carried out to find the transmitted vector.

$$z = [z_1, z_2 \dots z_{N_t}]^T$$

$z_k = (h_k)^\dagger y$ ,  $(h_k)^\dagger = \frac{h_k^H}{h_k^H h_k}$  where  $k \in [1, 2, 3 \dots N_t]$ . To measure the reliability of each TAC, the absolute squared values have been calculated.

$w_i = z_{i1}^2 + z_{i2}^2 + \dots + z_{iN_a}^2 = \sum_{n=1}^{N_a} z_{in}^2$  where  $i \in \{1, 2, 3 \dots N\}$ . Now sort the weighting factors in descending order to obtain the combination of radiating antennas.

$$[k_1, k_2 \dots k_n] = \arg \text{sort}(w)$$

In order to estimate symbol from the corresponding active transmit antenna

$$\begin{aligned} \tilde{S}_{j1} &= Q1 \left( \left( (H_{I_{k_j}})^H H_{I_{k_j}} + \sigma^2 I \right)^{-1} (H_{I_{k_j}})^H y \right) \\ \tilde{S}_{j2} &= Q2 \left( \left( (H_{I_{k_j}})^H H_{I_{k_j}} + \sigma^2 I \right)^{-1} (H_{I_{k_j}})^H y \right) \end{aligned}$$

Due to the rotation angle introduced in the second transmit symbol in DSM, rotated constellation map has to be considered in its detection. We define digital modulator functions  $Q1(\cdot)$  and  $Q2(\cdot)$  with respect to the MQAM and rotated MQAM constellation maps. In order to reduce the computational complexity for detecting all possible  $N$  transmit antenna combinations the block MMSE detector will terminate the output if  $(k_j, \tilde{S}_j)$  satisfies the threshold rule then antenna and constellation points are updated.

$$d_j = \left\| y - H_{I_{k_j}} \tilde{S}_j \right\|_F^2 \leq V_{th}; \quad \hat{I} = I_{k_j} \quad \hat{S} = \tilde{S}_j$$

Else the detector updates and continue with the next estimate, if  $j > N$  then the detector is equivalent to the optimal ML detector.

$$u = \arg \min_j \left\| y - H_{I_{k_j}} \tilde{S}_j \right\|_F^2 \text{ for } j \in \{1, 2, 3 \dots N\}$$

update the value  $\hat{I} = I_{k_u}$   $\hat{S} = S_u$ .

### 5.3 Analytical treatment for DSM under fading scenarios:

Analytical framework for the ABEP of DSM system under Rayleigh, Rician and Nakagami-m fading environments with P-CSI and Imp-CSI has been derived in this section.

When the symbol  $S$  is transmitted and it is erroneously detected as  $\hat{S}$ , then conditional pairwise error probability (CPEP) can be calculated as shown in [Yigit and Basar (2016), Duman and Ghrayeb (2008), Simon and Alouini (2005), Forenza et al. (2004)].

#### 5.3.1 Case 1: Perfect-CSI

$PEP(S \rightarrow \hat{S}|H)$

$$\begin{aligned} CPEP &= P_r(\|y - HS\|^2 > \|y - H\hat{S}\|^2 | H) \\ &= P_r(\|HS\|^2 - \|H\hat{S}\|^2 - 2\Re\{y^H(HS - H\hat{S})\} > 0) \\ P(S \rightarrow \hat{S}|H) &= \frac{1}{\pi} \int_0^{\pi/2} \exp\left(-\frac{\|H(S - \hat{S})\|^2}{4N_0 \sin^2 \theta}\right) d\theta \end{aligned} \quad (5.11)$$

for Rayleigh channel PEP can be expressed as follows:

$$P(S \rightarrow \hat{S}) = \frac{1}{\pi} \int_0^{\pi/2} \left( \frac{\sin^2 \theta}{\sin^2 \theta + \frac{H\|S - \hat{S}\|^2}{4N_0}} \right)^{N_r} d\theta \quad (5.12)$$

From [Simon and Alouini (2005)] we know that

$$J_m(a, b) \triangleq \frac{a^m}{\gamma(m)} \int_0^\infty e^{-at} t^{m-1} Q(\sqrt{bt}) dt = \frac{1}{2} \left[ 1 - \mu(c) \sum_{k=0}^{m-1} \binom{2k}{k} \left( \frac{1 - \mu^2(c)}{4} \right)^k \right] \quad (5.13)$$

$$\mu(c) \triangleq \left( \sqrt{\frac{c}{1+c}} \right); \quad c = \frac{H\|S - \hat{S}\|^2}{4N_0} \quad (5.14)$$

the R.H.S term in equation (5.12) is of the form

$$\frac{1}{\pi} \int_0^{\pi/2} \left( \frac{\sin^2 \theta}{\sin^2 \theta + C} \right)^m d\theta = \frac{a^m}{\pi} \int_0^{\pi/2} \left( \frac{1}{a^m \left( 1 + \frac{c}{\sin^2 \theta} \right)^m} \right) d\theta \quad (5.15)$$

equation (5.15) can be simplified as

$$= \frac{a^m}{\pi \gamma(m)} \int_0^{\pi/2} \left( \frac{\gamma(m)}{\left( a + \frac{ac}{\sin^2 \theta} \right)^m} \right) d\theta \quad \text{where, } \gamma(m) = \int_0^\infty e^{-at} t^{m-1} dt \quad (5.16)$$

Let us consider,

$$J_m(a, b) = \frac{a^m}{\Gamma(m)} \int_0^\infty e^{-at} t^{m-1} \left( \frac{1}{\pi} \int_0^{\pi/2} e^{-\frac{bt}{2\sin^2 \theta}} d\theta \right) dt \quad (5.17)$$

Interchanging the order of integration and simplifying equation (5.15) we get

$$J_m(a, b) \cong \frac{a^m}{\pi \Gamma(m)} \int_0^{\pi/2} \int_0^\infty t^{m-1} e^{-\left(a + \frac{b}{2\sin^2 \theta}\right)t} dt d\theta \quad (5.18)$$

We know that by definition the gamma function is given by,

$$\Gamma(m) = \left( a + \frac{b}{2\sin^2 \theta} \right)^m \int_0^\infty t^{m-1} e^{-\left(a + \frac{b}{2\sin^2 \theta}\right)t} dt \Rightarrow \frac{\Gamma(m)}{\left( a + \frac{b}{2\sin^2 \theta} \right)^m} \int_0^\infty t^{m-1} e^{-\left(a + \frac{b}{2\sin^2 \theta}\right)t} dt \quad (5.19)$$

$$J_m(a, b) \cong \int_0^{\pi/2} \left( \frac{1}{\left( 1 + \frac{c}{\sin^2 \theta} \right)} \right)^m d\theta = \int_0^{\pi/2} \left( \frac{\sin^2 \theta}{(\sin^2 \theta + c)} \right)^m d\theta \quad (5.20)$$

From the above analysis, the closed form expression for DSM systems over Rayleigh fading environments can be derived by using [Yigit and Basar (2016), Simon and Alouini (2005)] as

$$P_{P-CSI} (S \rightarrow \hat{S}) = \frac{1}{2} \left[ 1 - \mu(c) \sum_{k=0}^{N_r-1} \binom{2k}{k} \left( \frac{1 - \mu^2(c)}{4} \right)^k \right] \quad (5.21)$$

$$\mu(c) \triangleq \left( \sqrt{\frac{c_{Rayleigh}}{1 + c_{Rayleigh}}} \right) \quad c_{Rayleigh} = \frac{H \|S - \hat{S}\|^2}{4N_0} \quad (5.22)$$

After evaluating equation (5.21) by considering the union bound [Yigit and Basar (2016), Simon and Alouini (2005)] we can approximate

$$ABER_{DSM} \leq \frac{1}{\eta 2^\eta} \sum_S \sum_{\hat{S}} P(S \rightarrow \hat{S}) e(S, \hat{S}) \quad (5.23)$$

where  $\{S \neq \hat{S}\}$ ,  $\eta$  is the number of bits for the transmitted vector  $S$  and  $e(S, \hat{S})$  is the total number of bits in error for the corresponding pairwise error event  $P(S \rightarrow \hat{S})$ .

Similarly for a DSM system under Rician fading channel condition we can write

$$P_{P-CSI}(S \rightarrow \hat{S}) = \frac{1}{\pi} \int_0^{\frac{\pi}{2}} \left( \frac{(1+K)\sin^2\theta}{(1+K)\sin^2\theta + a^2\bar{\gamma}/2} \times \exp \left\{ -\frac{Ka^2\bar{\gamma}/2}{(1+K)\sin^2\theta + a^2\bar{\gamma}/2} \right\} \right) d\theta \quad (5.24)$$

where,  $a^2 = \|S - \hat{S}\|_F^2$ ,  $\bar{\gamma}$  is the average SNR per bit given by

$$\bar{\gamma} = \frac{E_S}{N_0} \left( \frac{1-K}{1+K} \right) \quad (5.25)$$

From (3.19) the upper bound can be deduced by using Chernoff [Younis (2014)].

$$PEP(S \rightarrow \hat{S}) \leq \frac{1}{2\pi} \frac{\exp \left( -\frac{1}{4\sigma_n^2} \text{vec}(\check{\mathbf{H}}^H)^H \check{\Gamma} \left( I_{N_r N_t} + \frac{1}{4\sigma_n^2} \mathcal{L}_H \check{\Gamma} \right)^{-1} \text{vec}(\check{\mathbf{H}}^H) \right)}{\left| I_{N_r N_t} + \frac{1}{4\sigma_n^2} \mathcal{L}_H \check{\Gamma} \right|} \quad (5.26)$$

where,  $\check{\Gamma} = \mathbf{R}_{\text{REC}} \otimes (\mathfrak{J}\mathfrak{J}^H \mathbf{R}_{\text{TRAN}})$ ,  $\mathcal{L}_H$  is the covariance matrix,  $\check{\mathbf{H}}$  is the mean matrix,  $\otimes$  is the Kronecker product,  $(\cdot)^H$  is the Hermitian and  $I_n$  is an  $n \times n$  identity matrix. For Rician fading channel mean matrix is defined as  $\check{\mathbf{H}} = \sqrt{\frac{K}{1+K}} \times 1_{N_r \times N_t}$  and covariance matrix is given as  $\mathcal{L}_H = \sqrt{\frac{1}{1+K}} \times I_{N_r \cdot N_t}$ .  $K$  represents the Rician factor.  $K=3$  (5 dB). However, same bound equation holds good for Nakagami-m fading channels also, provided, mean matrix and the covariance matrix are given by

$$\check{\mathbf{H}} = \left[ \frac{\Gamma(\frac{m}{2}) + \frac{1}{2}}{\Gamma(\frac{m}{2}) \cdot \sqrt{\frac{m}{2}}} e^{j\frac{\pi}{4}} \right] \times 1_{N_r \times N_t}; \quad \mathcal{L}_H = \left( 1 - \frac{2}{m} \left[ \frac{\Gamma(\frac{m}{2}) + \frac{1}{2}}{\Gamma(\frac{m}{2})} \right]^2 \right) \times I_{N_r \times N_t}$$

Furthermore, adapting the same procedure used for Rayleigh fading, the closed form solution for a DSM system evaluated over Nakagami-m fading channels can be written as given in [Simon and Alouini (2005)]

$$P(S \rightarrow \hat{S}) = \frac{1}{\pi} \int_0^{\pi/2} \left( \frac{\sin^2\theta}{\sin^2\theta + \frac{H\|S-\hat{S}\|_F^2}{4N_0}} \right)^{N_r} d\theta \quad (5.27)$$

$$\bar{\gamma} = \frac{E_S}{N_0} \left( 1 - \frac{2}{m} \left[ \frac{\Gamma\left(\left(\frac{m}{2}\right) + \frac{1}{2}\right)}{\Gamma\left(\frac{m}{2}\right)} \right]^2 - \left[ \frac{\Gamma\left(\frac{m}{2}\right) + \frac{1}{2}}{\Gamma\left(\frac{m}{2}\right) \cdot \frac{\sqrt{m}}{2}} e^{j\frac{\pi}{4}} \right]^2 \right) \quad (5.28)$$

The closed form expression for Nakagami-m fading channels can be derived by using [Simon and Alouini (2005)]

$$P_{P-CSI}(S \rightarrow \hat{S}) = \frac{1}{2} \left[ 1 - \mu(c) \sum_{k=0}^{N_r-1} \binom{2k}{k} \left( \frac{1 - \mu^2(c)}{4} \right)^k \right] \quad (5.29)$$

$$\mu(c) \triangleq \left( \sqrt{\frac{c_{nak}}{1 + c_{nak}}} \right) \quad c_{nak} = \frac{\bar{\gamma} \|S - \hat{S}\|^2}{4N_0} \quad (5.30)$$

### 5.3.2 Case 2: Imperfect-CSI

Following equation (5.12) given in [Badarneh et al. (2014), Basar et al. (2012), Badarneh and Mesleh (2015)] the analysis can be extended to DSM systems.

$$P(S \rightarrow \hat{S}) = \frac{1}{\pi} \int_0^{\pi/2} \left( \frac{\sin^2 \theta}{\sin^2 \theta + \frac{\gamma \rho^2}{4(N_0 + (1 - \rho^2))}} \right)^{N_r} d\theta \quad (5.31)$$

where,

$$\gamma = \begin{cases} 2, & \text{if } l_t \neq l \\ \|S - \hat{S}\|^2, & \text{if } l_t = l \end{cases}$$

Equation (5.31) is reproduced from [Basar et al. (2012)]. Most of the times practical systems employ channel estimation at the receiver to understand the fading coefficient estimates  $\beta_{tr}$ . If the channel is estimated with least squares (LS), the estimation error model has the form  $\beta_{tr} = \alpha_{tr} + \varepsilon_{tr}$ , where  $\varepsilon_{tr}$  represents the channel estimation error which is independent of  $\alpha_{tr}$  and is distributed according to  $C \mathcal{N}(0, \sigma_e^2)$ . Consequently, the distribution of  $\beta_{tr}$  becomes  $C \mathcal{N}(0, 1 + \sigma_e^2)$ , and  $\beta_{tr}$  is dependent on  $\alpha_{tr}$  with the correlation coefficient  $\rho = \frac{1}{\sqrt{1 + \sigma_e^2}}$ .

In our simulations we have not made use of channel estimation procedure but we have used fixed  $\sigma_e^2$ .  $\sigma_e^2$  is fixed for all SNR values in order to determine the pure effect of the imperfect channel knowledge on the error performance.



The closed form expression for DSM systems over Rayleigh fading channel with Imp-CSI is given by

$$P_{Imp-CSI} (S \rightarrow \hat{S}) = \frac{1}{2} \left[ 1 - \mu(c) \sum_{k=0}^{N_r-1} \binom{2k}{k} \left( \frac{1 - \mu^2(c)}{4} \right)^k \right] \quad (5.32)$$

$$\mu(c) \triangleq \left( \sqrt{\frac{c_{Rayleigh}}{1 + c_{Rayleigh}}} \right) \quad c_{Rayleigh} = \frac{\|S - \hat{S}\|^2 \rho^2}{4(N_0 + (1 - \rho^2))} \quad (5.33)$$

where,  $\sigma_e^2 = \frac{1}{SNR} = 0.01$ .

DSM system under Rician fading channel conditions with Imp-CSI, is given by

$$P_{Imp-CSI} (S \rightarrow \hat{S}) = \frac{1}{\pi} \int_0^{\frac{\pi}{2}} \left( \frac{(1+K)\sin^2\theta}{(1+K)\sin^2\theta + a^2\bar{\gamma}/2} \times \exp \left\{ -\frac{Ka^2\bar{\gamma}/2}{(1+K)\sin^2\theta + a^2\bar{\gamma}/2} \right\} \right) d\theta \quad (5.34)$$

where,  $a^2 = \|S - \hat{S}\|_F^2$ ,  $\bar{\gamma}$  is the average SNR per bit given by

$$\bar{\gamma} = \frac{\|S - \hat{S}\|^2 \rho^2}{4(N_0 + (1 - \rho^2))} \left( \frac{1-K}{1+K} \right) \quad (5.35)$$

DSM system over Nakagami-m fading channel conditions with Imp-CSI is given by,

$$P_{Imp-CSI} (S \rightarrow \hat{S}) = \frac{1}{2} \left[ 1 - \mu(c) \sum_{k=0}^{N_r-1} \binom{2k}{k} \left( \frac{1 - \mu^2(c)}{4} \right)^k \right] \quad (5.36)$$

$$\mu(c) \triangleq \left( \sqrt{\frac{c_{nak}}{1 + c_{nak}}} \right) \quad c_{nak} = \frac{\|S - \hat{S}\|^2 \rho^2}{4(N_0 + (1 - \rho^2))} \quad (5.37)$$

## 5.4 Simulation Results and observations:

In this section, two spectral efficiencies were targeted for DSM as well as for other variants of SM schemes. First set comprises of  $N_t=4$ ,  $N_r=4$ , yielding a spectral efficiency  $\eta=8$  bpcu. The second set comprises of  $N_t=8$ ,  $N_r=8$  and produces a spectral efficiency  $\eta=10$  bpcu. These values are compared with the derived mathematical upper bound. Analytical BER performance of the DSM scheme over Rayleigh, Rician,

Nakagami-m fading channels has been substantiated through Monte Carlo simulations. A close correlation is observed between simulation and analytic results. The BER values under conditions of P-CSI and Imp-CSI has been plotted. It is observed that ABER performance of the DSM scheme is superior to other conventional SM schemes.

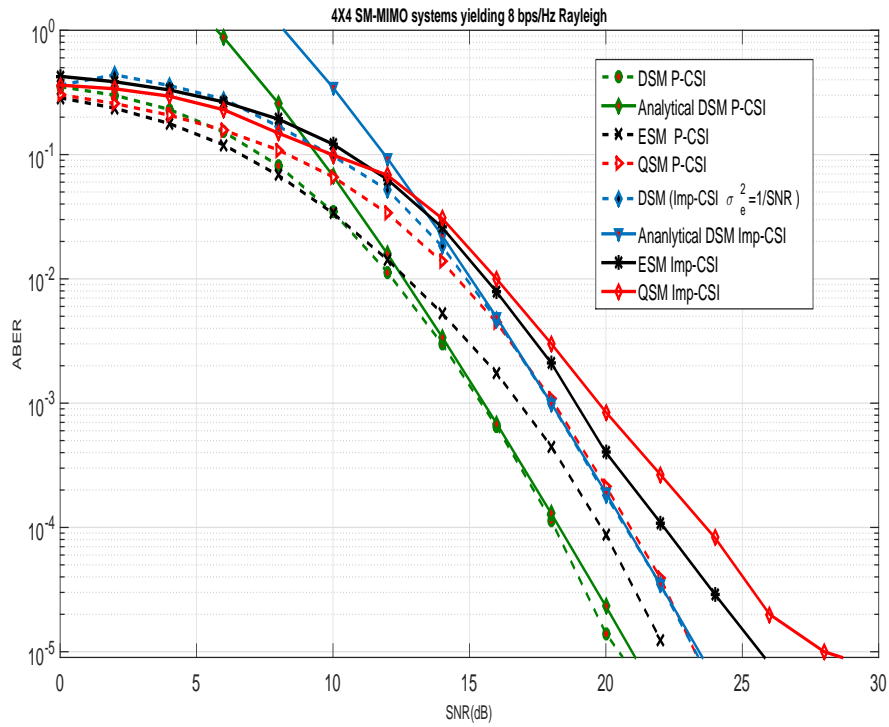


Figure 5.2 BER performance analysis of DSM in Imp-CSI ( $\sigma_e^2 = \frac{1}{SNR} = 0.01$ ) and variants of SM schemes (DSM,ESM,QSM) over a Rayleigh fading environment with  $N_t = 4, N_r = 4$ , yielding  $\eta = 8$  bpcu.

In Figure 5.2, we have shown the BER performance comparison of a DSM scheme with variants of SM (QSM and ESM) for a  $4 \times 4$  MIMO arrangement yielding a spectral efficiency  $\eta = 8$  bpcu over a Rayleigh fading channel. It has been observed that DSM system outperforms ESM and QSM systems by 1.8 dB and 2.3 dB respectively in P-CSI environment. If the channel is imperfect ( $\sigma_e^2 = \frac{1}{SNR}$ ) there exists a performance deterioration of about 2 dB in comparison to DSM system with P-CSI under lower SNR regime. Amount of performance degradation increases with increase in the value of SNR. Additionally, DSM scheme in Imp-CSI scenario perform better by about 2 dB over ESM systems and 3.5 dB over QSM systems which possesses Imp-CSI. Finally,

simulations were terminated for the error floor value of  $(9 \times 10^{-6})$ .

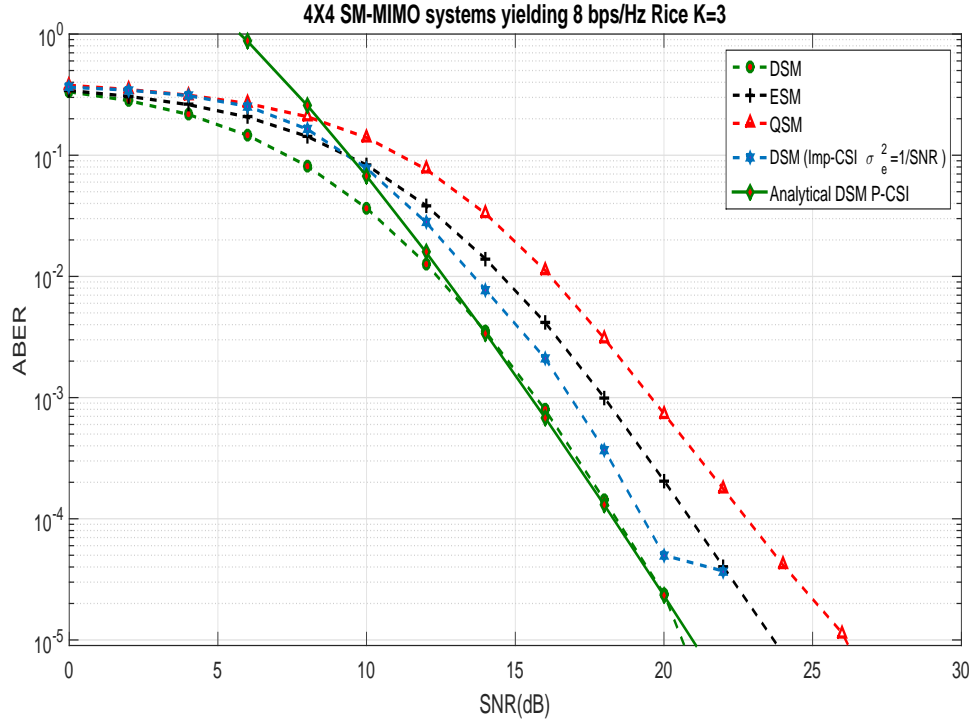


Figure 5.3 BER performance analysis of DSM in Imp-CSI ( $\sigma_e^2 = \frac{1}{SNR} = 0.01$ ) and variants of SM schemes (DSM,ESM,QSM) in P-CSI over a Rician fading environment ( $K=3$ ) with  $N_t = 4, N_r = 4$ , yielding  $\eta = 8$  bpcu.

Figure 5.3, compares the BER performance of DSM scheme with variants of SM (QSM and ESM) for a  $4 \times 4$  MIMO arrangement yielding a spectral efficiency  $\eta = 8$  bpcu over a Rician fading channel with  $K=3$ . Close examination of the simulation results explains DSM system with P-CSI outperforms ESM and QSM systems by 1.9 dB and 2.7 dB respectively. On comparing DSM performance in Imp-CSI condition with P-CSI, a degradation of about 1.6 dB is observed in lower SNR regime. Amount of performance degradation increases with higher values of SNR which is similar to that observed in Rayleigh fading. Furthermore, it is noted that the DSM scheme under Imp-CSI scenario performs better by approximately 2 dB and 3 dB over ESM and QSM systems with P-CSI respectively. Finally, simulations were terminated at the error floor value of  $(6 \times 10^{-5})$ .

Figure 5.4, illustrates the relative performance of SM variants for a  $4 \times 4$  MIMO

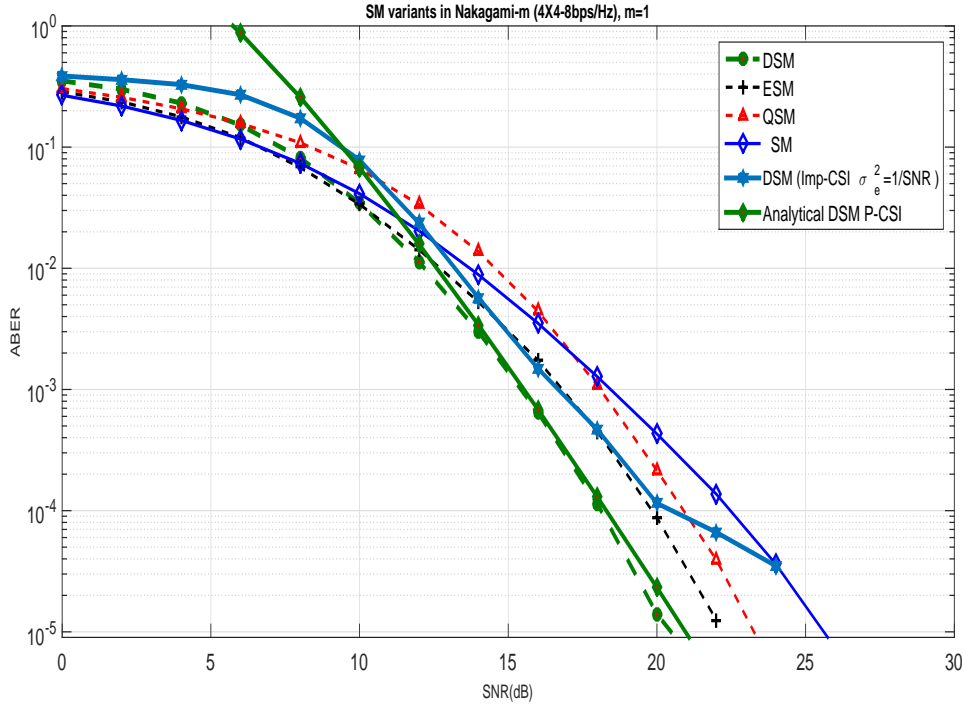


Figure 5.4 BER performance analysis of DSM in Imp-CSI ( $\sigma_e^2 = \frac{1}{SNR} = 0.01$ ) and variants of SM schemes (DSM,ESM,QSM,SM) in P-CSI over Nakagami-m fading environment ( $m=1$ ) with  $N_t = 4$ ,  $N_r = 4$ , yielding  $\eta = 8$  bpcu.

arrangement yielding a spectral efficiency of 8bps/Hz over a Nakagami-m fading channel with  $m=1$ . It is observed that DSM outperforms QSM, ESM and SM systems by approximately 1.9 dB, 2.7 dB and 4 dB respectively. It is also seen that DSM scheme under Imp-CSI scenario performs better by approximately 1.3 dB over QSM system and 2.1 dB over SM systems with P-CSI availability. The performance of DSM in Imp-CSI has a downfall of about 1.9 dB when compared to DSM with P-CSI for low SNR values.

A  $4 \times 4$  MIMO DSM system which produces 8 bpcu is compared in Figure 5.5. Figure 5.5 demonstrates the effect of various channel parameters such as  $m = 1, 2, 3, 4$  and the idea of non-uniform phase distribution on the performance of DSM scheme over Nakagami fading channel. The instance of  $m = 1$  relates to Rayleigh fading and the result is similar to the one revealed in [Yigit and Basar (2016)]. The performance deterioration of at least 1 dB is observed for every increasing value of  $m$ . In order to show the incre-

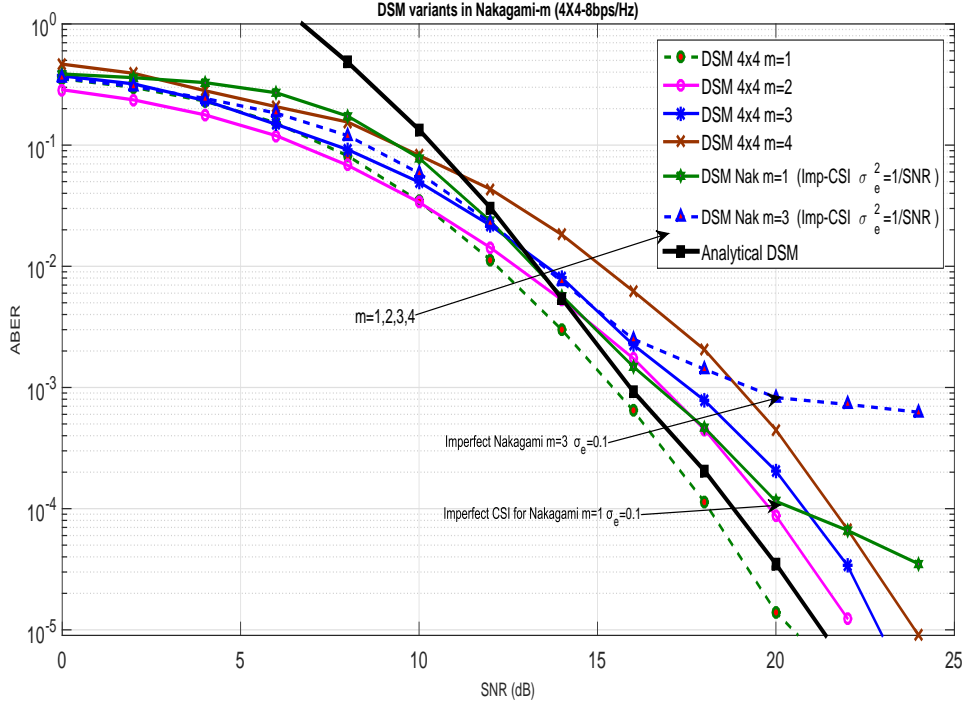


Figure 5.5 BER performance analysis of DSM in Imp-CSI ( $\sigma_e^2 = \frac{1}{SNR} = 0.01$ ) ( $m=1,3$ ) and DSM in P-CSI over Nakagami- $m$  fading environment ( $m=1,2,3,4$ ) with  $N_t = 4$ ,  $N_r = 4$ , yielding  $\eta = 8$  bpcu.

mental error floor values under Imp-CSI scenario. Performance degradation of about 3 dB is observed from the value of  $m=1$  to  $m=3$ .

Figure 5.6 gives the performance analysis of DSM and other variants of SM schemes in Nakagami- $m$  fading environment with  $m=4$ . At lower SNR values SM system outperforms all the other variants but in higher SNR values DSM scheme gives the best performance. This characteristic of both the frameworks can be justified as follows. At lower SNR values the error in distinguishing the active antenna index dominates, whereas at high SNR values the information symbol error detection predominates. It is also observed that at high values of SNR, DSM system outperform SM scheme by approximately 3 dB.

The comparison of performance of ML and OB-MMSE detection strategies for a DSM system has been demonstrated in Figure 5.7. Varied fading channel environments such as Rayleigh, Rician and Nakagami- $m$  are considered for simulation. Close obser-

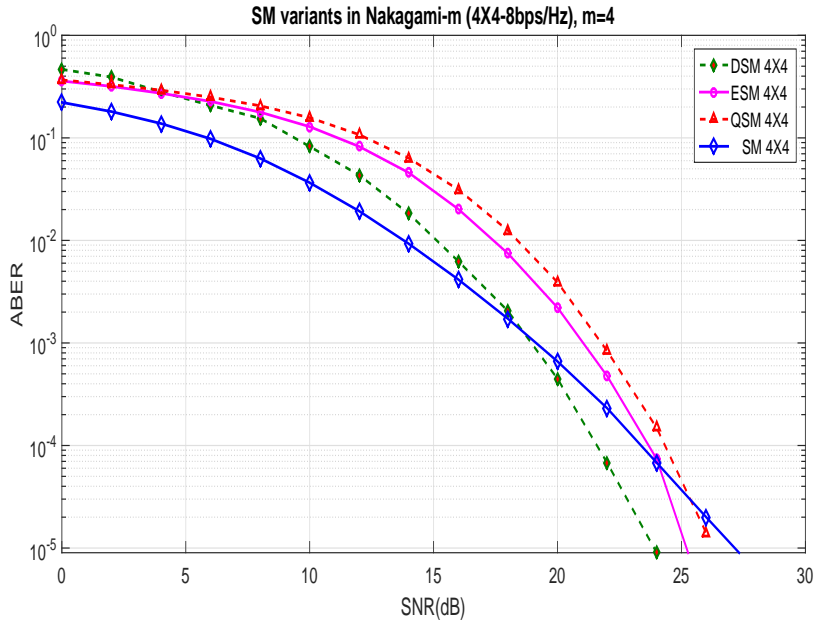


Figure 5.6 BER performance analysis of DSM and variants of SM schemes (ESM, QSM and SM) in P-CSI over Nakagami-m possesses non-uniform fading environment ( $m=4$ ) with  $N_t = 4$ ,  $N_r = 4$ , yielding  $\eta = 8$  bpcu.

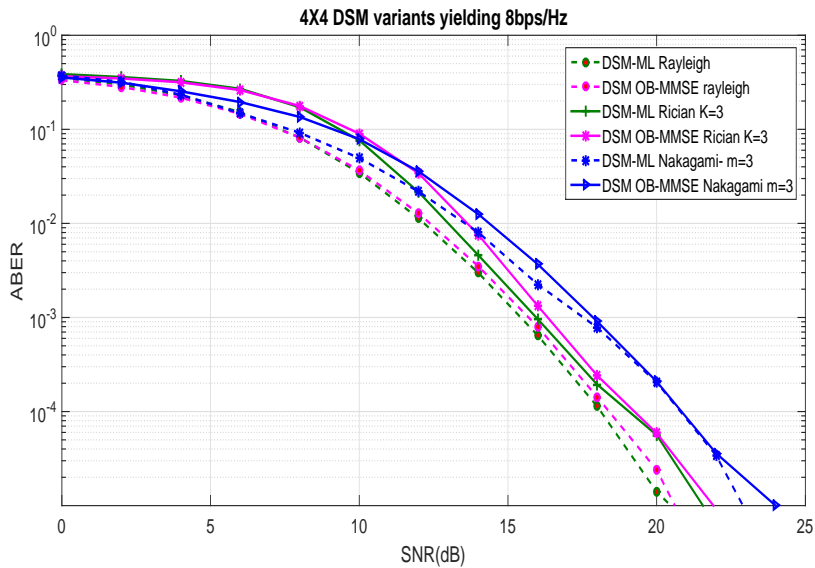


Figure 5.7 BER performance analysis of DSM schemes in Rayleigh, Rician and Nakagami-m fading environments comparison of ML and OB-MMSE with  $N_t = 4$ ,  $N_r = 4$ , yielding  $\eta = 8$  bpcu.

variation of the Figure 5.7 indicates that for pragmatic values, OB-MMSE performance is almost comparable to ML decoding strategy. At the same time OB-MMSE also pro-

vides a 80 percent reduction in computational complexity over ML detection strategies [Xiao et al. (2014)].

In Figure 5.8, we have shown the BER performance comparison of a DSM scheme for a  $8 \times 8$  MIMO arrangement. DSM employs 4 QAM to produce a spectral efficiency  $\eta=10$  bps/Hz over a Nakagami-m fading channel. The performance deterioration of at least 1 dB is observed for every increasing value of m. The examined results follow the similar trend that was contemplated in Figure 5.5.

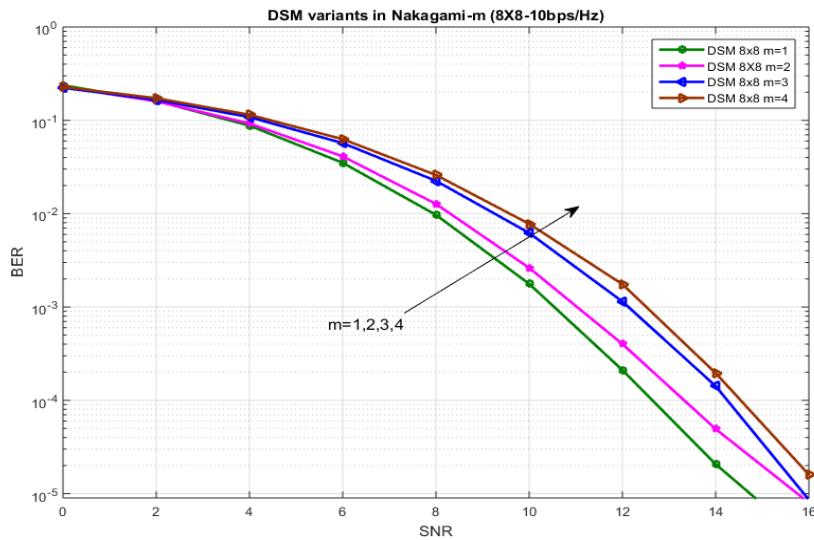


Figure 5.8 BER performance analysis of DSM in P-CSI over Nakagami-m fading environment ( $m=1,2,3,4$ ) with  $N_t = 8$ ,  $N_r = 8$ , yielding  $\eta = 10$  bpcu.

The final set of results reported in Figure 5.9 delineate the effect of Nakagami-m channel phase distribution on the execution of DSM frameworks. The realistic non-uniform phase parameter with phase  $m=2,4$  is plotted. When considering uniform phase distribution and expanding value of m, the DSM execution upgrades by an amount of almost 3 dB. The results indicate approximately 4.5 dB improvement for non-uniform phase distributed DSM system over uniform phase with  $m=4$ . Similarly, when the value of m is reduced, the performance gap between the plots increases to approximately 7 dB.

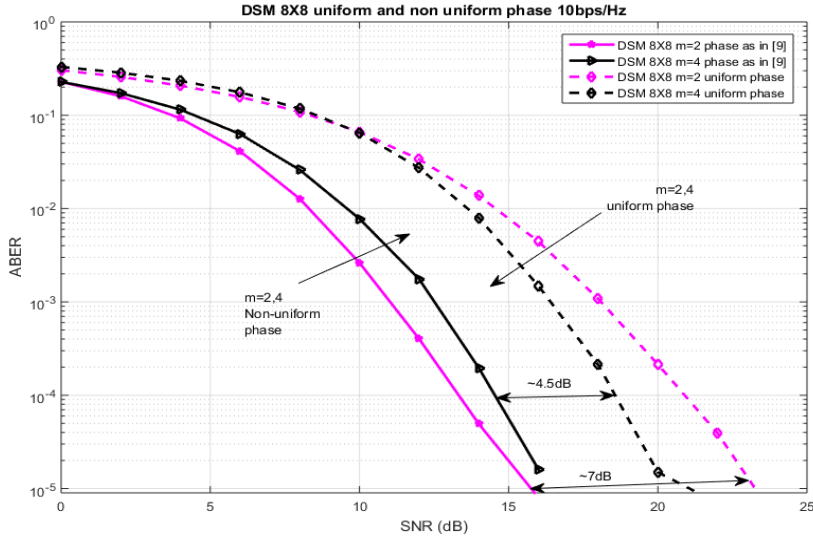


Figure 5.9 BER performance analysis of DSM in P-CSI over Nakagami- $m$  fading environment ( $m=2,4$ ) comprising uniform and non-uniform phase distribution with  $N_t = 8$ ,  $N_r = 8$ , yielding  $\eta = 10$  bpcu.

## 5.5 Summary

DSM is a high rate spectrally efficient MIMO scheme proposed recently. We have analyzed the performance of DSM schemes to work efficiently under conditions of P-CSI and Imp-CSI for channels perturbed by Rayleigh, Rician and Nakagami- $m$  distributions. The ABER performance under these conditions is also evaluated analytically. DSM system shows exceptional performance improvement of the order of 2 dB for different system configurations and channel parameters. Considering that phase distribution associated with the Nakagami distribution is non-uniform, the second part of the work deals with evaluating the performance of DSM schemes under channels perturbed by Nakagami- $m$  distribution for varying values of  $m$ . Under conditions of non-uniform phase distributed Nakagami channels an increase in the value of  $m$  results in performance deterioration of the order of approximately 1 dB. In the case of Nakagami channel with uniform phase distribution performance improvement is observed with the increasing values of  $m$ . DSM scheme outperforms all the conventional SM schemes by at least 2 dB, over all possible channel environments. This is true irrespective of whether CSI is perfectly or imperfectly available. Finally, modified suboptimal OB-



MMSE algorithm is designed for a DSM scheme which gives a near ML performance with reduced computational complexity. Hence these schemes can be advantageously deployed in the next generation 5G wireless communication systems as a realistic and efficient modulation technique.

The next contributory chapter deals with the idea of energy efficient as well as spectrally efficient scheme which is well suited to meet the requirements of LTE-Advanced and any 5G systems employing MIMO architecture and non-uniform constellations.



## Chapter 6

# Signal Constellations Employing Multiplicative Groups of Gaussian and Eisenstein Integers for Enhanced Spatial Modulation

<sup>1</sup> In this work, we propose two new signal constellation designs employing Gaussian and Eisenstein Integers for Enhanced Spatial Modulation (ESM). ESM is a novel technique which was propounded by Cheng et.al. The advantage of ESM over other Spatial Modulation (SM) schemes lies in its ability to enhance spectral efficiency while keeping energy efficiency intact. This is done by activating either one or two antennas judiciously depending upon the required trade-off. In ESM, information radiated from the antennas depends upon index of the active transmit antenna combination(s) and also on the set of constellation points chosen, which may include points from multiple constellations. In this chapter, we propose signal constellations based on multiplicative groups of Gaussian and Eisenstein integers. The set comprising of Gaussian and Eisenstein integers serves as primary and secondary constellation points for Gaussian Enhanced Spatial Modulation (GESM) scheme. The secondary constellation points are deduced from a single geometric interpolation from the primary constellation points. The Monte Carlo simulation results indicate that the proposed non-uniform constellations achieve impressive SNR gains compared to conventional constellation points used in the design of ESM. This new design has been described for MIMO employing  $4 \times 4$  and  $8 \times 8$  antenna configurations with only two active antennas. Furthermore, a closed

---

<sup>1</sup>Goutham Simha G.D., et al., Signal constellations employing multiplicative groups of Gaussian and Eisenstein integers for Enhanced Spatial Modulation, Volume 25 Part-2 pp 546-554, Physical Communication (2017) Elsevier.

form expression for the PEP of GESM scheme has been deduced. The PEP is utilized to determine the upper bound on the ABEP. Our simulations indicate that the proposed GESM from Gaussian and Eisenstein integers scheme outperforms all the other variants of SM including conventional ESM by at least 2.5 dB at an ABER of  $10^{-5}$ . Close correspondence between the theoretical analysis and the Monte Carlo simulation results are observed.

## 6.1 Introduction

Multiple Input Multiple Output (MIMO) transmission techniques are broadly utilized as a part of wireless communication frameworks and are an integral part of the next generation 5G wireless communication systems, due to their ability to provide enhanced spectral efficiency along with improved reliability [Wen et al. (2016)]. The likelihood of restricted direct device-to-device (D2D) communication has been introduced as an augmentation with the 4G/LTE-A specifications. In the next generation 5G era, exhaustive use of D2D communication as a feature of the general wireless communication is envisaged. The goal of incorporating these innovations is to have improved information throughput between devices in close proximity. A spectral efficiency of almost 10 bpcu to 16 bpcu has to be achieved between Base Station (BS) and Mobile Station (MS) in every cell to meet the data transfer requirements pertaining to 5G standards [Wen et al. (2016),Basar (2016)]. One of the fundamental limitations for mobile device is its physical size and antenna placement. A minimum spectral efficiency of 10 bpcu has to be extracted from a  $4 \times 4$  system and 16 bpcu through a  $8 \times 8$  system. To satisfy this demand, modulation schemes proposed for 5G should possess high spectral efficiency and energy efficiency [Basar (2016)]. Unlike MIMO spatial multiplexing (SMX) techniques, primary work on SM considers activation of single RF chain (single antenna) [Mesleh et al. (2008),Di Renzo et al. (2014)]. In order to compensate for the reduction in spectral efficiency due to single active antenna, additional data bits in the form of active antenna indices are used to communicate information. Enhanced Spatial Modulation (ESM) given by [Cheng et al. (2014),Cheng et al. (2015),Cheng et al. (2016)] and Quadrature Spatial Modulation (QSM) introduced by [Mesleh et al. (2015)].

ESM was designed by consolidating new concepts in MIMO based on individual

trade offs. First and foremost was to transmit information through single active antenna combination from primary constellation points followed by two active antennas which employs secondary constellation points. For multistream SM transmission techniques a single geometric interpolation has been carried out to activate two antenna combinations all the time, that was designated as ESM type1 and ESM type2 [Cheng et al. (2016)]. The demand for lower energy consumption per transmitted symbol, lead us to explore non-uniform signal constellations with minimum symbol energy and higher distance of separation, as compared to the conventional constellation points.

The primary contributions of this chapter are specified as below:

- We have proposed two new signal designs for ESM technique (GESM) from Gaussian and Eisenstein integers which pave the way to increased spectral efficiency and performance with minimum symbol energy.
- Determination of a tight upper bound on the performance of GESM scheme which is in excellent agreement with performance plots obtained by Monte Carlo simulations.
- Performance analysis of high rate GESM scheme under conditions of Rayleigh fading environment.

## 6.2 System and Channel Model

Before examining the idea of proposed Gaussian and Eisenstein signal designs used in GESM, the notion of Gaussian integers, Eisenstein integers and other framework models are described, which are utilized as the basis for relative comparison.

### 6.2.1 Gaussian and Eisenstein-Jacobi integers

Gaussian integers are numbers from the complex field of the form  $Z = a + bi$  and  $q = 4k + 1 = a^2 + b^2, (k = 0, 1, 2, 3 \dots)$ . Here  $a, b, k$  are integers and  $q$  is a prime number. The Gaussian prime number is defined as  $\Pi = a + bi$ . The set of integers  $\left\{ z_i = i \bmod \Pi = i - \left[ \frac{i\Pi^*}{\Pi\Pi^*} \right] \Pi; i = 0, 1 \dots q - 1 \right\}$ , where,  $\Pi^*$  is the complex conjugate of

$\Pi$ . In this chapter, we define  $F_{\Pi}$  as field of Gaussian integers isomorphic to  $GF(k)$  [Huber (1994b)].

Table 6.1  $q, \Pi, a$  and  $b$  values

$q$	$\Pi$	$a$	$b$
5	$2+i$	-1	$1+i$
13	$3+2i$	-2	$1+2i$
17	$4+i$	-2	$2+i$

In [Huber (1994a)], Huber defined a map called as the Eisenstein map for prime numbers of the form  $q' = 6b + 1$  i.e.  $q' = 7, 13, 19 \dots$ . Eisenstein-Jacobi (EJ) integer  $\omega$  is a complex number of the form  $\omega = u + \rho\beta$  where,  $\rho = \left(\frac{-1+i\sqrt{3}}{2}\right)$  such that  $q' = u^2 + 3\beta^2$  where,  $u$  and  $\beta$  are integers. These primes are product of two conjugate Eisenstein-Jacobi integers  $\zeta, \zeta^*$  defined as  $\zeta = u + \beta + \rho \cdot 2\beta$  and its conjugate  $\zeta^* = u + \beta + \rho^2 \cdot 2\beta$ . The set of integers  $\left\{ \zeta(i) = i \bmod \Pi \triangleq i - \left[\left(\frac{i\Pi^*}{\Pi\Pi^*}\right)\right]\Pi \text{ for } i = 0, 1, 2 \dots q' - 1 \right\}$  form a field  $E_{\zeta}$  isomorphic to  $GF(q')$ .

Table 6.2  $q', \Pi, u$  and  $\beta$  values

$q'$	$\Pi$	$u$	$\beta$
7	$3+2\rho$	2	1
13	$3+4\rho$	1	2
19	$5+2\rho$	4	1

In communication scenario, the multiplicative groups  $F_{\Pi} \setminus \{0\}$  and  $E_{\zeta} \setminus \{0\}$  can be considered as a two dimensional signal constellations. In this chapter, we explore the use of above signal constellations for ESM systems. The systems employing these are named as Gaussian ESM (GESM) systems.

## 6.2.2 Enhanced SM (ESM)

Example: Table 6.3 of ESM system reproduced for the sake of understanding from [Cheng et al. (2014)]. ESM scheme for single stream SM systems are designed to have

Table 6.3 ESM

	$T_{x1}$	$T_{x2}$	$T_{x3}$	$T_{x4}$
C1	QPSK	0	0	0
C2	0	QPSK	0	0
C3	0	0	QPSK	0
C4	0	0	0	QPSK
C5	BPSK 0	BPSK 0	0	0
C6	BPSK 0	0	BPSK 0	0
C7	BPSK 0	0	0	BPSK 0
C8	0	BPSK 0	BPSK 0	0
C9	0	BPSK 0	0	BPSK 0
C10	0	0	BPSK 0	BPSK 0
C11	BPSK 1	BPSK 1	0	0
C12	BPSK 1	0	BPSK 1	0
C13	BPSK 1	0	0	BPSK 1
C14	0	BPSK 1	BPSK 1	0
C15	0	BPSK 1	0	BPSK 1
C16	0	0	BPSK 1	BPSK 1

maximum distance between the points chosen for transmission. ESM schemes employ primary and secondary constellations (for example: QPSK and BPSK). Single antenna combinations are activated through the primary constellation and two antenna combinations are activated through secondary constellation. When secondary constellation points are radiated from two antennas then each radiated symbol possesses exactly half the energy of the symbol radiated from the primary constellation. The spectral efficiency provided by this scheme is quantified as shown below [Cheng et al. (2014)].

$$\eta = \log_2 \left( \binom{N_t}{1} \times P_c + 2 \binom{N_t}{2} \times S_c \right) \quad (6.1)$$

where,  $P_c$  represents the number of combinations from primary constellation and  $S_c$  is the number of combinations from secondary constellation.

### 6.2.3 Quadrature SM (QSM)

A new methodology was proposed by Mesleh et.al, which uses the aspects of in-phase and quadrature phase points of the constellation. These are transmitted independently from separate active antennas (1 or 2). This method is known as Quadrature Spatial Modulation (QSM). QSM technique produces an improvement in spectral efficiency as compared to conventional SM schemes. It exhibits a spectral efficiency as given below [Mesleh et al. (2015)],

$$\eta = 2 \times \log_2(N_t) + \log_2(M) \quad (6.2)$$

### 6.2.4 Enhanced SM (ESM) type-1 and type-2

ESM type-1,type-2 schemes are used to enhance the throughput of multistream SM system. The idea behind these schemes is to increase the number of active antenna combinations by initiating single step geometrical interpolation in the signal constellation plane. This new designed constellation points possess higher Euclidean distance and are involved in reducing the total transmit energy [Cheng et al. (2016)].

### 6.2.5 ESM design from Gaussian and Eisenstein integers (GESM)

We consider a MIMO system operating on Rayleigh fading channel, then the received signal is denoted by:

$$\mathbf{Y} = \mathbf{H}\mathbf{X} + \mathbf{n} \quad (6.3)$$

where,  $\mathbf{H}$  is a  $N_r \times N_t$  channel matrix,  $N_r$  is the number of receive antennas,  $N_t$  is the number of transmit antennas,  $\mathbf{X}$  is a transmitted vector which possess normalized power of  $X = \frac{s}{\sqrt{E_s}}$ , vector  $\mathbf{X}$  is transmitted over a frequency flat MIMO channel of size  $N_t \times 1$ ,  $\mathbf{n}$  is a circularly symmetric complex Gaussian noise and a column vector which is denoted as  $C \mathcal{N}(0, \sigma^2)$  independent and identically distributed (i.i.d).

Similar to conventional ESM, the proposed GESM scheme activates one antenna for radiating symbol from primary constellation and activates two antennas while communicating symbols from secondary constellation in order to achieve the required through-



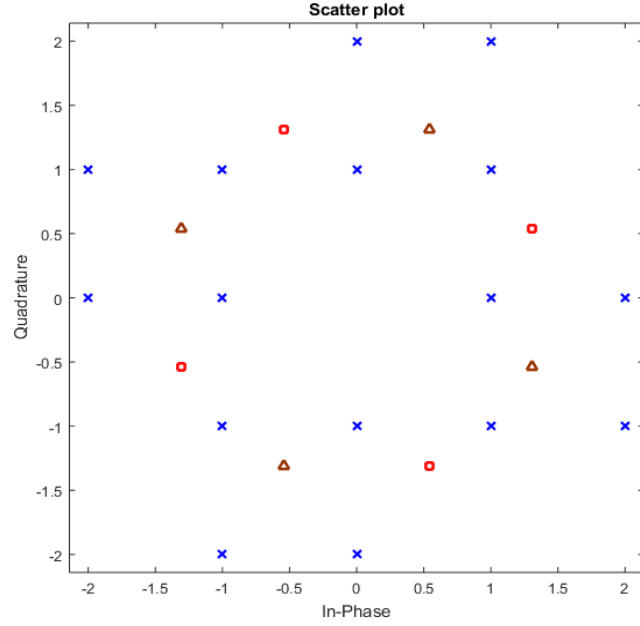


Figure 6.1 Gaussian constellations used for  $4 \times 4$  MIMO system yielding  $\eta= 8$  bpcu: The blue crosses represent  $\{GF(17) \setminus \{0\}, \cdot\}$ , the red square and brown triangle represents the rotated  $\{GF(5) \setminus \{0\}, \cdot\}$  signal constellations

put (bpcu) this has been displayed in Figure 6.1. A similar mapping for GSM systems over Eisenstein integers is shown in [Freudenberger and Shavgulidze (2017)].

$$\mathbf{X} \in \{\mathbf{L1}, \mathbf{L2}, \mathbf{L3}\} \quad (6.4)$$

In the proposed design, transmitted codeword vector  $\mathbf{X}$  is given by (6.4) and it can be inferred that  $\{\mathbf{L1}, \mathbf{L2}, \mathbf{L3}\}$  is the set of transmission vectors chosen to yield a spectral efficiency of 8 bpcu for a  $4 \times 4$  MIMO system. Here, x1 refers to (blue cross) constellation points obtained from the multiplicative group  $\{GF(17) \setminus \{0\}, \cdot\}$ . A detailed explanation is given in the next page.

$$\mathfrak{L}1 = \left\{ \begin{array}{l} \begin{bmatrix} x1 \\ 0 \\ 0 \\ 0 \end{bmatrix}, \begin{bmatrix} 0 \\ x1 \\ 0 \\ 0 \end{bmatrix}, \begin{bmatrix} 0 \\ 0 \\ x1 \\ 0 \end{bmatrix}, \begin{bmatrix} 0 \\ 0 \\ 0 \\ x1 \end{bmatrix} \end{array} \right\} \quad (6.5)$$

$$\mathfrak{L}2 = \left\{ \begin{array}{l} \begin{bmatrix} x2 \\ x2 \\ 0 \\ 0 \end{bmatrix}, \begin{bmatrix} x2 \\ 0 \\ x2 \\ 0 \end{bmatrix}, \begin{bmatrix} x2 \\ 0 \\ 0 \\ x2 \end{bmatrix}, \begin{bmatrix} 0 \\ x2 \\ x2 \\ 0 \end{bmatrix}, \begin{bmatrix} 0 \\ x2 \\ 0 \\ x2 \end{bmatrix}, \begin{bmatrix} 0 \\ 0 \\ x2 \\ x2 \end{bmatrix} \end{array} \right\} \quad (6.6)$$

$$\mathfrak{L}3 = \left\{ \begin{array}{l} \begin{bmatrix} x3 \\ x3 \\ 0 \\ 0 \end{bmatrix}, \begin{bmatrix} x3 \\ 0 \\ x3 \\ 0 \end{bmatrix}, \begin{bmatrix} x3 \\ 0 \\ 0 \\ x3 \end{bmatrix}, \begin{bmatrix} 0 \\ x3 \\ x3 \\ 0 \end{bmatrix}, \begin{bmatrix} 0 \\ x3 \\ 0 \\ x3 \end{bmatrix}, \begin{bmatrix} 0 \\ 0 \\ x3 \\ x3 \end{bmatrix} \end{array} \right\} \quad (6.7)$$

$$x1 = \left\{ \begin{array}{l} 1, \quad 1+1i, \quad 2i-1, \quad -2i, \quad 1i, \quad -1+1i, \\ -2, \quad 2-1i, \quad -1, \quad -1-1i, \quad -2i, \quad 1+2i, \\ -1i, \quad 1-1i, \quad 2, \quad -2+1i \end{array} \right\} \quad (6.8)$$

$$x2 = \left\{ \begin{array}{l} -1.3066 - 0.5412i, \quad 0.5412 - 1.3066i, \\ -0.5412 + 1.3066i, \quad 1.3066 + 0.5412i \end{array} \right\} \quad (6.9)$$

$$x3 = \left\{ \begin{array}{l} -1.3066 + 0.5412i, \quad -0.5412 - 1.3066i, \\ 0.5412 + 1.3066i, \quad 1.3066 - 0.5412i \end{array} \right\} \quad (6.10)$$

It is observed that, if we increase the number of codeword vectors by including  $\mathfrak{L}4$

the spectral efficiency is increased to 8.5 bpcu.

$$\mathbb{L}_4 = \left\{ \begin{array}{c} \begin{bmatrix} x_2 \\ x_3 \\ 0 \\ 0 \end{bmatrix}, \begin{bmatrix} x_2 \\ 0 \\ x_3 \\ 0 \end{bmatrix}, \begin{bmatrix} x_2 \\ 0 \\ 0 \\ x_3 \end{bmatrix}, \begin{bmatrix} 0 \\ x_2 \\ x_3 \\ 0 \end{bmatrix}, \begin{bmatrix} 0 \\ x_2 \\ 0 \\ x_3 \end{bmatrix}, \begin{bmatrix} 0 \\ 0 \\ x_2 \\ x_3 \end{bmatrix} \end{array} \right\} \quad (6.11)$$

$x_2$  refers to (Red circle) rotated constellation points obtained from the multiplicative group  $\{GF(5) \setminus \{0\}, \cdot\}$ . The angle of rotation of  $x_2$  is chosen to be  $22.5^\circ$ .  $x_3$  refers to (Brown Triangle) rotated constellation points obtained from the multiplicative group  $\{GF(5) \setminus \{0\}, \cdot\}$ .

The angle of rotation between the constellation points of  $x_2$  and  $x_3$  is optimally selected in order to satisfy the following two conditions.

- i) Distance of separation between the corresponding points of  $x_2$  and  $x_3$  is maximum.
- ii) The cumulative difference of spacing between all the points of  $x_2$  and  $x_3$  together is large enough to be identified at the receiving end.

The second most important aspect in designing this constellation is the average energy required to transmit the codeword. The average energy per transmitted codeword for a conventional ESM scheme which employs a  $4 \times 4$  system by using 16 QAM as primary and QPSK1, QPSK2 as secondary constellation points to produce a spectral efficiency of 8 bpcu is given by

$$E_{avg}(ESM) = 10 + 4 + 4 = 18 \quad (6.12)$$

While the average energy per transmitted codeword for the proposed GESM which employs a  $4 \times 4$  system with  $(\{GF(17) \setminus \{0\}, \cdot\}, \{GF(5) \setminus \{0\}, \cdot\}, \{GF(5) \setminus \{0\}, \cdot\})$  as primary and secondary constellation points to produce a spectral efficiency of 8 bpcu is given by:

$$E_{avg}(GESM) = 3 + 4 + 4 = 11 \quad (6.13)$$

for 8.5 bpcu, considering  $\mathbb{L}_4$  from equation (6.11)

$$E_{avg}(GESM) = 3 + 4 + 4 + 4 = 15 \quad (6.14)$$

The above observation indicates that the average energy per transmitted codeword required for the proposed scheme is  $\sim 39\%$  less than the energy required for the conventional ESM scheme.

Note: Squared minimum Euclidean distance between transmit symbol vectors is denoted as  $\ell_{min}^2$  as given in [Cheng et al. (2015)].

$$\ell_{min}^2 = \min_{X \neq X'} \|X - X'\|^2 \quad (6.15)$$

The squared minimum Euclidean distance between codeword vectors is observed to be 43.03 in the proposed GESM scheme (employing the points shown in Figure 6.1 where the blue crosses represent primary constellation of  $\{GF(17) \setminus \{0\}, \cdot\}$  and the secondary constellation is denoted by the red square and brown triangles given by  $\{GF(5) \setminus \{0\}, \cdot\}$ ) while the squared minimum Euclidean distance is 23.03 for the conventional ESM scheme (employing the primary constellation as 16 QAM and the secondary constellations as QPSK1 and QPSK2).

Table 6.4 Squared Minimum Euclidean distance of ESM and GESM

$\eta$	ESM	GESM
8bpcu (4 × 4)	23.03	43.03
10bpcu (4 × 4)	45	57
12bpcu (8 × 8)	92	122

Table 6.4 and Table 6.5 show the comparison between conventional ESM and GESM in terms of squared minimum Euclidean distance between two transmit codeword vectors and maximum energy consumption per symbol.

Since the spectral efficiency is directly proportional to the number of codeword

Table 6.5 Maximum symbol energy of ESM and GESM

$\eta$	ESM	GESM
8bpcu (4 × 4)	18	11
10bpcu (4 × 4)	32.4	15
12bpcu (8 × 8)	18	11

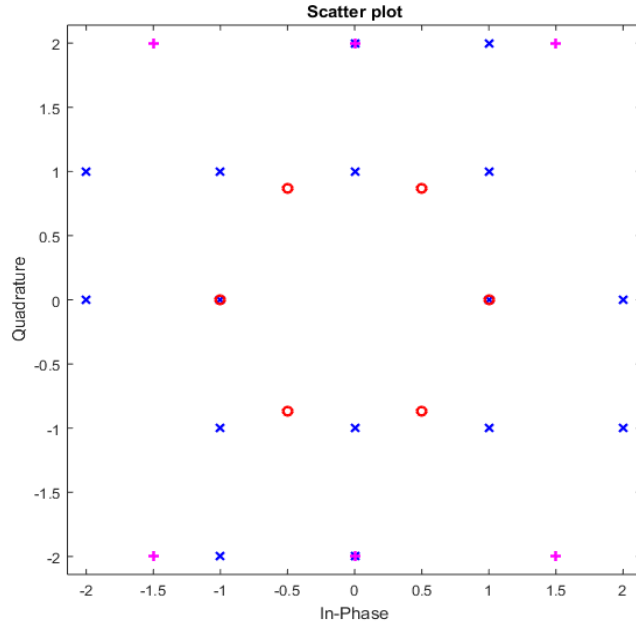


Figure 6.2 Gaussian constellations used for  $4 \times 4$  MIMO system yielding  $\eta = 9.5$  bpcu: The blue crosses represent  $\{GF(17) \setminus \{0\}, \cdot\}$ , the red circle represents Eisenstein  $\{GF(7) \setminus \{0\}, \cdot\}$  and magenta plus symbol indicates the subset of  $\{GF(17) \setminus \{0\}, \cdot\}$  constellations.

vectors, an increase in the size of the codebook increases the spectral efficiency. To achieve a spectral efficiency of 9.5 bpcu in a  $4 \times 4$  MIMO system, we have considered  $x_2$  as Eisenstein multiplicative group  $\{GF(7) \setminus 0, \cdot\}$  and  $x_3 \not\subseteq x_1$  as shown below (some points are subsets of  $\{GF(19) \setminus \{0\}, \cdot\}$  and the remaining points have undergone single geometric interpolation to have maximum distance of separation).

$$\rho = (-1 + \sqrt{3}i)/2 \quad (6.16)$$

$$x2 = \{1, 1 + \rho, \rho, -1, -1 - \rho, -\rho\}$$

$$x3 = \{1.5 - 2i, 1.5 + 2i, -1.5 - 2i, -1.5 + 2i, 2i, -2i\} \quad (6.17)$$

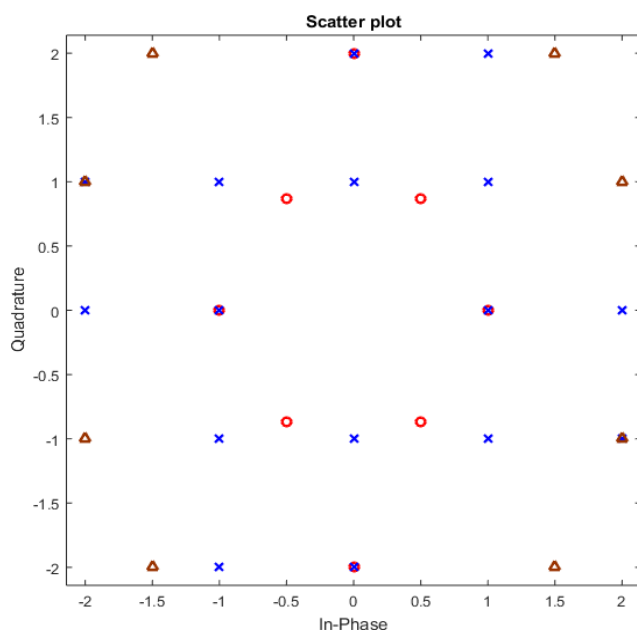


Figure 6.3 Gaussian constellations used for  $4 \times 4$  MIMO systems yielding  $\eta = 10.3$  bpcu: The blue crosses represent  $\{GF(17) \setminus \{0\}, \cdot\}$ , the red circle represents Eisenstein  $\{GF(7) \setminus \{0\}, \cdot\}$

Similarly, to achieve a spectral efficiency of 10.3 bpcu in a  $4 \times 4$  MIMO system, we have constructed  $x2$  by interpolating the Eisenstein multiplicative group  $\{GF(7) \setminus \{0\}, \cdot\}$  and  $x3 \not\subseteq x1$  and brown triangle symbol indicates some points are subsets of  $\{GF(19) \setminus \{0\}, \cdot\}$  and remaining points are interpolated to have maximum distance of separation.

$$\rho = (-1 + \sqrt{3}i)/2 \quad (6.18)$$

$$x2 = \{1, 1 + \rho, -2i, \rho, -1, 2i, -1 - \rho, -\rho\}$$

$$x3 = \{1.5 - 2i, 1.5 + 2i, -1.5 - 2i, -1.5 + 2i, 2 + 1i, 2 - 1i, -2 + 1i, -2 - 1i\} \quad (6.19)$$

In general, spectral efficiency is given by

$$\eta = \log_2 \left( \binom{N_t}{1} \times P_c + 3 \binom{N_t}{2} \times S_c \right) \quad (6.20)$$

where,  $P_c$  is the number of possible combinations from primary constellation given by  $(F_{4+i} \setminus \{0\})$  and  $S_c$  is the number of possible combinations from secondary constellation given by  $(F_{\Pi} \setminus \{0\}, G_{\zeta} \setminus \{0\})$ . It is to be noted that  $\eta$  can be increased by employing higher order multiplicative groups of Gaussian and Eisenstein integers. Furthermore, the proposed scheme can be generalized for any number of transmit antennas. Simulation results for constructions over  $8 \times 8$  MIMO system is shown in Section 6.5.

## 6.2.6 Generalization to Multistream SM systems

In this section, we propose an extended version of GESM to Multistream SM systems. Considering the same number of signal constellation points as given in Equation (6.5-6.7) the extended scheme for  $4 \times 4$  MIMO systems, is described as below

$$\mathbf{X} \in \{\mathbf{X}1, \mathbf{X}2, \mathbf{X}3\} \quad (6.21)$$

$$\mathbf{X}1 = \left\{ \begin{bmatrix} x11 \\ x12 \\ 0 \\ 0 \end{bmatrix}, \begin{bmatrix} x11 \\ 0 \\ x12 \\ 0 \end{bmatrix}, \begin{bmatrix} x11 \\ 0 \\ 0 \\ x12 \end{bmatrix}, \begin{bmatrix} 0 \\ x11 \\ x12 \\ 0 \end{bmatrix}, \begin{bmatrix} 0 \\ x11 \\ 0 \\ x12 \end{bmatrix}, \begin{bmatrix} 0 \\ 0 \\ x11 \\ x12 \end{bmatrix} \right\} \quad (6.22)$$

$$\mathbf{X}2 = \left\{ \begin{bmatrix} x2 \\ x2 \\ 0 \\ 0 \end{bmatrix}, \begin{bmatrix} x2 \\ 0 \\ x2 \\ 0 \end{bmatrix}, \begin{bmatrix} x2 \\ 0 \\ 0 \\ x2 \end{bmatrix}, \begin{bmatrix} 0 \\ x2 \\ x2 \\ 0 \end{bmatrix}, \begin{bmatrix} 0 \\ x2 \\ 0 \\ x2 \end{bmatrix}, \begin{bmatrix} 0 \\ 0 \\ x2 \\ x2 \end{bmatrix} \right\} \quad (6.23)$$

$$\mathfrak{L}_3 = \left\{ \begin{array}{l} \begin{bmatrix} x_3 \\ x_3 \\ 0 \\ 0 \end{bmatrix}, \begin{bmatrix} x_3 \\ 0 \\ x_3 \\ 0 \end{bmatrix}, \begin{bmatrix} x_3 \\ 0 \\ 0 \\ x_3 \end{bmatrix}, \begin{bmatrix} 0 \\ x_3 \\ x_3 \\ 0 \end{bmatrix}, \begin{bmatrix} 0 \\ x_3 \\ 0 \\ x_3 \end{bmatrix}, \begin{bmatrix} 0 \\ 0 \\ x_3 \\ x_3 \end{bmatrix} \end{array} \right\} \quad (6.24)$$

$$\mathfrak{L}_4 = \left\{ \begin{array}{l} \begin{bmatrix} x_2 \\ x_3 \\ 0 \\ 0 \end{bmatrix}, \begin{bmatrix} x_2 \\ 0 \\ x_3 \\ 0 \end{bmatrix}, \begin{bmatrix} x_2 \\ 0 \\ 0 \\ x_3 \end{bmatrix}, \begin{bmatrix} 0 \\ x_2 \\ x_3 \\ 0 \end{bmatrix}, \begin{bmatrix} 0 \\ x_2 \\ 0 \\ x_3 \end{bmatrix}, \begin{bmatrix} 0 \\ 0 \\ x_2 \\ x_3 \end{bmatrix} \end{array} \right\} \quad (6.25)$$

$$x_{11} = \left\{ \begin{array}{l} 1, \quad 1 + 1i, \quad 1i, \quad -1 + 1i, \\ -1, \quad -1 - 1i, \quad -1i, \quad 1 - 1i, \end{array} \right\} \quad (6.26)$$

$$x_{12} = \left\{ \begin{array}{l} 2i - 1, \quad -2i, \quad -2, \quad 2 - 1i, \\ -2i, \quad 1 + 2i, 2, \quad -2 + 1i \end{array} \right\} \quad (6.27)$$

$$x_2 = \left\{ \begin{array}{l} -1.3066 - 0.5412i, \quad 0.5412 - 1.3066i, \\ -0.5412 + 1.3066i, \quad 1.3066 + 0.5412i \end{array} \right\} \quad (6.28)$$

$$x_3 = \left\{ \begin{array}{l} -1.3066 + 0.5412i, \quad -0.5412 - 1.3066i, \\ 0.5412 + 1.3066i, \quad 1.3066 - 0.5412i \end{array} \right\} \quad (6.29)$$

From the above analysis, it can be noted that the spectral efficiency has been increased to 9.4 bpcu. That is, in general for a Multistream SM system the spectral efficiency can be enhanced by increasing the number of codeword vectors. The generalization defined above for Multistream systems results in a spectral efficiency given by

$$\eta = \log_2(|\mathfrak{L}_1| + |\mathfrak{L}_2| + |\mathfrak{L}_3| + |\mathfrak{L}_4|) \quad (6.30)$$



### 6.2.7 Quasi Static Rayleigh Fading Channels

Following [Younis (2014), Jeganathan et al. (2008)] realization of any fading channel is given by channel matrix.

$$\mathbf{H} = \check{\mathbf{H}} + \dot{\mathbf{H}} \quad (6.31)$$

where  $\check{\mathbf{H}}$  is the mean matrix and  $\dot{\mathbf{H}}$  is a  $N_r \times N_t$  channel matrix whose entries are i.i.d complex gaussian random numbers with zero mean and unit variance ( $C \mathcal{N} (0, 1)$ ). The mean matrix for a Rayleigh fading channel can be evaluated as  $\check{\mathbf{H}} = \mathbf{0}_{N_r \times N_t}$  matrix [Younis (2014)]. Optimal ML detection strategy is employed for the considered GESM scheme. Joint estimation of the antenna indices and MQAM information symbols are formulated as

$$\log_2 \left( \binom{N_t}{1} \times P_c + 3 \binom{N_t}{2} \times S_c \right) \quad (6.32)$$

$$(\hat{t}, \hat{X}) = \underset{X \in \{\mathbb{L}1, \mathbb{L}2, \mathbb{L}3, \mathbb{L}4\}}{\arg \min} \|Y - HX\|_F^2 \text{ where, } \|\cdot\|_F \text{ is the Frobenius norm.}$$

### 6.3 Analytical treatment for proposed GESM

A mathematical analysis for the ABEP of the proposed GESM scheme is presented in this section. A quasi static Rayleigh fading environment is considered for our analysis. The Conditional Pairwise Error Probability (CPEP) for erroneous detection of  $\hat{X}$  (when  $X$  is transmitted and ( $\hat{X} \neq X$ )) is calculated as given below, [Cheng et al. (2015), Cheng et al. (2016)].

$$PEP(X \rightarrow \hat{X}|H) = P_r(\|Y - HX\|_F^2 > \|Y - H\hat{X}\|_F^2 | H)$$

$$= P_r(\|HX\|^2 - \|H\hat{X}\|^2 - 2\Re\{y^H(HX - H\hat{X})\} > 0)$$

$$P(X \rightarrow \hat{X}|H) = \frac{1}{\pi} \int_0^{\pi/2} \exp\left(-\frac{\|H(X - \hat{X})\|^2}{4N_0 \sin^2 \theta}\right) d\theta \quad (6.33)$$

$$P(X \rightarrow \hat{X}) = \frac{1}{\pi} \int_0^{\pi/2} \left( \frac{\sin^2 \theta}{\sin^2 \theta + \frac{H \|X - \hat{X}\|^2}{4N_0}} \right)^{N_r} d\theta \quad (6.34)$$

Following [Proakis (1998)], the closed form expression for the PEP over quasi static Rayleigh fading channel can be given as

$$P(X \rightarrow \hat{X}) = \left( \frac{1 - \mu(c)}{2} \right)^{N_r - 1} \sum_{k=0}^{N_r - 1} \binom{N_r - 1}{k} \left( \frac{1 + \mu(c)}{4} \right)^k \quad (6.35)$$

where,

$$\mu(c) \triangleq \left( \sqrt{\frac{c_{Rayleigh}}{1 + c_{Rayleigh}}} \right); \quad c_{Rayleigh} = \frac{H \|X - \hat{X}\|^2}{4N_0} \quad (6.36)$$

## 6.4 Computational Complexity Analysis

Following [Cheng et al. (2016)], receiver computational complexity analysis has been calculated in this section. To evaluate equation (6.31) the number of complex and real multiplications required can be described with a following example. For a 4 transmit MIMO system with  $\eta=8$  bpcu, GESM ML decoder needs to compute  $w_{ij}=y - h_i x_j$  for three sets of antenna/constellation combinations, where  $h_i$  denote the  $i^{th}$  column of H matrix and  $x_j \in F_{4+i} \setminus \{0\}$ . First set  $\ell_1$  comprises of four possible antenna combinations hence computation of  $w_{ij}$  results in 64 complex multiplications equivalently 256 real multiplications. Second set  $\ell_2$  having two active antenna combinations has  $w_{ij}$  given by  $w_{ij}=y - h_{i1}x_{j1} - h_{i2}x_{j2}$ . Since  $x_2 \in F_{1+2i} \setminus \{0\}$ , the number of complex multiplication involved are  $4 \times 4 = 16$ . Similarly,  $\ell_3$  results in 16 complex multiplications. Further, computation for the squared modulus of each one of the  $w_{ij}$  terms, requires another 256 complex multiplications. Therefore, the total number of complex multiplications required in estimating 1 possible transmitted vector is given by  $64+16+16+256=352$ . One complex multiplication is equivalent to 4 real multiplications hence total number of real multiplications required are  $352 \times 4 = 1408$ . From the above analysis it is observed that for a 4 transmit 8 bpcu GESM framework, the computational complexity remains same as that of conventional ESM scheme. Extending the above analysis for

Table 6.6 Receiver Complexity

<b>Spectral Efficiency</b>	<b>8bpcu(4×4)</b>	<b>10bpcu(4 × 4)</b>	<b>12bpcu(8×8)</b>
<b>ESM</b>	352	1344	4320
<b>GESM</b>	352	1184	4320

the proposed schemes the obtained computational complexity values are tabulated in Table 6.6.

From Table 6.6, it is observed that for a 4 transmit antenna 10 bpcu system the proposed GESM scheme results in a complexity reduction of 11.9%.

## 6.5 Simulation Results and Observations

In this section, we have compared the performance of proposed GESM scheme with the variants of SM (ESM,QSM,SM). Simulations were performed for three spectral efficiencies  $\eta = 8, 10, 12$  bpcu. To achieve a spectral efficiency of  $\eta = 8, 10$  bpcu, the proposed GESM employs a  $4 \times 4$  MIMO system. Further, to achieve a  $\eta = 12$  bpcu a  $8 \times 8$  MIMO system is considered. A minimum of  $10^6$  channel realizations have been considered for the estimation of ABER. To justify the effectiveness, these values are compared with the derived mathematical upper bound. Monte Carlo simulation method is used to substantiate the analytical BER performance of the proposed GESM scheme. A close correlation is observed between simulation and theoretic results.

In Figure 6.4, we have shown the BER performance of a proposed GESM scheme with the variants of SM (QSM, ESM and SM) for a system employing  $4 \times 4$  MIMO arrangement producing a spectral efficiency  $\eta = 8$  bpcu over a quasi static flat Rayleigh fading channel. Proposed GESM uses  $F_{4+i} \setminus \{0\}$  as primary constellation,  $e^{j\theta_1} F_{2+i} \setminus \{0\}$  and  $e^{j\theta_2} F_{2+i} \setminus \{0\}$  as the two secondary constellation points ( $\theta_1 = 22.5, \theta_2 = 67.5$ ), conventional ESM uses 16 QAM and QPSK1, QPSK2 as the primary and secondary constellation points, QSM uses 16 QAM while SM uses 64 QAM. It is observed that the proposed GESM system outperforms conventional ESM, QSM and SM systems by approximately 2 dB, 2.5 dB and 5 dB respectively. Further it is observed that simulation

results are in close correspondence with analytical upper bound at SNRs greater than 10 dB (Asymptotic values).

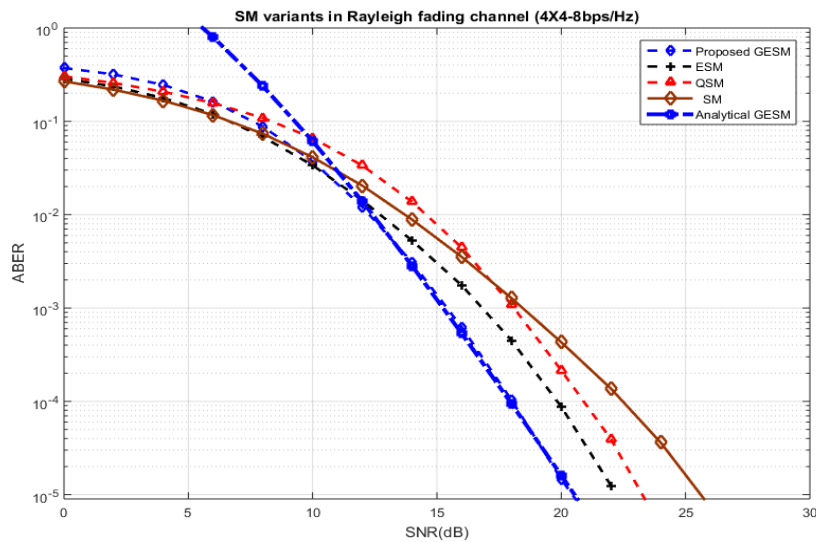


Figure 6.4 BER performance analysis of GESM and variants of SM schemes in a  $4 \times 4$  MIMO system yielding  $\eta = 8$  bpcu.

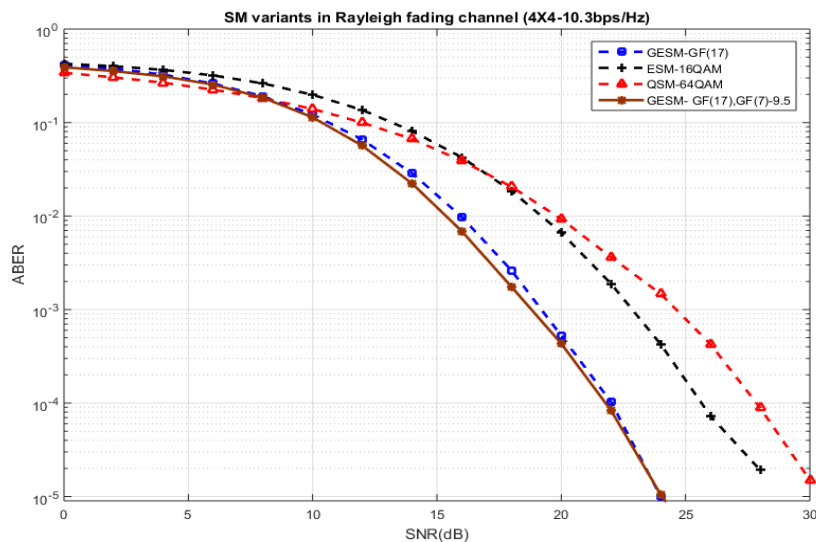


Figure 6.5 BER performance analysis of GESM and variants of SM schemes in a  $4 \times 4$  MIMO system yielding  $\eta = 10.3$  bpcu. (Exception: GESM brown line, represents secondary constellation extension producing 9.5 bpcu).

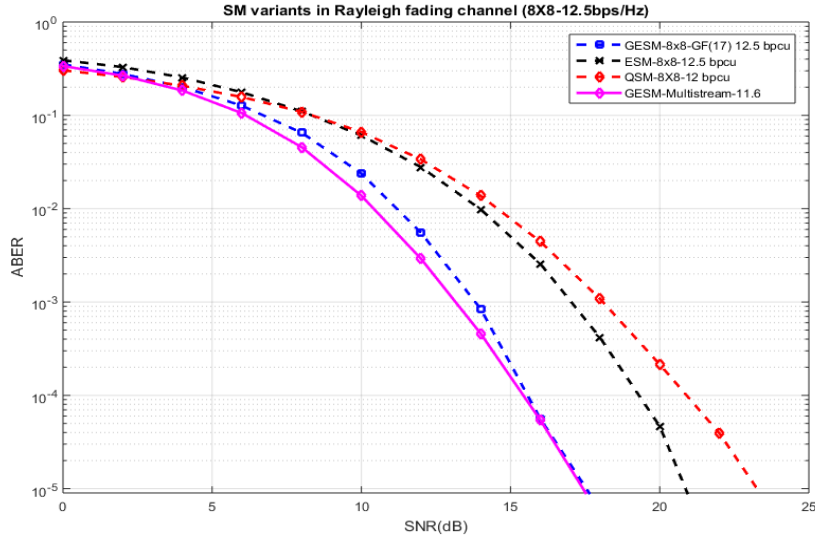


Figure 6.6 BER performance analysis of GESM and variants of SM schemes in a  $8 \times 8$  MIMO systems yielding  $\eta = 12.5$  bpcu. (Exception: GESM magenta line, represents secondary constellation extension producing 11.3 bpcu).

Figure 6.5, shows two important observations: First, GESM scheme employing  $e^{j\theta_1}F_{2+i} \setminus \{0\}$  and  $e^{j\theta_2}F_{2+i} \setminus \{0\}$  as the two secondary constellations can be extended to yield a spectral efficiency of 9.5 bpcu that is marked in brown line. Second: If we choose GESM scheme with  $F_{4+i} \setminus \{0\}$ ,  $F_{3+2\rho} \setminus \{0\}$  and geometric interpolation of points pertaining to  $F_{3+2\rho} \setminus \{0\}$ , a spectral efficiency of 10.3 bpcu is achieved, while the conventional ESM uses 16 QAM and 8 PSK1,8 PSK2 as the primary and secondary constellation points, QSM uses 64 QAM. It is observed that the proposed GESM system has an improvement of approximately 4 dB and 5 dB over conventional ESM and QSM systems respectively.

Figure 6.6, gives the performance analysis of GESM and other variants of SM schemes in a  $8 \times 8$  MIMO arrangement producing a spectral efficiency  $\eta=12.5$  bpcu over a quasi static flat Rayleigh fading channel. Proposed GESM uses  $F_{4+i} \setminus \{0\}$  as primary constellation,  $e^{j\theta_1}F_{2+i} \setminus \{0\}$  and  $e^{j\theta_2}F_{2+i} \setminus \{0\}$  as the two secondary constellation points ( $\theta_1 = 22.5, \theta_2 = 67.5$ ), conventional ESM uses 16 QAM and QPSK1,QPSK2 as the primary and secondary constellation points and QSM uses 16 QAM to produce 12 bpcu. It is observed that the proposed GESM system is superior to conventional ESM and QSM systems by approximately 4 dB and 6 dB respectively. Furthermore, this

GESM scheme can be extended to Multistream SM systems as discussed previously, is demonstrated in Figure 6.6.

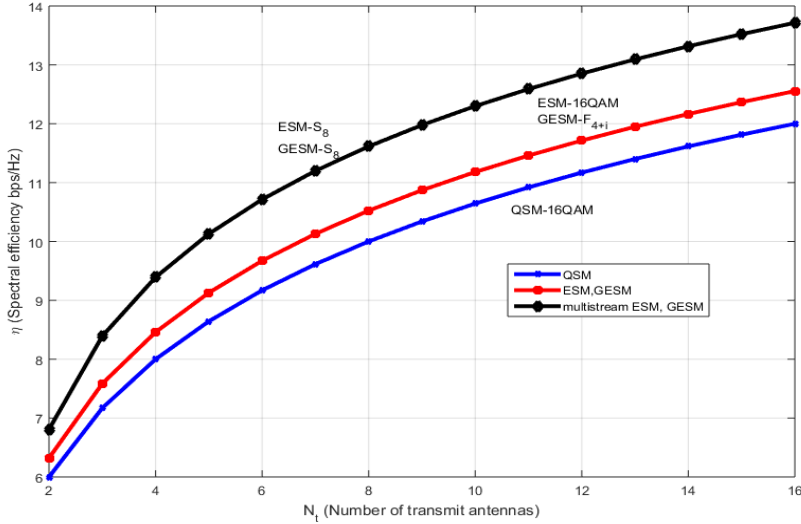


Figure 6.7 A comparison of achievable spectral efficiencies with variable number of transmit antennas,  $N_t$ , and with  $M = 16$  QAM and  $F_{4+i}$  modulation for various SM systems.

Figure 6.7, shows the comparison of maximum achievable spectral efficiency with variable number of antennas. It is observed that for  $N_t = 4$  the proposed GESM scheme achieves a average spectral efficiency of 8.5 bpcu, Multistream GESM scheme attains spectral efficiency of 10.3 bpcu. QSM system achieves spectral efficiency of 8 bpcu. Note that all these schemes activate either one or two transmit antennas only.

## 6.6 Summary

In this work, we have investigated signal constellations for ESM systems from multiplicative groups of Gaussian and Eisenstein integers and named it as GESM. This scheme can be generalized to single stream SM as well as Multistream SM configurations. Moreover, extension of this construction and mapping to higher antenna configurations has been devised and analyzed. The derived mathematical upper bound and Monte Carlo simulation results show that proposed new constellation design for ESM exhibits remarkable improvement in SNR gains (approximately 2.5 dB) as compared

to traditional ESM systems employing standard constellation points. Since the signal points are not a power of two, fractional bpcu values are obtained in our Monte Carlo simulations. In conclusion, it is observed that the new GESM scheme is energy efficient as well as spectrally efficient and this scheme is well suited to meet the requirements of LTE-Advanced and any 5G wireless systems employing MIMO architecture that may evolve in the future.

After exploring the advantages of a Multistream Spatial Modulation scheme we are convinced that this scheme can yield impressive SNR gains in all possible fading environments. The major constraint for any SM-MIMO scheme implementation is its performance in spatially correlated fading channels. Synthesis of schemes which can yield good BER performance under conditions of high spatial correlation between antennas leads us to our final contributory chapter which concentrates on the design and performance analysis of Multistream SM systems over spatially correlated fading channels.





## Chapter 7

# Modified Signal Design for Multistream Spatial Modulation over Spatially Correlated Channels

<sup>1</sup> In this work, we describe a modified signal design for Multistream Spatial Modulation (MSM). The fundamental idea behind MSM is to activate multiple antennas and transmit complex symbols along with active antenna indices. Here, a modified MSM technique explicitly designed to combat the effect of spatial correlation in realistic channel scenarios is proposed. In this MSM scheme, two antennas are made active all the time, mapping for antenna selection is judiciously adopted from primary and secondary constellation points. Secondary constellations are obtained through single geometric interpolation of the primary constellation points. Simulation studies show that for a fixed number of antenna combinations and spectral efficiency, the proposed scheme produces a performance improvement of at least 4 dB at a ABER of  $10^{-5}$  over all traditional Spatial Modulation (SM) systems, more specifically Enhanced Spatial Modulation (ESM), Quadrature Spatial Modulation (QSM) and Double Spatial Modulation (DSM) systems when employed over dense spatially correlated channels. Furthermore, an upper bound on the average bit error probability (ABEP) for the modified MSM scheme has been derived and quantified. Monte Carlo simulation results corroborate the close correspondence between analytical and the obtained simulation results.

---

<sup>1</sup>Goutham Simha G.D, et.al, "Modified Signal Design for Multistream Spatial Modulation over Spatially Correlated Channels", published in Proceedings of the 6th IEEE "International conference on Advances in Computing, Communications and Informatics " Manipal Institute of Technology, Manipal, Karnataka , September 2017.

## 7.1 Introduction

It is for the most part observed that the execution of all SM schemes disintegrate under Spatially Correlated (SC) channel conditions. To reduce the impact of SC conditions, Trellis Coded Spatial Modulation (TCSM) was presented by [Mesleh et al. (2010)] . Spatial Multiplexing (SMX) systems expands the complexity and cost of the MIMO systems since it activates all the antennas while transmitting information, this increases the RF chain requirement. Keeping in view of this disadvantage, Multistream SM techniques have been proposed whose performance is superior to that of SMX systems under conditions of spatial correlation [Ntontin et al. (2013a)]. Targeting the goal of obtaining a twofold increment in spectral efficiency compared with the conventional SM frameworks, Zehra and Basar proposed a high rate Index Modulation scheme for use in MIMO and large scale MIMO systems. This scheme is known as Double Spatial Modulation (DSM) [Yigit and Basar (2016)].

In compact mobile hand held devices, placing and activating multiple number of antennas, especially more than 4 working in a same frequency band becomes a tedious task predominantly due to size and space constraints. Antennas working in the same frequency band, if placed near i.e. less than  $0.5\lambda$  distance from each other results in very high spatial correlation between them. An increase in spectral efficiency achieved through higher order modulation schemes with the large number of transmit antennas will result in a deterioration of the ABER performance.

Inspired by ESM and MSM techniques, the present work concentrates on proposing a technique for design and selection of constellation points which yield good results in spatially correlated Rayleigh and Rician fading channels. The advantage of the proposed MSM method is to produce performance improvement over the existing SM techniques in SC channel conditions without increasing the number of active transmit antenna configurations. Throughout this work we use  $\hat{\mathbf{X}}$  as the estimation of transmitted symbol  $\mathbf{X}$ ,  $x \in j, q$  is defined to be  $1 \leq j \leq N_t$ ,  $1 \leq q \leq M$  respectively.  $N_t$  is the transmit antenna and  $M$  is the modulation order.

The contributions of this chapter is categorized as follows:

- Design a modified MSM to work in spatially correlated fading channel environ-

ments.

- Derive an analytical expression for the Pairwise Error Probability (PEP) and further enhancement of this result to characterize upper bound on the ABEP for modified MSM scheme.

## 7.2 System Models

Before discussing the concept of modified MSM designed for spatially correlated channel scenarios, let us first briefly describe the other system models which are used as the basis for relative study.

### 7.2.1 Enhanced SM (ESM)

The ESM scheme uses the special combinations of number of active antennas and modulation scheme that is employed. Maximum two antennas can be activated in this scheme. If only single antenna is activated then higher order modulation scheme is adopted (Assume QPSK). While, if double antennas are excited then lower order modulation scheme (exactly half the constellation energy of the primary is selected, here BPSK0,BPSK1). The spectral efficiency provided by this scheme is quantified as,

$$\eta_{ESM} = \log_2 \left( \binom{N_t}{1} \times P_c + 2 \binom{N_t}{2} \times S_c \right) \quad (7.1)$$

where,  $P_c$  (higher order modulation scheme) denotes the number of combinations possible from the primary constellation points and  $S_c$  (lower order modulation schemes) represents the number of combinations from secondary constellation points.

### 7.2.2 Quadrature SM (QSM)

A new method utilizing the spatial dimension was introduced by Mesleh et.al which employs quadrature and in-phase components separately. This new approach was named as Quadrature Spatial Modulation (QSM). This scheme yields an improvement in spectral efficiency as compared to conventional SM schemes. Spectral efficiency of this scheme is given by

$$\eta = 2 \times \log_2(N_t) + \log_2(M) \quad (7.2)$$

where,  $M$  is the constellation size.

### 7.2.3 Double SM (DSM)

Zehra and Basar have proposed a scheme referred to as Double Spatial Modulation (DSM) in 2016, in which the single framework comprises of two individual SM schemes. The two subordinate SM schemes are distinguished by angle rotation principle. This scheme yields an improvement in spectral efficiency as compared to conventional SM [Yigit and Basar (2016)]. Spectral efficiency of this scheme is given by:

$$\eta_{DSM} = \log_2(N_t^2 M^2) \quad (7.3)$$

### 7.2.4 Modified Multistream SM (MSM)

Motivated by the approach of considering two active antenna combinations and two level constellation point selection [Cheng et al. (2016)] we have carried out the following studies. Throughout the work presented in this chapter, we have considered  $4 \times 4$  MIMO communication systems ( $N_t = 4$   $N_r = 4$ ) and active antennas  $N_a = 2$ .

Systems with only two antennas are active can be represented as

$$\mathbf{X} = [0 \cdots, 0, X_{s1}, 0, \cdots, 0, X_{s2}, 0 \cdots, 0]^T \quad (7.4)$$

where,  $X_{s1}$  and  $X_{s2}$  are the indexes of the active antennas.  $X_{s1} \neq X_{s2}$ .  $\mathbf{X}$  has dimensions  $N_t \times 1$  and  $X_{s1}, X_{s2}$  ranges from  $X_{s1} = X_{s2} = 1, \cdots, N_t$ .

### 7.2.5 Antenna Selection in modified MSM

In the proposed MSM, we use two different constellation points to activate two antenna elements, primary constellation points and secondary constellation points. The secondary constellation points are chosen from the geometrical interpolation of the primary. Primary points denote M-QAM constellation and the secondary points denote mPSK (where m represents inner constellation points of  $M$ ). Here, we have made use of 16 QAM and QPSK to obtain a spectral efficiency of 8 bpcu. Mathematically it is

explained in (7.6). In (7.6),  $P_c$  is the primary constellation points, represented as red crosses in Figure 7.1.  $S_c$  is the secondary constellation points, represented as blue dots in Figure 7.1.

Note: Unlike ESM, (one or two antennas are made active at any time instant) in the proposed MSM scheme, all the time two antennas are made active and radiating two

different set of constellation points.  $\binom{4}{2} = 6$  out of which only 4 antenna combination pair as given in (7.5) are dynamically chosen in such a way that, the existence of correlation between the successive transmit antenna pair is made very minimal.

$\binom{4}{2} = 6$  though it is possible to choose all 6 antenna combinations to increase the spectral efficiency  $\eta \geq 8$  bpcu. In the proposed scheme, it has been restricted to use only uncorrelated antenna pairs to improve the ABER performance specifically in SC channel conditions).

$$x \in \left\{ \begin{array}{l} \left[ \begin{array}{c} P_c \\ S_c \\ 0 \\ 0 \end{array} \right] \left[ \begin{array}{c} 0 \\ 0 \\ P_c \\ S_c \end{array} \right] \left[ \begin{array}{c} P_c \\ 0 \\ S_c \\ 0 \end{array} \right] \left[ \begin{array}{c} 0 \\ S_c \\ 0 \\ P_c \end{array} \right] \end{array} \right\} \quad (7.5)$$

The spectral efficiency calculation for the proposed MSM technique is given as follows, here

$$\eta = 2 + \log_2(P_c) + \log_2(S_c) \quad (7.6)$$

$\eta$  is defined to be Antenna selection bits + Constellation bit.

In the signal space, we have four antenna and signal constellation combinations as follows.

(a) Total antenna selection combinations are  $\binom{4}{2} = 6$ , out of which to combat the

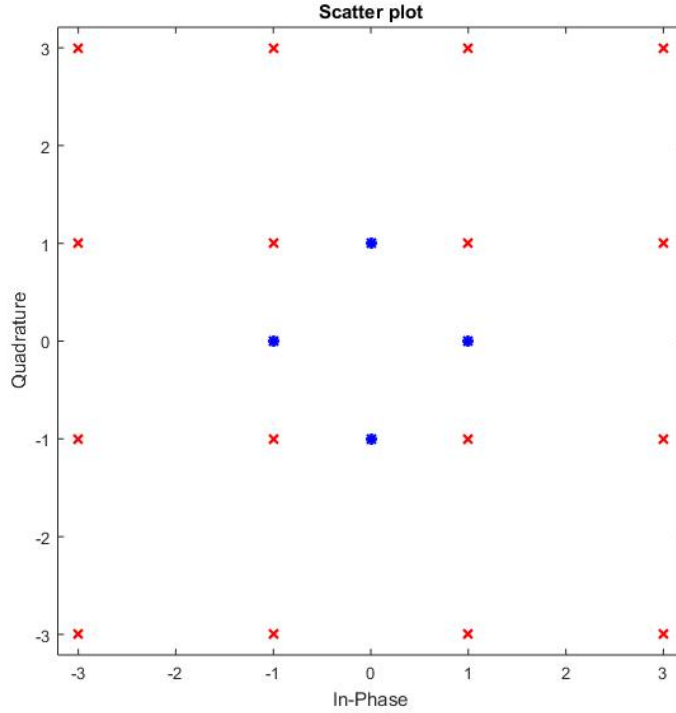


Figure 7.1 The primary (red) and secondary (blue) constellations used in the proposed MSM

effect of spatial correlation we choose combinations in such a way that the signal detection is less error prone.

(b) In selecting the antenna transmission, first two codewords of equation (7.5) indicates that transmission happens with collocated antennas (1,2) (3,4). The last two codewords from equation (7.5) which are transmitting constellation symbols from antennas (1,3) (2,4) are deemed to be unambiguous data transmission pairs as they are spatially separated sufficiently apart. Same performance is observed when antennas 1 and 4 are activated instead of 1 and 3. The total throughput of this scheme is 8 bpcu.

(c) Examining the average energy per codeword transmission, we consider primary and secondary constellation points. By observing Figure 7.1 scatter-plot, the average energy for 16 QAM is  $E_{16QAM_{avg}} = 10$ ,  $E_{QPSK_{avg}} = 1$ . Considering the average energy for all the other SM schemes, the modified MSM scheme has lesser average transmit energy of 11 in producing the throughput of 8 bpcu. Hence, the overall performance improvement is at least 2 dB in comparison with other competing schemes ESM, QSM.

This has been demonstrated in simulation section.

Consider a MIMO framework operated on spatially correlated Rayleigh or Rician fading channels, the received signal can then be modeled as given below:

$$\mathbf{Y} = \mathbf{H}_c \mathbf{X} + \mathbf{n}, \quad (7.7)$$

where,  $N_t$  signifies number of transmitting antennas,  $N_r$  denotes number of receiving antennas,  $N_a$  is the number of active transmit antennas,  $\mathbf{H}_c$  possesses  $N_r \times N_t$  dimension channel matrix,  $\mathbf{X}$  is  $N_t \times 1$  symbol vector which is transmitted from the transmitter and  $\mathbf{n}$  is the complex circularly symmetric i.i.d Additive White Gaussian Noise. Finally assuming perfect channel state information available at the receiver, an optimum ML detection scheme has been carried out.

$$\hat{\mathbf{X}}_{ML} = \arg \min_{X \in j, q} \|\mathbf{Y} - \mathbf{H}\hat{\mathbf{X}}\|_F^2 \quad (7.8)$$

### 7.3 Analytical Treatment for Modified MSM

To substantiate the correctness of Monte Carlo simulations performed for the proposed MSM and obtain a legitimate comprehension into its attributes under SC channel conditions bounds on the PEP are considered in this segment. It is presumed that perfect Channel State Information (CSI) is accessible at the receiver and optimum ML detection strategy is utilized. From [Younis (2014)], the APEP can be calculated from the union bound and ABER for the proposed MSM scheme and can be deduced for spatially correlated channel conditions as

$$ABER_{MSM} = \frac{1}{2\eta} \sum_{N_t, x_{st}} \sum_{N_t, x} \frac{N(X_{N_t, x_{st}}, X_{N_t, x})}{\eta} E_H \{PEP\} \quad (7.9)$$

In the above equation,  $x_{st}$  is the transmitted symbol from the active antenna  $N_t$ ,  $N(X_{N_t, x_{st}}, X_{N_t, x})$  is the total number of error bits between the two.  $E_H \{PEP\}$  is the expectation across the channel  $H$ .

$$PEP(X \rightarrow \hat{X}) = P_r \left( \|Y - H_c X_{n_t, x_t}\|^2 > \|Y - H_c X_{n_t, x}\|^2 | H \right) \quad (7.10)$$

$$= Q \left( \sqrt{\frac{\|H_c \mathfrak{Z}\|^2}{2\sigma_n^2}} \right) \quad (7.11)$$

equation (7.10) can be reduced to a  $Q$  function  $Q(\cdot)$ ,  $\mathfrak{Z} = (x_{N_t, x_{st}}) - (x_{N, x})$ . Simplifying the above equation we get the upper bound as given in (7.12) [Younis (2014)].

$$ABER_{MSM} \leq \frac{1}{2\eta} \frac{N(X_{N_t, x_{st}}, X_{N, x})}{\Sigma_{N_t, x_{st}} \Sigma_{N, x}} \times \frac{1}{2\pi} \frac{\exp(-\frac{1}{4\sigma_n^2} \text{vec}(\check{\mathbf{H}}^H)^H \Gamma (I_{N_r N_t} + \frac{1}{4\sigma_n^2} L_H \Gamma)^{-1} \text{vec}(\check{\mathbf{H}}^H))}{\left| I_{N_r N_t} + \frac{1}{4\sigma_n^2} L_H \Gamma \right|} \quad (7.12)$$

(Note:  $\Gamma = \mathbf{R}_{\text{REC}} \otimes (\mathfrak{Z} \mathfrak{Z}^H \mathbf{R}_{\text{TRAN}})$ ,  $\mathcal{L}_H$  is the covariance matrix,  $\check{\mathbf{H}}$  is the mean matrix,  $\otimes$  is the Kronecker product,  $(\cdot)^H$  is the Hermitian, in equation (7.12) This is the same chernoff bound derived in chapter 3).

## 7.4 Simulation Results and Observations

This section is dedicated to a portrayal of the implementation of modified MSM schemes in spatially correlated Rayleigh and Rician environments. The proposed MSM technique has been compared with other schemes with two active antennas that were defined in the literature. Monte Carlo simulations have been carried out with a minimum of  $10^6$  realizations. The ABER values are plotted against SNR. A Rician factor of  $K=3$  has been chosen to replicate the behavior of spatially correlated indoor environment.

By observing Figure 7.2 the derived asymptotic upper bound on the performance of a modified MSM scheme follows the Monte Carlo simulations at higher SNR values. This simulation has been carried out for a SC channel with transmit antenna element spacing of  $0.5\lambda$  and receive antenna element spacing of  $0.5\lambda$ .

From Figure 7.3, it is observed that the proposed MSM outperforms all the other variants of multiple active SM systems. The performance analysis is carried out for a realistic mobile radio environment. The transmit antenna separation (TX separation) of  $0.5\lambda$  and receiver separation (RX separation) of  $0.5\lambda$  leads to moderate fading. These comparisons have been carried out at ABER of  $10^{-5}$ . Proposed MSM scheme offers a



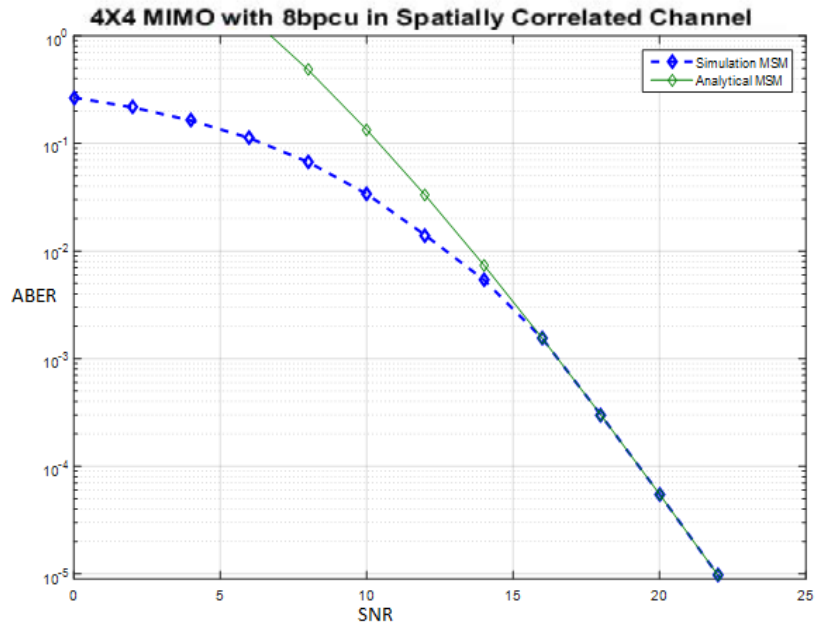


Figure 7.2 Analytical upper bound on the performance of proposed MSM for spatially correlated (SC) channel with transmit antenna element spacing of  $0.5\lambda$  and  $0.5\lambda$  at the receiver.

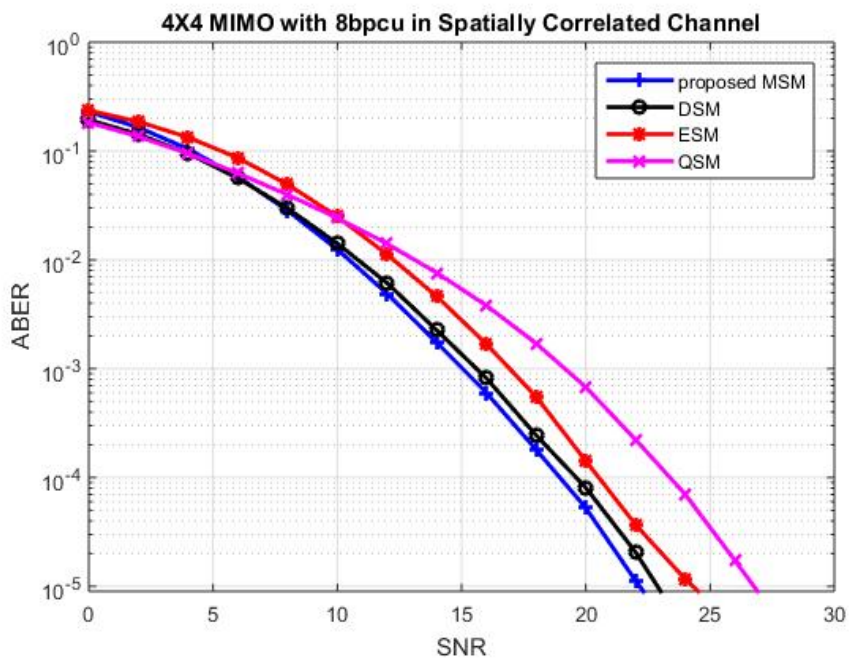


Figure 7.3 BER performance of  $4 \times 4$  MIMO systems with TX separation  $=0.5\lambda$  and RX separation  $=0.5\lambda$  yielding  $\eta=8$  bpcu spectral efficiency, over a SC channel.

performance improvement over DSM, ESM and QSM schemes by  $\sim 1$  dB,  $\sim 2$  dB and  $\sim 4$  dB respectively.

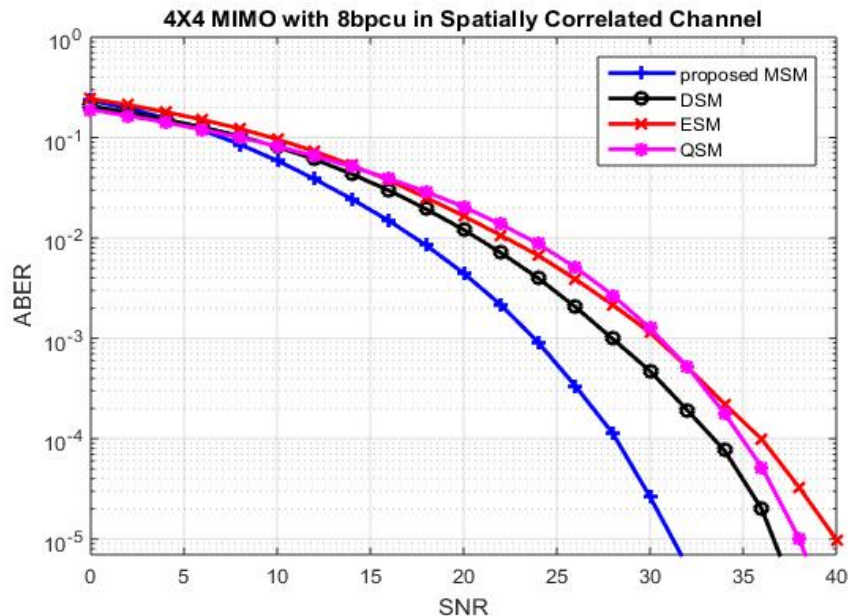


Figure 7.4 BER performance of  $4 \times 4$  MIMO systems with TX separation  $=0.1\lambda$  and RX separation  $=0.5\lambda$  yielding  $\eta=8$  bpcu spectral efficiency, over a Rayleigh SC channel.

The idea of dense spatial correlation is depicted in Figure 7.4. A subtle change in the transmit antenna correlation distance causes a significant degradation in the performances of all the competing schemes. Since correlation become dense the values pertaining to transmit antenna become similar. This effect causes change in performance of all the contending schemes. This is clearly recorded in Figure 7.4. From this we can conclude that even under these dense SC channel conditions, the proposed MSM shows superior performance compare to all the other schemes. MSM offers an SNR improvement over DSM, QSM and ESM systems in higher SNR regime by 5 dB, 7.4 dB and  $\sim 9$  dB respectively. An interesting phenomenon observed here in this simulation is, whenever the correlation becomes dense the BER performance of the proposed MSM system improves because of the antenna selection pattern, moreover the antenna selection (codeword of active antennas) combination is so chosen such that transmission happens from the unambiguous codeword patterns.

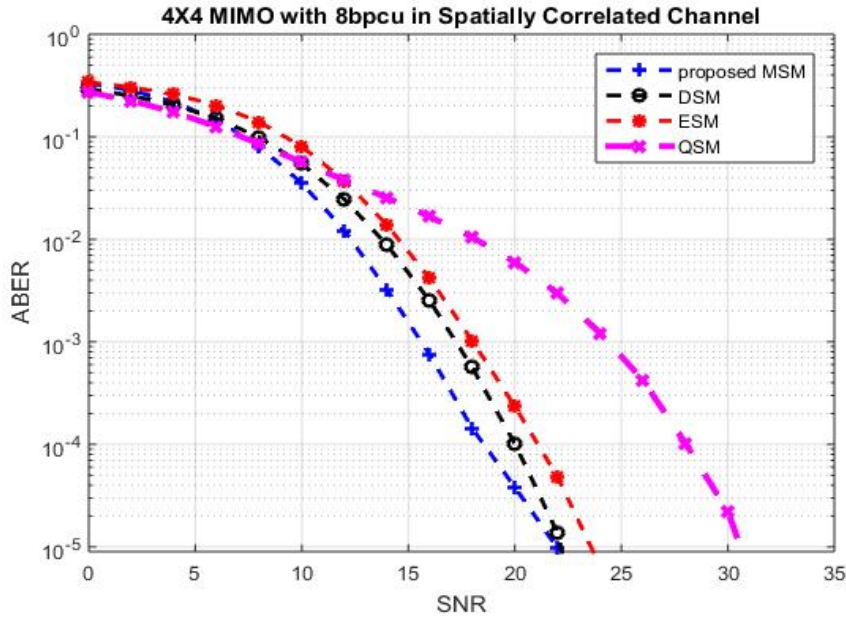


Figure 7.5 BER performance of  $4 \times 4$  MIMO systems with TX separation  $=0.5\lambda$  and RX separation  $=0.5\lambda$  yielding  $\eta=8$  bpcu spectral efficiency, over a Rician fading SC channel with  $K=3$ .

The phenomenon of moderate spatial correlation is depicted in Figure 7.5. Two important aspects of Figure 7.5 are these set of moderate SC channel conditions are carried over Rician fading channels. When the dominant LoS component is available generally the SNR performance for MIMO systems are high. Since error in detecting the antenna combination dominates at lower SNR values and spatial constellation error dominates at higher SNR regime. The Rician  $K$  factor 3 is chosen such that the distribution behaves identical to the indoor propagation channel. Hence, the proposed MSM shows performance enhancements compare to all the other schemes. MSM produces 1.5 dB performance improvement in lower SNR values over DSM schemes, 2.5 dB and  $\sim 9$  dB over ESM and QSM systems respectively. Figure 7.6 shows varying spectral efficiency for a  $4 \times 4$  MIMO system. The advantage of using this scheme is that even in case of dense correlation the performance deterioration is not high. Adding to the above fact, for a  $4 \times 4$  MIMO yielding 10 bpcu the performance is degraded by 4 dB and  $4 \times 4$  MIMO producing 12 bpcu and SNR degradation is 8 dB in comparison with  $4 \times 4$  MIMO systems yielding 8 bpcu. This is highly acceptable compared to all the

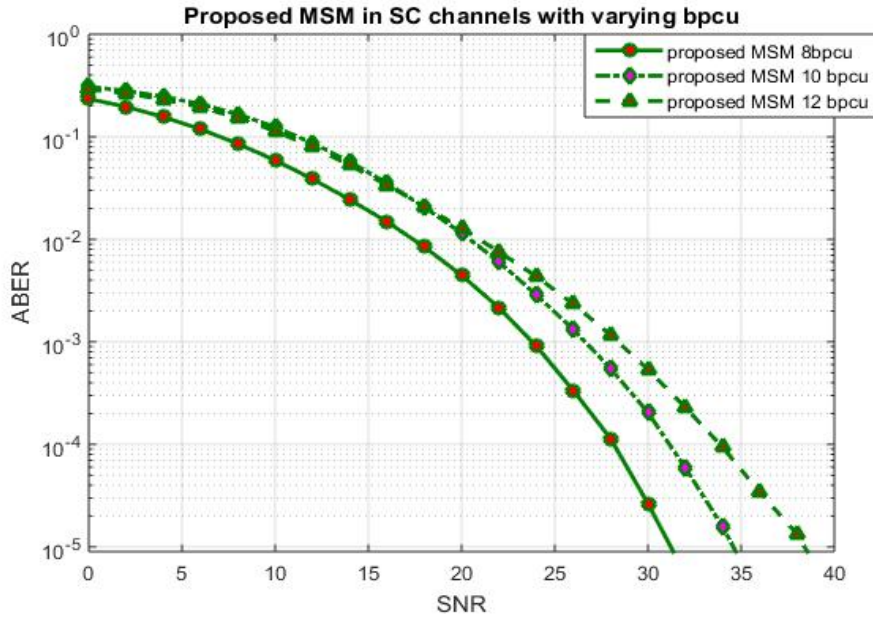


Figure 7.6 BER performance of  $4 \times 4$  MIMO systems with TX separation  $=0.1\lambda$  and RX separation  $=0.5\lambda$  yielding  $\eta=8,10,12$  bpcu spectral efficiency, over a Rayleigh SC channel.

other multiple active antenna SM schemes which retrograde their performances over  $\sim 6$  dB while considering the same channel scenarios.

## 7.5 Summary

In this chapter, we have proposed a modified MSM scheme to work in various SC channel conditions specifically dense correlated Rayleigh and Rician environments. Modified MSM scheme offers lot of advantages when compared with other competing schemes, especially DSM,ESM and QSM systems. The proposed MSM scheme offers a performance gain of over 5 dB in very high correlated fading environments. These performance enhancements are acquired with no additional computational complexity. ABER gains acquired by mathematical upper bound expressions were compared with Monte Carlo simulations and close correspondence between the two sets of results were quantified. This dynamic modification of MSM scheme can be utilized in realistic scenarios where channel is in a state of deep fade. Finally, the proposed MSM scheme can be profitably installed on mobile hand-held devices to achieve higher performance improvements, where antenna spacing becomes very critical.

## Chapter 8

### Conclusions and Future works:

The Research work presented in this thesis, started with a complete study of Spatial Modulation and the design of novel modulation and detection strategies in varied channel conditions. During the study, we became familiar with the concepts of Spatial Modulation and its implications in SC channels. SM-MIMO systems were primarily developed to work in uncorrelated environments considering its energy efficiency as the major advantage. The Primary drawback of conventional SM-MIMO systems include the performance deterioration in SC channels. We, in our first contributory chapter (Chapter-3) provide an alternative solution to SM systems to work efficiently in SC channels and the proposed technique is named as ReSM. We have also derived the upper bound on the performance of the proposed system. ReSM is a special case of SM scheme designed to support reliable communication in SC channels exhibiting flat fading. The major advantage of ReSM is the absence of complex encoder/decoder when compared with TCSM, it also provides BER advantage of  $\sim 4$  dB. Practical measurements were made to prove our claim in an indoor environment.

In order to improve the reliability of data transfer we have studied the concept of Space Time Block Codes and its implementation for SM Systems. During this process we found some of the important aspects of rank distance properties of  $n$ -length cyclic codes over  $GF(q^m)$ , constructed by utilizing the concept of Galois Field Fourier Transforms Sripati et al. (2004). In Chapter 4, we have designed a novel way of choosing antennas and derived the upper bound for the proposed NSTBC-SM scheme. This scheme has the potential to correct errors induced in the communication channel due to its inherent structure. A generalized procedure for designing NSTBC-SM schemes for

any number of transmit antennas ( $N_t$ ) has been devised. For a fixed spectral efficiency of 6 bpcu and two active transmit antenna ( $N_a$ ) configuration, a coding gain of at least 2.2 dB over varied STBC-SM schemes is observed. Our schemes exhibit coding gains superior to those described in literature for comparable spectral efficiencies. We have derived an upper bound on the performance of these codes and have carried out analysis of the computational complexity involved in decoding. The proposed NSTBC-SM scheme offers coding gains ranging from  $\sim 1.2$  dB to 2.8 dB over STBC-SM and  $\sim 4$  dB over SM systems.

The third contributory chapter (Chapter 5) in the thesis analyzes the effect of Imperfect channel state information on the performance of the designed scheme. The motivation behind this work started with the idea of analyzing the performance deterioration of conventional SM systems in the presence of varied channel state information. As a special case study we have also come across the effect of non-uniform phase distribution on the performance of DSM systems. In this chapter, we have investigated and analyzed the impact of imperfect channel knowledge on the performance of DSM system under Rayleigh, Rician and Nakagami-m fading channels. Later, a low complexity decoder for the DSM scheme has been designed using Ordered Block Minimum mean Square Error (OB-MMSE) criterion. Its performance under varied fading environments have been quantified via Monte Carlo simulations. Considering that phase distribution associated with the Nakagami distribution is non uniform, the second part of the work deals with evaluating the performance of DSM schemes under channels perturbed by Nakagami-m distribution for varying values of m. Under conditions of non-uniform phase distributed Nakagami channels an increase in the value of m results in performance deterioration of the order of approximately 1 dB. In the case of Nakagami channel with uniform phase distribution performance improvement is observed with the increasing values of m. DSM scheme outperforms all the conventional SM schemes by at least 2 dB, over all possible channel environments.

In Chapter 6, we have designed a novel SM scheme from non-uniform constellation designs. In this work we propose signal constellations based on multiplicative groups of Gaussian and Eisenstein integers. The set comprising of Gaussian and Eisenstein

integers serves as primary and secondary constellation points for Gaussian Enhanced Spatial Modulation (GESM) scheme. The Monte Carlo simulation results indicate that the proposed nonuniform constellations achieve impressive SNR gains compared to conventional constellation points used in the design of ESM. This new design has been described for MIMO employing  $4 \times 4$  and  $8 \times 8$  antenna configurations with only two active antennas. GESM scheme is energy efficient as well as spectrally efficient and this scheme is well suited to meet the requirements of LTE-Advanced and any 5G wireless systems employing MIMO architecture that may evolve in the future.

Finally, in Chapter 7, we have introduced the concept of modified MSM technique explicitly designed to combat the effect of spatial correlation in realistic channel scenarios. In this modified MSM scheme, two antennas are made active all the time, mapping for antenna selection is judiciously adopted from primary and secondary constellation points. Modified MSM scheme offers lot of advantages when compared with other competing schemes, especially DSM, ESM and QSM systems. The proposed MSM scheme offers a performance gain of over 5 dB in very high correlated fading environments. Finally, the proposed MSM scheme can be profitably installed on mobile hand-held devices to achieve higher performance improvements.

## 8.1 Future work

- A low complexity decoder can be proposed for the ReSM and NSTBC-SM scheme that has been designed in our work. The use of sphere decoder reduces the complexity issues when compared with the ML detection strategies.
- Practical Implementation and design of DSM technique to understand the behavior of non-uniform phase distributed Nakagami-m fading channels will be our futuristic study.
- Since Spatial Correlation cant be avoided in any hand-held device there is a need to understand the effectiveness of SC channel conditions and design of low complexity decoder strategies without compromising the spectral efficiency.





## Bibliography

- Adachi, F., Feeney, M., Parsons, J., and Williamson, A. (1986). Crosscorrelation between the envelopes of 900 mhz signals received at a mobile radio base station site. In *IEE Proceedings F (Communications, Radar and Signal Processing)*, 133, 506–512. IET.
- Afana, A., Atawi, I., Ikki, S., and Mesleh, R. (2015). Energy efficient quadrature spatial modulation mimo cognitive radio systems with imperfect channel estimation. In *Ubiquitous Wireless Broadband (ICUWB), 2015 IEEE International Conference on*, 1–5. IEEE.
- Alamouti, S. M. (1998). A simple transmit diversity technique for wireless communications. *IEEE Journal on selected areas in communications*, 16(8), 1451–1458.
- Babich, F. and Lombardi, G. (2000). Statistical analysis and characterization of the indoor propagation channel. *IEEE Transactions on Communications*, 48(3), 455–464.
- Badarneh, O. S. and Mesleh, R. (2015). On the performance of space modulations over  $\kappa$ - $\mu$  fading channels with imperfect csi. In *Wireless Communications and Networking Conference (WCNC), 2015 IEEE*, 189–194. IEEE.
- Badarneh, O. S., Mesleh, R., Ikki, S. S., and Aggoune, H. M. (2014). Performance analysis of space modulation techniques over alpha-mu fading channels with imperfect channel estimation. In *Vehicular Technology Conference (VTC Fall), 2014 IEEE 80th*, 1–5. IEEE.
- Basar, E. (2016). Index modulation techniques for 5g wireless networks. *IEEE Communications Magazine*, 54(7), 168–175.

- Basar, E., Aygolu, U., Panayirci, E., and Poor, H. V. (2011). Space-time block coded spatial modulation. *IEEE Transactions on Communications*, 59(3), 823–832.
- Basar, E., Aygolu, U., Panayirci, E., and Poor, H. V. (2012). Performance of spatial modulation in the presence of channel estimation errors. *IEEE Communications Letters*, 16(2), 176–179.
- Blahut, R. E. (1983). *Theory and practice of error control codes*, 126. Addison-Wesley Reading (Ma) etc.
- Bossert, M. (1999). *Channel coding for telecommunications*. John Wiley & Sons, Inc.
- Cheng, C.-C., Sari, H., Sezginer, S., and Su, Y. T. (2014). Enhanced spatial modulation with multiple constellations. In *Communications and Networking (BlackSeaCom), 2014 IEEE International Black Sea Conference on*, 1–5. IEEE.
- Cheng, C.-C., Sari, H., Sezginer, S., and Su, Y. T. (2015). Enhanced spatial modulation with multiple signal constellations. *IEEE Transactions on Communications*, 63(6), 2237–2248.
- Cheng, C.-C., Sari, H., Sezginer, S., and Su, Y. T. (2016). New signal designs for enhanced spatial modulation. *IEEE Transactions on Wireless Communications*, 15(11), 7766–7777.
- Clerckx, B. and Oestges, C. (2013). *MIMO wireless networks: Channels, techniques and standards for multi-antenna, multi-user and multi-cell systems*. Academic Press.
- Constantine, A. B. et al. (2005). Antenna theory: analysis and design. *MICROSTRIP ANTENNAS, third edition, John wiley & sons*.
- Di Renzo, M., Haas, H., Ghayeb, A., Sugiura, S., and Hanzo, L. (2014). Spatial modulation for generalized mimo: Challenges, opportunities, and implementation. *Proceedings of the IEEE*, 102(1), 56–103.
- Di Renzo, M., Mesleh, R. Y., Haas, H., and Grant, P. M. (2010). Upper bounds for the analysis of trellis coded spatial modulation over correlated fading channels. In  *Vehicular Technology Conference (VTC 2010-Spring), 2010 IEEE 71st*, 1–5. IEEE.

- Duman, T. M. and Ghrayeb, A. (2008). *Coding for MIMO communication systems*. John Wiley & Sons.
- Erceg, V. (2004). Tgn channel models, ieee p802. 11 wireless lans std. *IEEE 802.11-03/940r4*.
- Forenza, A., Love, D. J., and Heath, R. W. (2004). A low complexity algorithm to simulate the spatial covariance matrix for clustered mimo channel models. In  *Vehicular Technology Conference, 2004. VTC 2004-Spring. 2004 IEEE 59th*, 2, 889–893. IEEE.
- Freudenberger, J. and Shavgulidze, S. (2017). Signal constellations based on eisenstein integers for generalized spatial modulation. *IEEE Communications Letters*, 21(3), 556–559.
- Gabidulin, E. M. (1985). Theory of codes with maximum rank distance. *Problemy Peredachi Informatsii*, 21(1), 3–16.
- Gesbert, D., Shafi, M., Shiu, D.-s., Smith, P. J., and Naguib, A. (2003). From theory to practice: An overview of mimo space-time coded wireless systems. *IEEE Journal on selected areas in Communications*, 21(3), 281–302.
- Goldsmith, A. (2005). *Wireless communications*. Cambridge university press.
- Group, G. et al. Spatial channel model, spatial channel model ahg (combined ad-hoc from 3gpp and 3gpp2), 3gpp std. *SCM-134 text*, 6.
- Hedayat, A., Shah, H., and Nosratinia, A. (2005). Analysis of space-time coding in correlated fading channels. *IEEE Transactions on Wireless Communications*, 4(6), 2882–2891.
- Hoehner, P. (1992). A statistical discrete-time model for the wssus multipath channel. *IEEE Transactions on vehicular technology*, 41(4), 461–468.
- Hottinen, A., Tirkkonen, O., and Wichman, R. (2004). *Multi-antenna transceiver techniques for 3G and beyond*. John Wiley & Sons.

- Huber, K. (1994a). Codes over eisenstein-jacobi integers. *Contemporary Mathematics*, 168, 165–173.
- Huber, K. (1994b). Codes over gaussian integers. *IEEE Transactions on Information Theory*, 40(1), 207–216.
- Ishibashi, K. and Sugiura, S. (2014). Effects of antenna switching on band-limited spatial modulation. *IEEE Wireless Communications Letters*, 3(4), 345–348.
- Jeganathan, J., Ghrayeb, A., and Szczecinski, L. (2008). Spatial modulation: optimal detection and performance analysis. *IEEE Communications Letters*, 12(8).
- K.Huber (1994). Codes over eisenstein-jacobi integers. *Contemporary Mathematics*, 168, 165–179.
- Kim, Y., Kang, H., and Kim, K. (2004). Performance of space-time block codes with qam under the spatially correlated channels. In *Vehicular Technology Conference, 2004. VTC 2004-Spring. 2004 IEEE 59th*, 2, 670–673. IEEE.
- Koca, M. and Sari, H. (2012). Performance analysis of spatial modulation over correlated fading channels. In *Vehicular Technology Conference (VTC Fall), 2012 IEEE*, 1–5. IEEE.
- Le, M.-T., Ngo, V.-D., Mai, H.-A., Tran, X. N., and Di Renzo, M. (2014). Spatially modulated orthogonal space-time block codes with non-vanishing determinants. *IEEE Transactions on Communications*, 62(1), 85–99.
- Lee, J., Kim, Y., Kwak, Y., Zhang, J., Papasakellariou, A., Novlan, T., Sun, C., and Li, Y. (2016). Lte-advanced in 3gpp rel-13/14: an evolution toward 5g. *IEEE Communications Magazine*, 54(3), 36–42.
- Lee, W.-Y. (1973). Effects on correlation between two mobile radio base-station antennas. *IEEE Transactions on Vehicular Technology*, 22(4), 130–140.
- Lee, Y., Yun, S., et al. (2005). Interchannel interference avoidance in mimo transmission by exploiting spatial information. In *Personal, Indoor and Mobile Radio Communi-*

- cations, 2005. PIMRC 2005. IEEE 16th International Symposium on*, 1, 141–145. IEEE.
- Li, X. and Wang, L. (2014). High rate space-time block coded spatial modulation with cyclic structure. *IEEE Communications Letters*, 18(4), 532–535.
- Luna-Rivera, J., Campos-Delgado, D. U., and Gonzalez-Perez, M. (2013). Constellation design for spatial modulation. *Procedia Technology*, 7, 71–78.
- Luna-Rivera, J. and Gonzalez-Perez, M. (2012). An improved spatial modulation scheme for mimo channels. In *Antennas and Propagation (EUCAP), 2012 6th European Conference on*, 1–5. IEEE.
- Lusina, P., Gabidulin, E., and Bossert, M. (2003). Maximum rank distance codes as space-time codes. *IEEE Transactions on Information Theory*, 49(10), 2757–2760.
- MacLeod, H., Loadman, C., and Chen, Z. (2005). Experimental studies of the 2.4-ghz ism wireless indoor channel. In *Communication Networks and Services Research Conference, 2005. Proceedings of the 3rd Annual*, 63–68. IEEE.
- Mesleh, R., Di Renzo, M., Haas, H., and Grant, P. M. (2010). Trellis coded spatial modulation. *IEEE Transactions on Wireless Communications*, 9(7), 2349–2361.
- Mesleh, R. and Ikki, S. S. (2015). On the impact of imperfect channel knowledge on the performance of quadrature spatial modulation. In *Wireless Communications and Networking Conference (WCNC), 2015 IEEE*, 534–538. IEEE.
- Mesleh, R., Ikki, S. S., and Aggoune, H. M. (2015). Quadrature spatial modulation. *IEEE Transactions on Vehicular Technology*, 64(6), 2738–2742.
- Mesleh, R., Stefan, I., Haas, H., and Grant, P. M. (2009). On the performance of trellis coded spatial modulation. In *Int. ITG Workshop on Smart Antennas*, 235–241.
- Mesleh, R. Y. (2007). *Spatial modulation: a spatial multiplexing technique for efficient wireless data transmission*. PhD thesis, Jacobs University Bremen.

- Mesleh, R. Y., Haas, H., Sinanovic, S., Ahn, C. W., and Yun, S. (2008). Spatial modulation. *IEEE Transactions on Vehicular Technology*, 57(4), 2228–2241.
- Moon, T. K. (2005). Error correction coding. *Mathematical Methods and Algorithms*. Jhon Wiley and Son.
- Ntontin, K., Di Renzo, M., Perez-Neira, A., and Verikoukis, C. (2013a). Performance analysis of multistream spatial modulation with maximum-likelihood detection. In *Global Communications Conference (GLOBECOM), 2013 IEEE*, 1590–1594. IEEE.
- Ntontin, K., Di Renzo, M., Pérez-Neira, A. I., and Verikoukis, C. (2013b). A low-complexity method for antenna selection in spatial modulation systems. *IEEE communications letters*, 17(12), 2312–2315.
- Panic, S., Stefanovic, M., Anastasov, J., and Spalevic, P. (2013). *Fading and interference mitigation in wireless communications*. CRC Press.
- Paulraj, A. J. and Papadias, C. B. (1997). Space-time processing for wireless communications. *IEEE Signal Processing Magazine*, 14(6), 49–83.
- Pedersen, K. I., Mogensen, P. E., and Fleury, B. H. (1998). Spatial channel characteristics in outdoor environments and their impact on bs antenna system performance. In *Vehicular Technology Conference, 1998. VTC 98. 48th IEEE*, 2, 719–723. IEEE.
- Proakis, J. G. (1998). *Digital communications fourth edition*, 2001.
- Puchinger, S., Stern, S., Bossert, M., and Fischer, R. F. (2016). Space-time codes based on rank-metric codes and their decoding. In *Wireless Communication Systems (ISWCS), 2016 International Symposium on*, 125–130. IEEE.
- Serafimovski, N., Younis, A., Mesleh, R., Chambers, P., Di Renzo, M., Wang, C.-X., Grant, P. M., Beach, M. A., and Haas, H. (2013). Practical implementation of spatial modulation. *IEEE Transactions on Vehicular Technology*, 62(9), 4511–4523.
- Simha, G. D. G., Koila, S., Neha, N., Raghavendra, M., and Sripati, U. (2017). Re-designed spatial modulation for spatially correlated fading channels. *Wireless Personal Communications, Springer*, 1–28.

- Simon, M. K. and Alouini, M.-S. (2005). *Digital communication over fading channels*, 95. John Wiley & Sons.
- Spencer, Q. H., Jeffs, B. D., Jensen, M. A., and Swindlehurst, A. L. (2000). Modeling the statistical time and angle of arrival characteristics of an indoor multipath channel. *IEEE Journal on Selected areas in communications*, 18(3), 347–360.
- Srinath, K. P. and Rajan, B. S. (2009). Low ml-decoding complexity, large coding gain, full-rate, full-diversity stbcs for 2x2 and 4x2 mimo systems. *IEEE Journal of Selected Topics in Signal Processing*, 3(6), 916–927.
- Sripati, U. and Rajan, B. S. (2003). On the rank distance of cyclic codes. In *Information Theory, 2003. Proceedings. IEEE International Symposium on*, page 72. IEEE.
- Sripati, U., Rajan, B. S., and Shashidhar, V. (2004). Full-diversity stbcs for block-fading channels from cyclic codes. In *Global Telecommunications Conference, 2004. GLOBECOM'04. IEEE*, 1, 566–570. IEEE.
- Stavridis, A., Sinanovic, S., Di Renzo, M., Haas, H., and Grant, P. (2012). An energy saving base station employing spatial modulation. In *Computer Aided Modeling and Design of Communication Links and Networks (CAMAD), 2012 IEEE 17th International Workshop on*, 231–235. IEEE.
- Tarokh, V., Jafarkhani, H., and Calderbank, A. R. (1999). Space-time block codes from orthogonal designs. *IEEE Transactions on information theory*, 45(5), 1456–1467.
- Tarokh, V., Seshadri, N., and Calderbank, A. R. (1998). Space-time codes for high data rate wireless communication: Performance criterion and code construction. *IEEE transactions on information theory*, 44(2), 744–765.
- Trefethen, L. N. and Bau III, D. (1997). *Numerical linear algebra*, 50. Siam.
- Tzeremes, G. and Christodoulou, C. (2002). Use of weibull distribution for describing outdoor multipath fading. In *Antennas and Propagation Society International Symposium, 2002. IEEE*, 1, 232–235. IEEE.

- Van Zelst, A. and Hammerschmidt, J. (2002). A single coefficient spatial correlation model for multiple-input multiple-output (mimo) radio channels. *Proc. 27th General Assembly of the Int. Union of Radio Science (URSI)*.
- Wang, L., Chen, Z., and Wang, X. (2014). A space-time block coded spatial modulation from  $(n, k)$  error correcting code. *IEEE Wireless Communications Letters*, 3(1), 54–57.
- Wen, M., Cheng, X., and Yang, L. (2016). Index modulation for 5g wireless communications.
- Wicker, S. B. (1995). *Error control systems for digital communication and storage*, 1. Prentice hall Englewood Cliffs.
- Xiao, Y., Yang, Z., Dan, L., Yang, P., Yin, L., and Xiang, W. (2014). Low-complexity signal detection for generalized spatial modulation. *IEEE Communications Letters*, 18(3), 403–406.
- Yacoub, M. D. (2009). Nakagami- $m$  phase-envelope joint distribution: An improved model. In *Microwave and Optoelectronics Conference (IMOC), 2009 SBMO/IEEE MTT-S International*, 335–339. IEEE.
- Yang, P., Xiao, Y., Yu, Y., and Li, S. (2011). Adaptive spatial modulation for wireless mimo transmission systems. *IEEE Communications Letters*, 15(6), 602–604.
- Yigit, Z. and Basar, E. (2016). Double spatial modulation: A high-rate index modulation scheme for mimo systems. In *Wireless Communication Systems (ISWCS), 2016 International Symposium on*, 347–351. IEEE.
- Younis, A. (2014). Spatial modulation: theory to practice.
- Younis, A., Mesleh, R., and Haas, H. (2016). Quadrature spatial modulation performance over nakagami- $m$  fading channels. *IEEE Transactions on Vehicular Technology*, 65(12), 10227–10231.



- Younis, A., Serafimovski, N., Mesleh, R., and Haas, H. (2010). Generalised spatial modulation. In *Signals, Systems and Computers (ASILOMAR), 2010 Conference Record of the Forty Fourth Asilomar Conference on*, 1498–1502. IEEE.
- Younis, A., Sinanovic, S., Di Renzo, M., Mesleh, R., and Haas, H. (2013). Generalised sphere decoding for spatial modulation. *IEEE Transactions on Communications*, 61(7), 2805–2815.

## Journal Publications:

- **Goutham Simha G.D**, Shriharsha K, Neha .N, Raghavendra M.A.N.S and U.Sripati, “Redesigned Spatial Modulation for Spatially Correlated Fading Channels”, Springer Wireless personal communications, Volume 97 Issue 4, pp 5003-5030 (2017).
- **Goutham Simha G.D**, Shriharsha K, Raghavendra M.A.N.S and U.Shripathi Acharya, “A comprehensive framework for Double Spatial Modulation under imperfect channel state information”, Elsevier Physical Communication, Volume 25 Part 2, pp 519-526 (2017).
- **Goutham Simha G.D**, Raghavendra M.A.N.S, Shriharsha K and U.Shripathi Acharya, “Signal Constellations Employing Multiplicative Groups of Gaussian and Eisenstein Integers for Enhanced Spatial Modulation”, Elsevier Physical Communication, Volume 25 Part 2 pp 546-554 (2017).
- **Goutham Simha G.D**, Raghavendra M.A.N.S, and U.Shripathi Acharya, “Non Orthogonal Space Time Block Coded Spatial Modulation for SM-MIMO systems”, ("Unpublished").

## Conference Papers

- **Goutham Simha G.D**, Shriharsha K, Raghavendra M.A.N.S, and U.Shripathi Acharya, “Modified Signal Design for Multistream Spatial Modulation over Spatially Correlated Channels”, published in Proceedings of the 6<sup>th</sup> IEEE “International conference on Advances in Computing, Communications and Informatics” Manipal Institute of Technology, Manipal, Karnataka , September 2017.
- **Goutham Simha G.D**, Shriharsha K, Raghavendra M.A.N.S, and U. Shripathi Acharya. “Performance of Spatial modulation and Spatial Multiplexing Systems over weibull fading channel”, “International Conference on Computing and Network Communications (CoCoNet’15)” December 16-19, 2015, Trivandrum, Kerala, India.

## BIO-DATA

**Name** : Goutham Simha G.D.

**Email Id** : goutham.mah@gmail.com

**Mobile** : +91-9482898354

**Date of Birth** : 01-June-1984

**Address** : Dept of Electronics and Communication Engineering NITK, Surathkal.

### Educational Qualifications and Teaching Experience:

<b>Degree</b>	<b>Year of Passing</b>	<b>University</b>
B.E.	2007	VTU Belgaum, SSIT Tumkur.
M.tech.	2009-10	VTU Belgaum, Dayananda Sagar Bangalore.
Lecturer	2010-2012	Dayananda Sagar Bangalore.
Ph.D.	2012-2017	National Institute of Technology Karnataka, Surathkal.